2007

Scalable Volumetric Three-dimensional Up-conversion Display Medium

Jung-Hyun Cho
University of Central Florida

SCALABLE VOLUMETRIC THREE-DIMENSIONAL UP-CONVERSION DISPLAY MEDIUM

by

JUNG-HYUN CHO
B.S. Sungkyunkwan University, 1997
M.S. Sungkyunkwan University, 1999

A dissertation submitted in partial fulfillment of the requirements
for the degree of Doctor of Philosophy
in the College of Optics and Photonics: CREOL & FPCE
at the University of Central Florida
Orlando, Florida

Fall Term
2007

Major Professor: Michael Bass

ABSTRACT

There are many different techniques to display 3D information. However, not many of them are able to provide sufficient depth cues to the observers to sense or feel the images as real three-dimensional objects. Volumetric three-dimensional displays generate images within a real 3D space, so they provide most of the depth cues automatically.

This thesis discusses the basic notions required to understand three-dimensional displays. Also discussed are different techniques used to display 3D information and their advantages and disadvantages as well as their current limitations. Several rare-earth doped fluoride crystals that are excited to emit visible light by sequential two photon absorption have been investigated as display medium candidates for static volumetric three dimensional displays. A scalable display medium is suggested to enable large 3D displays. This medium is a dispersion of particles of the rare earth doped fluoride crystals in a refractive index-matched polymer matrix. Detailed experiments are described to prepare such a scalable display medium using a wide variety of polymers. The scattering problem in such a medium was greatly reduced by index-matching the polymer to the crystalline particles. An index-matching condition that optimizes the performance was identified and demonstrated. A potential near-future solution is demonstrated and improvements are suggested.

Dedicated to my wife Soyoung,
my mother, my family
and my late father

ACKNOWLEDGMENTS

First of all, I would like to thank to Dr. Michael Bass. I have learnt not just invaluable knowledge but also an attitude of a scientist from Dr. Bass. He is not just an advisor, but also he is my mentor. I also thank to my committee members Dr. Aristide Dogariu, Dr. Shin-Tson Wu, Dr. Kevin Belfield for their guidance and advices. I am really grateful to Dr. Hans Jenssen, Arlete Cassanho for their support and beautiful crystals. Many thanks to past Bass group members Ferenc, Janet and Alexandra, also, current Bass group members: Giorgio Turri, Ying Chen, Hong Shu, William Hageman. It is so great to work with such brilliant people. My great thanks to my Turkish best friends Sarper, Pinar and Ozan. I thank all the prior and current Korean students in CREOL and UCF. Thanks to Sung-soo Kim and all of my old college friends who have studied and studying to get the PhD in the United States. I am truly grateful to Dr. Bongjin Kim, my best friend since middle school, who saved rest of my life by giving me a chance to meet the most special person in my life.

Special thanks to my family: the Chos and the Parks. I am really grateful to my grandmother and late grandfather who believed in me all the time, and to all the uncles, aunts and cousins. I am truly thankful to my brother and sister-in-law for their support and their beautiful work: my adorable nephew. I would like to thank to my father-, mother-in-law and my brother-in-law for their belief and support. I am especially grateful to my mother and late father for their love and the endless support. My late father was a physicist and a brilliant inventor and he is the one who led me to the world of Physics. I would not have made it this far without them.

Finally, I would like to thank to my wife, Dr. Soyoung Park. She was always there for me as a friend and gave me priceless advices and support as a colleague and as a wife. There are no words to convey how much I love her and how much I am thankful to her.

This work was supported by the U.S. Army Office of Research Grant No. DAAD19-99-1-0220 and DURIP Award No. DAAD19-00-10132.

TABLE OF CONTENTS

LIST OF FIGURES

LIST OF TABLES

LIST OF ACRONYMS

2D	two-dimensional
3D	three-dimensional
CRT	cathode ray tube
TSTF	two-step two-frequency
UC	up-conversion
IR	infrared
TPA	two-photon absorption
CGH	computer-generated holograms
SLM	spatial light modulator
CBD	crossed-beam display
wt%	weight percent
Nd:YAG	neodymium-doped yttrium aluminum garnet
MOPO	master oscillator-power oscillator
PMMA	Polymethylmethacrylate
PFCB	Perfluorocyclobutyl

CHAPTER ONE: INTRODUCTION

1.1 3D Display

It has been about one hundred years since the invention of the cathode ray tube (CRT) and, since then, thousands of researchers have been developing this and other two dimensional (2D) display systems. Thanks to these efforts, there are many excellent displays in common use. Three dimensional (3D) displays, on the other hand have received much less attention and are much less developed. Even though there are some commercial 3D displays on the market, most of them are not 'true' 3D displays. They do not provide all the depth cues that are required for observers to sense a certain object shown in a display as a real three-dimensional object. Also, they cannot provide enough information, so that the observer sees same views for different viewing angles. For example, stereoscopic 3D display systems, such as in a 3D movie, provide only binocular parallax by presenting slightly different images to each eye. Such a 3D display can be simple and effective for a large number of viewers. However, they have an innate accommodation-convergence mismatch that makes many viewers uncomfortable. In addition, viewers must wear special glasses to view the 3D images and the system does not provide different views for different viewing angles [1]. More advanced autostereoscopic display systems that utilize a lenticular screen or parallax barrier technique do not require the viewer to wear special glasses [2][3]. However, they still have accommodation-convergence mismatch problems and provide only a limited number of views for different viewing angles. Further, there are restrictions on the positions from which viewers can see a proper image [4].

Volumetric 3D displays generate images within a real 3D space, so they provide most of the depth cues automatically. Swept volume 3D displays, one of a few commercialized volumetric 3D displays, generate volume-filling images by rotating a two-dimensional screen and projecting images from different directions at appropriate times [5]. However, generating a volume filling screen by mechanical rotation has consequent problems. For example, to generate images at a high enough refresh rates to prevent visual jitter, the screen must rotate at a high speed. Such moving parts in a system are problematic because of short life, noise, and instability. Also the image will be dim because the rapid refresh rate allows only short illumination of any point on the rotating screen negating taking advantage of the integration of light in the retina [6]. However, in a static volumetric display there are no moving parts [7][8].

1.2 Static volume 3D display

Static volumetric 3D displays can be classified by how their volume pixels (voxels) are activated and what kind of display medium is used [9]. In our work, we mainly consider a 3D display with a passive display medium based on a rare earth doped material. Its voxels can be activated by sequential absorption of light from two invisible near infrared laser beams, as shown in Figure 1-1. The excitation process can be considered in three steps. 1) Absorption of near infrared light to populate an intermediate energy level of ions in the medium. 2) A second absorption of a different wavelength of infrared light at the intersection point of the two beams excites the ions in the intermediate level to an upper level. 3) Ions in the upper level then decay to the ground state while emitting visible light. This process is called two-step, two-frequency up-conversion (TSTF-UC). Downing et al. demonstrated a display utilizing this concept within

rare-earth doped heavy metal fluoride glasses in 1996 [7]. Even though the potential of this type of display was demonstrated more than 10 years ago there are currently no such display systems on the market. There are several practical difficulties related to voxel addressing and beam scanning. However, major limitations concern the display medium itself. Since it is the display medium that generates visible emission by conversion of infrared light, the display medium in this type of display is the heart of the system. It must be able to create voxels bright enough to be seen in the ambient lighting environment. Also, a useful volumetric 3D display medium must have good optical properties (that is must be scatter and stress free). It must be transparent to visible wavelengths and to the wavelengths used to excite visible emission from a voxel. It must have good mechanical properties and it must be possible to produce it in large enough samples to be useful in a volumetric display. More specifically, it must be possible to produce the display medium in volumes about 30 cm on a side at reasonable cost while retaining the desired optical properties.

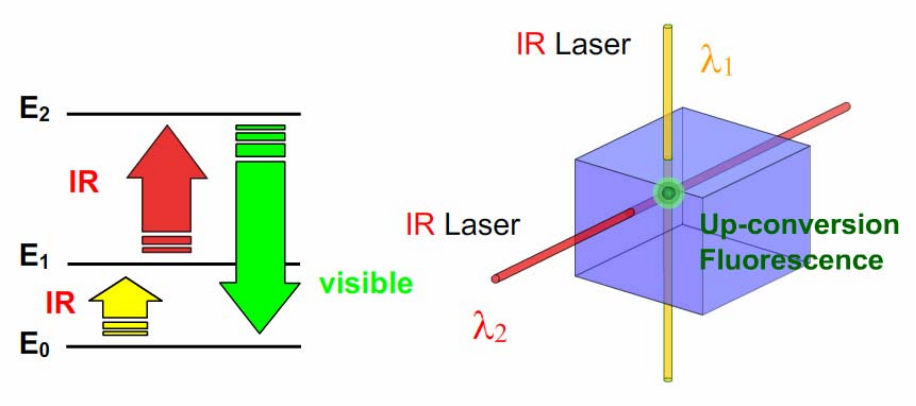

Figure 1-1: Schematic diagram of static volume 3D display. A two frequency two step up conversion process is diagramed on the left. A voxel is sketched in which visible light is generated in the display medium by two different frequency IR laser beams intersecting in the voxel.

Candidates for static 3D volumetric display media are investigated that can be excited to emit visible light by two-step two-frequency up-conversion (TSTF-UC) of near infrared laser light and that may meet the criteria discussed above. Part of this work was presented in SID 2007 conference held in Long Beach, CA and received a distinguished student paper award [10]. Also, it will be published in the Journal of SID on December 2007.

1.3 Thesis

In this thesis, several different display materials for use as static volume 3D display media with high efficiency and good optical and mechanical properties are discussed. Also, a potential solution to make a scalable display medium is examined.

In chapter 2, the basics of up-conversion are discussed and considered as applied to understand three-dimensional displays. Also, different techniques to display 3D information and their advantages and disadvantages as well as their current limitations are discussed.

In chapter 3, different materials as display medium candidates for static volumetric 3D display are discussed such as organic dyes and rare-earth doped single crystals. A rare-earth doped single crystal, that is the most promising candidate, is examined in detail.

In chapter 4, a method is described to make a scalable display medium by placing particles of the rare earth doped crystal in a passive, index matched host. Detailed experiments on many different polymer candidate host materiasl are described. A possible near-future solution is demonstrated and several issues and their solutions are suggested.

Finally, in chapter 5, results are summarized and future work is suggested.

CHAPTER TWO: BACKGROUND

2.1 Basics on up-conversion

2.1.1 Definitions

Luminescence is light emission which is not caused by heating. Luminescence is a collective term for different phenomena where a substance emits light without being strongly heated, i.e., the emission is not simply thermal radiation. This definition is also reflected by the term "cold light". Important kinds of luminescence are explained below [11].

Fluorescence is light emission caused by irradiation with light (normally visible or ultraviolet light) and typically occurring within nanoseconds to milliseconds after irradiation. It involves the excitation of electrons into states with a higher energy, from which radiative decay is possible. Typically, the emitted wavelengths are longer than the excitation wavelengths; otherwise one speaks of up-conversion fluorescence.

Phosphorescence is a light emission that can occur over much longer times (sometimes hours) after irradiation. It involves storage of energy in metastable states and its release through relatively slow (often thermally activated) processes. The phenomenon was discovered early on for phosphorus.

Photoluminescence is a less specific term which embraces both fluorescence and phosphorescence.

Thermoluminescence is a type of phosphorescence which occurs at elevated temperatures. It is not to be confused with thermal radiation: the thermal excitation only triggers the release of energy from another source.

Electroluminescence is light emission triggered by electric influences. In case of excitation by an electron beam, this is also often called cathodoluminescence.

Up-conversion is a process where light can be emitted with higher energy photons than those of the light causing the excitation. When a medium absorbs incident light and emits fluorescence as a result the wavelength of emitted light is usually longer than that of incident light. However, under some circumstances it is possible to have up-conversion fluorescence emitted at a shorter wavelength. This is possible by excitation mechanisms which involve more than one absorbed photon per emitted photon.

2.1.2 Two-step up-conversion process

There are several up-conversion processes that involve two photons as shown in Figure 2-1. One of the mechanisms that of interest in this dissertation is sequential absorption of pump photons by excited state absorption in Figure 2-1(b). This is called two-step (or more generally; stepwise) up-conversion process. A first absorption process populates a metastable excited level, and then the second absorption can take the ion to a higher level. In some energy level configurations, a single wavelength pump can be used for all excitation steps, but there are cases where multiple pump wavelengths are required.

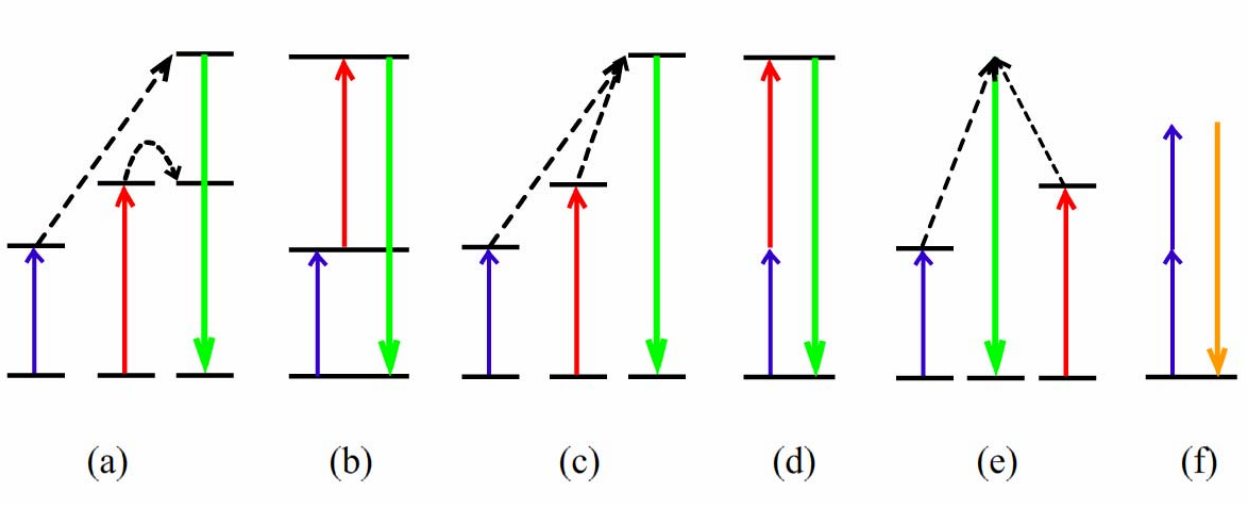

Figure 2-1: Schematic diagrams for different two-photon up-conversion processes [12]: (a)up-conversion by energy transfer (b) two-step up-conversion (c) cooperative sensitization (d) two-photon absorption excitation, (e) cooperative luminescence and (f) Second Harmonic Generation (SHG).

2.1.3 Two-step two-frequency up-conversion

In the case of the static volumetric display, the up-conversion fluorescence should be well defined in 3D space. Thus, instead of single wavelength pump beam, the use of two pump beams of different wavelengths is required. Two beams of infrared lasers are usually used to excite the quantum system to an energy state from which visible fluorescence may be emitted.

This system can be described by a simplified three-level system. In general, more than three levels are involved but the system often occupies the other states transiently. As a result their effect can be incorporated into the transition parameters for one of the states in the three-level model. Rate equations that describe such a system have been reported [1][13][14]. Figure

2-2 shows the schematic diagram of three-level system and the parameters associated with the transitions [1].

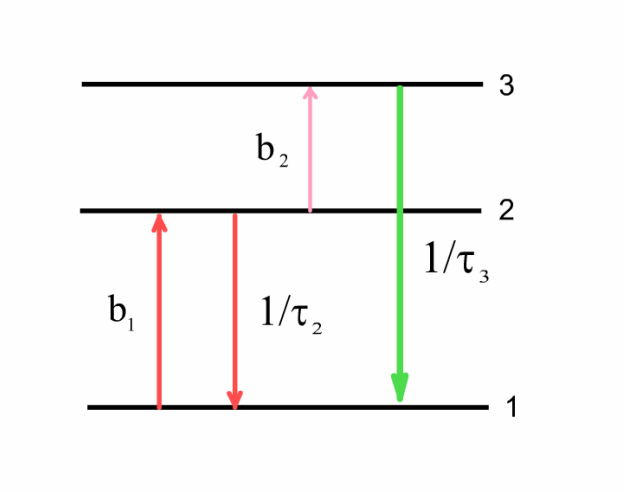

Figure 2-2: Schematic diagram for three-level two-step two-frequency up-conversion system. The parameters b_1 and b_2 are the product of the pulse intensity and absorption cross section, divided by the photon energy. Stimulated emission is given by b_1 and b_2. τ_1 and τ_2 are the spontaneous decay lifetime.

Parameters b_1 and b_2 are the coefficients related to the absorption rates of levels 1 and 2 respectively and can be written as

$$b_i = \frac{\sigma_i I_i}{\Delta E_i} \quad [s^{-1}] \tag{1}$$

where σ_i is the resonance absorption coefficient for the transition i to i+1, I_i is the peak intensity of the activation radiation with this transition and ΔE_i is the energy difference between the two states i and i+1. The lifetime τ_1 and τ_2 govern the spontaneous decay of levels 2 and 3. When

we denote the population density of each level as N_i (number per unit volume) the rate equations can be written as

$$\begin{aligned}
\frac{dN_1}{dt} &= \frac{1}{\tau_2}N_2 + \frac{1}{\tau_3}N_3 + p_1(t)b_1[N_2 - N_1] \\
\frac{dN_2}{dt} &= -\frac{1}{\tau_2}N_2 - p_1(t)b_1[N_2 - N_1] + p_2(t)b_2[N_3 - N_2] \\
\frac{dN_3}{dt} &= -\frac{1}{\tau_3}N_3 - p_2(t)b_2[N_3 - N_2]
\end{aligned} \tag{2}$$

where $p_j(t)$ (j=1,2) represent the normalized temporal profile of the activation pulses, $N_i=N_i(t)$ and $N=N_1+N_2+N_3$. These equations can be written in more convenient form as the matrix equation

$$\frac{d}{dt}\begin{bmatrix} N_1 \\ N_2 \\ N_3 \end{bmatrix} = \begin{bmatrix} -p_1(t)b_1 & \frac{1}{\tau_2} + p_1(t)b_1 & \frac{1}{\tau_3} \\ p_1(t)b_1 & -\frac{1}{\tau_2} - p_1(t)b_1 - p_2(t)b_2 & p_2(t)b_2 \\ 0 & p_2(t)b_2 & -\frac{1}{\tau_3} - p_2(t)b_2 \end{bmatrix}\begin{bmatrix} N_1 \\ N_2 \\ N_3 \end{bmatrix} \tag{3}$$

The total population excited to the fluorescent state is then

$$S_3 = \int_{t_2}^{t_2+T_P} [b_2 p_2(t)(N_2(t) - N_3(t))]dt \tag{4}$$

where T_p is pulse duration and t_2 is the time at which the radiation of the second beam arrives at the voxel location. The total energy (E_v) output from a voxel due to a two-pulse excitation is proportional to the total number (S_3) of fluorescent centers excited to the state 3, the fluorescent efficiency(η), and energy (E_{fl}) of each fluorescent photon.

$$E_v = \eta E_{fl} S_3 \ \text{[J]} \tag{5}$$

If the excitation pulse intensity does not saturate the transition, we can assume $N \approx N_1 >> N_2 >> N_3$. Then from Eqs (3) and (4) S_3 becomes

$$S_3 = b_1 b_2 N T_p^2 \tag{6}$$

The beam intensities are $I_j=P_j/a$, where a is the cross-sectional area of each beam. Using Eqs. (1), (5) and (6) the power output from a single voxel occupying volume V excited by two-pump beams can be expressed as

$$P_v = \eta N V \frac{E_{fl}}{\Delta E_1 \Delta E_2} \sigma_1 \sigma_2 \frac{P_1 P_2}{a^2} \frac{T_p^2}{\tau_3} \quad [\mathrm{W}] \tag{7}$$

when the life time of the third level is longer than the pulse duration.

The time-averaged output power per volume is determined by the duty cycle $\tau_3/\ \tau_r$, where τ_r is the image space refresh period.

$$P_v^{av} = P_v(\tau_3/\ \tau_r) \tag{8}$$

Voxel brightness is an important factor for volumetric 3D display applications. Some parameters that affect voxel brightness can be found from Eqs. (7) and (8). For example, an increase in the density of the fluorescent centers can lead to increased voxel brightness. This can be accomplished by an increase in the concentration of active ions or inclusion of more particles in the passive matrix host in the case of the scalable display medium discussed in Chapter 4. Longer voxel activation time can result increase in voxel intensity. However, this may reduce the number of voxels that can be activated per unit time. Increase in pump intensities by reducing the beam size can be employed to increase voxel brightness, but this may cause saturation in level 2 and decrease in the volume occupied by voxel. Therefore, there can be an optimum voxel size that can result in brightest voxel emission for any given system.

2.2 Human 3D perception

We live in three-dimensional world and receive innumerable information through our eyes everyday. The brain then interprets the received information in order to perceive the surroundings based on different depth information. It is important to know that how humans recognize three-dimensional objects by interpreting different depth cues to design or understand a 3D display system. There are different ways to categorize these depth cues [15][16]. One grouping scheme is based on the visual projections received on the retinas (retinal image cues) and feedback from muscle groups in eyes (physiological cues) [1][15].

2.2.1 Retinal image cues

Retinal image cues can be subdivided into static monocular cues, which function with a single retinal projection, and parallax cues, which make use of information from more than one projection [1]

2.2.1.1 Static monocular cues

- Occlusion (or interposition): Objects occluding each other suggest their relative depth ordering. The brain interprets a partially occluded object as lying farther away than the interposing one.
- Linear perspective: Object at greater distances from the observer subtend a smaller angle in the visual field than do nearby objects, and hence appear smaller [17].
- Aerial perspective: Because of the light scattering caused by the dust, fog or rain in the atmosphere, distant objects look hazy, colors loose saturation and hue tends to shift towards the blue.

- Shading: The shading pattern provides cues to depth relations.
- Height and the visual field: During normal viewing objects that are higher in our visual field are assumed to be farther away, as the vertical positioning of objects in the visual field generally increases toward a horizon line (at eye level) as their distances approach that of the horizon. Similarly, objects above the eye level appear to be farther away as they descend toward the horizon [1][18].

One can find most of the monocular cues described in Figure 2-3.

Figure 2-3: A photograph showing most of the monocular cues

2.2.1.2 Parallax cues.

- Binocular parallax (or stereopsis): Human have two eyes in front of the head with an average separation of 6.5 cm. The typical field of view of each eye is 208º, with 130º overlap. Each eye thus provides slightly different views of almost the same scene (binocular disparity). The brain then interprets these slightly different images into a 3D pattern which gives the sense of depth [19][20].
- Motion parallax (or temporal parallax): When an observer is in motion, a closer object will move faster than the object in greater distance in the observer's field of view. This relative motion of near and far objects gives a cue to distance.

2.2.2 Physiological cues

- Accommodation: The ciliary muscles adjust the curvature of the lens, and hence the refraction of the eye, to bring the images of objects at a particular distance into clear focus. This response is known as accommodation [21]. The brain interprets the magnitude of the tension applied to the muscles to provide depth cues for the field of view.
- Convergence: When an observer looks at an object nearby, the angle between two eyes' direction of gaze is larger than when looking at a distant object. This angle is called the angle of convergence. The brain makes use of the muscular forces exerted on the two eyes so that they swivel inward by an amount necessary in order that they both center their gaze on an object of interest [19][1].

2.3 Different types of 3D displays

Two-dimensional displays may depict three-dimensional images by utilizing only static monocular cues. However, because of its lack of parallax cues and physiological cues, it is not enough to make the observers 'feel' the images as real three-dimensional images. Many different techniques were developed to provide more depth cues in addition to the monocular cues. For example, stereoscopic and autostereoscopic displays can provide binocular parallax by offering two different images to the eyes while electro-holography and volumetric displays can provide most of the depth cues. The different types of displays employing different techniques to provide more depth cues are discussed next in this section.

2.3.1 Stereoscopic display

Stereoscopic display systems provide binocular parallax by presenting slight different images to each eye. Stereoscopic display systems require viewers to wear special glasses to direct the proper image to the designated eye. Many different systems have been proposed and different techniques have been commercialized. They often utilize color filters, polarizing glasses or liquid crystal shutters in synchronization with a projector (In Figure 2-4, a system employing color filters is shown). Stereoscopic display systems are suitable for large number of viewers such as in a cinema since the system is rather simple but still gives a strong 3D impression by just employing binocular parallax. [1][22][23][24][25]

However, they require users to wear devices and they have innate accommodation-convergence mismatch that makes many viewers uncomfortable. Additionally, the system does not provide different views for different viewing angles (no motion parallax is provided) [1][23] .

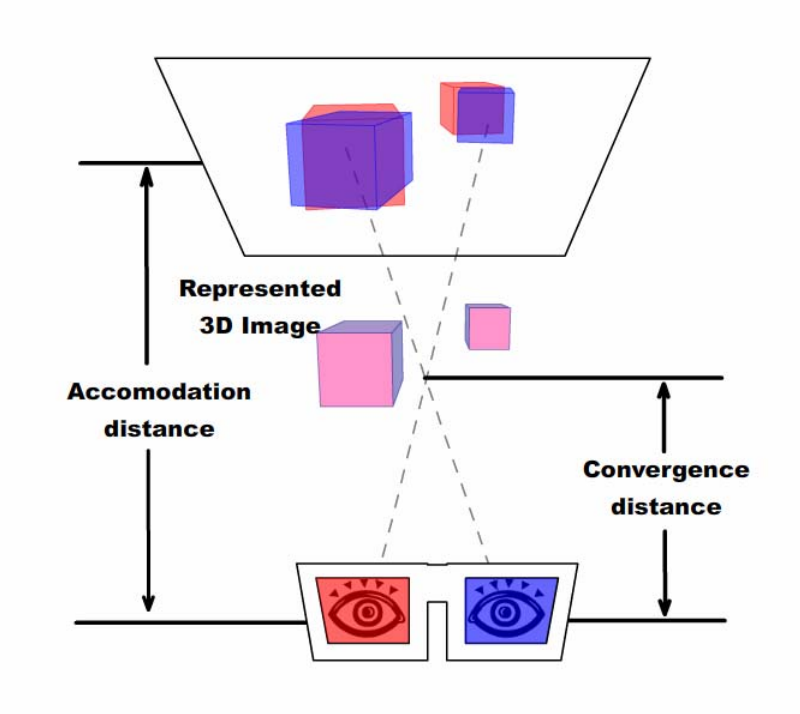

Figure 2-4: Typical stereoscopic display principle. Two slightly different images which are taken by special cameras are projected on the screen and using proper filter glasses (color filters, polarizers, liquid crystal shutters in synchronization with projector, etc. depending on the system) different images are delivered to each eye. The fact that the focus (accommodation point) is at the screen in contrast to the convergence point causes discomfort to some viewers.

2.3.2 Autostereoscopic display

Wearing additional devices is not very comfortable even for those who wears eye glasses already because most of the times that kind of devices restrict some of wearer's field of view. In some cases, it can limit the number of viewers depending on the system such as liquid crystal shutter glasses which need to be connected and be synchronized with the projection system. An

autostereoscopic display is a system that does not require additional devices other than the display itself. Some examples are presented next.

2.3.2.1 Parallax barrier and lenticular screen technique

The parallax stereogram was first introduced by F. E. Ives in 1903 [25]. A slit is used to direct the light from the special screen which containing alternating right and left views of an images to right and left eyes respectively as shown in Figure 2-5.

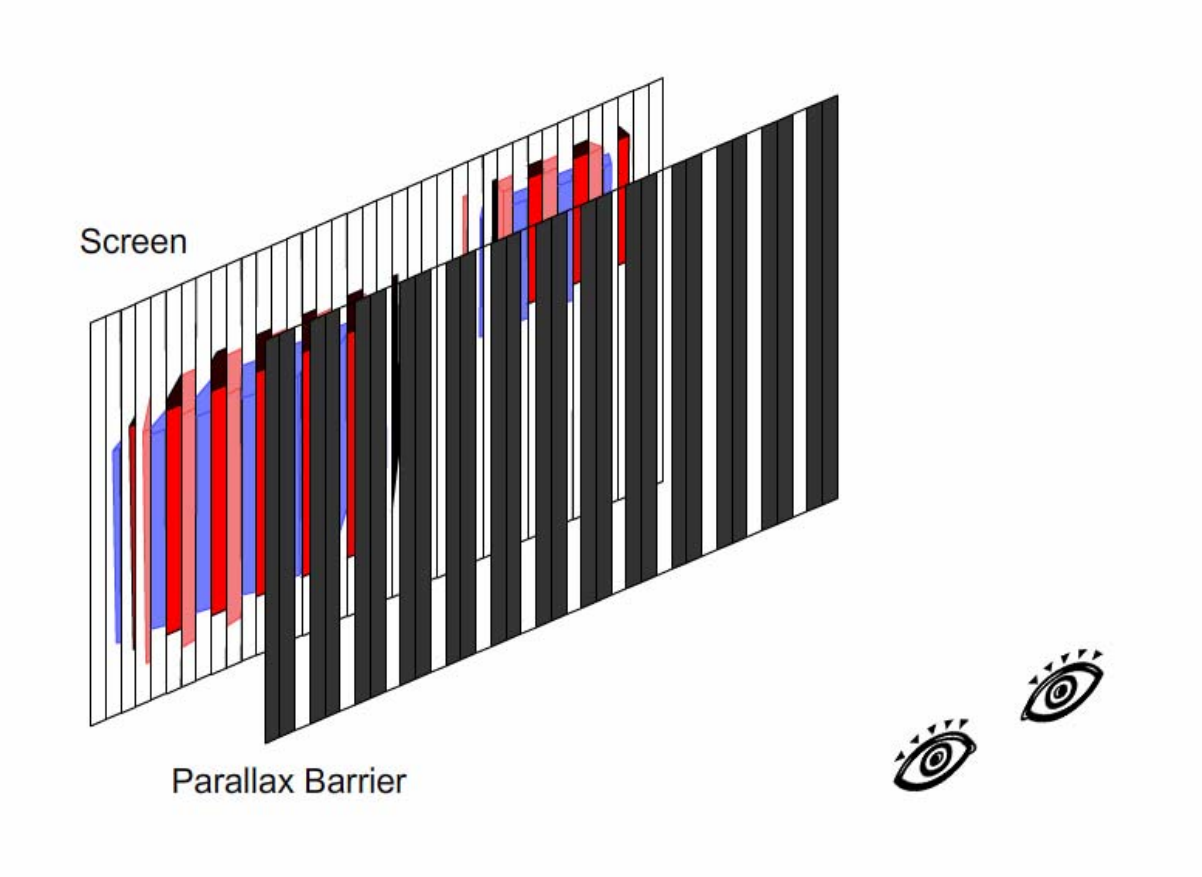

Figure 2-5: Simple diagram of parallax barrier display system. The difference between this and the lenticular screen technique is the use of the parallax barrier. The system shown can only gives horizontal parallax.

A new method is required to record that kind of special picture. Lippmann invented the integral photography technique which provides a way to record many different views of images on a single photographic plate using a lenslet array [26]. The original technique utilized a large array of small convex lenses to record an image. Reconstruction of recorded image was achieved by viewing through the same lens sheet but the resulting image was reversed in depth (pseudoscopic). The reversal could be solved by second integral imaging of the original image but this process degraded the image quality [25]. Simpler techniques were tried by using an array of horizontal cylindrical lenses called lenticular screen instead of tiny convex lens array [1][27]. However, this caused the loss of vertical parallax. The lenticular screen can be replaced by a horizontal slit (parallax barrier) or diffraction grating [28].

Technical advancement in engineering allows one to replace the lenticular screen and photographic plate with imagery obtained by multiple video cameras and displayed on a flat panel display such as liquid crystal display (LCD). In this way, instead of static images acquired in a photographic plate, active real-time images captured by multiple video cameras can be processed and displayed in LCD screen in certain ways as shown in Figure 2-6 and 2-7. A simple diagram shown in Figure 2-6 shows the basic idea of the parallax barrier display technique. First, the image is recorded by two or more video cameras. It is then processed in an image integration system to combine those images into a stream of data to alternately display the right and then the left images. These images are displayed in a flat panel display and the parallax screen placed in front of the display directs the appropriate images to the viewers' eyes [2]. In a single-view display shown in Figure 2-6 all the observers will see the same view. The screen will have only alternating information for right and left eye images so that the image resolution will be half of the screen resolution.

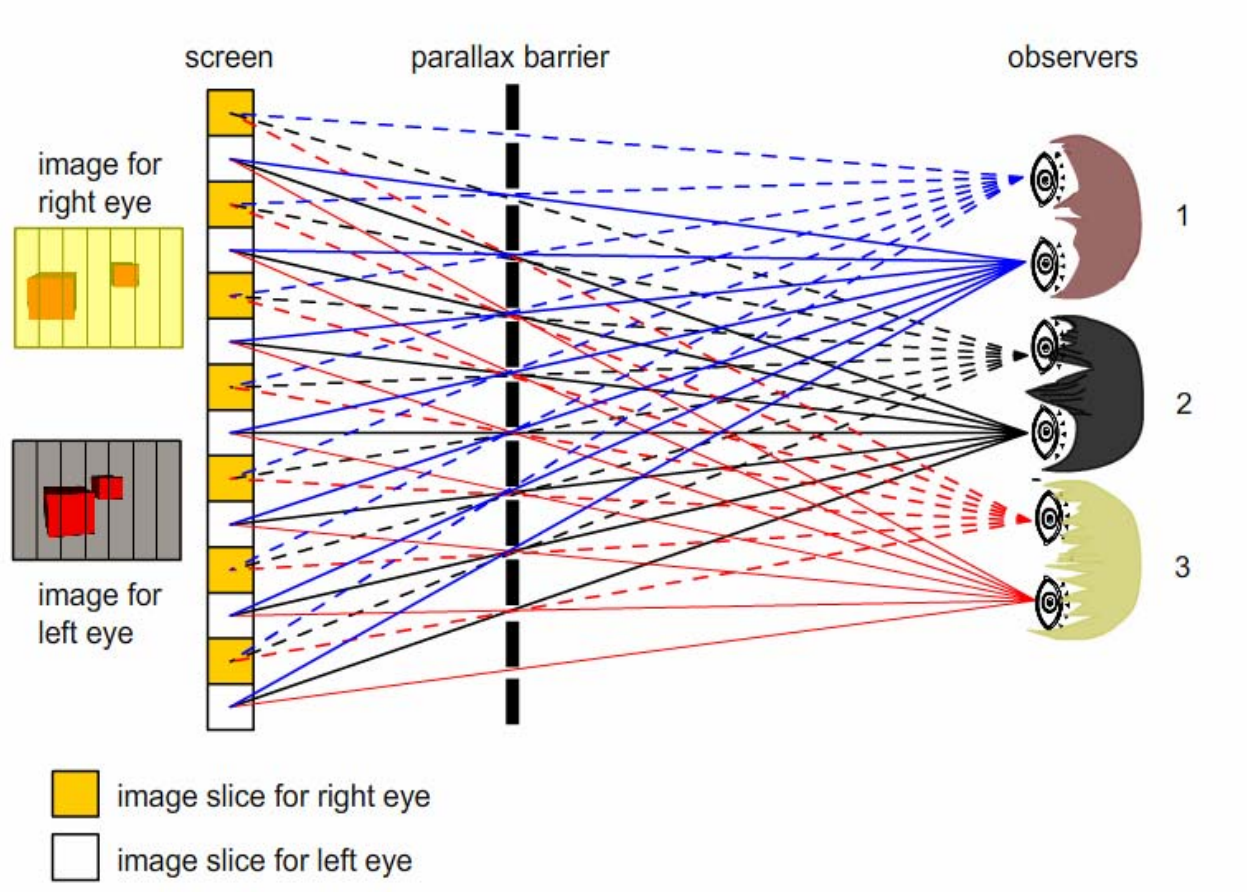

Figure 2-6: Simple diagram of parallax barrier display system (single view). All three observers see the same image. Observers must be seated in a designated position to see a proper image.

In a multi-view display such as sketched in Figure 2-7 different observers will see different perspectives of an image. For example as shown in Figure 2-7, observer 1 will see image 6 with right eye and image 5 with left eye which are then fused in the brain generating the experience of viewing a 3D object. Observer 2 sees image 4 with right eye and 3 with left eye and observer 3 sees image 2 (right eye) and 1 (left eye). All three observers will see the object with different perspective. This means that a single viewer who moves around the display will see different aspects of the object (This is a "look around" capability of the display system).

However, observers need to be in the proper position to see a correct image. Also, to have more views the resolution will be reduced by the number of views (image resolution = resolution of display / # of views). Providing more views also requires more computing power.

In another multi-view display technique that can only reduces the display resolution by a factor of two (right and left images). head-tracking is utilized with to located the viewer's eyes and send each the proper images. [29][30].

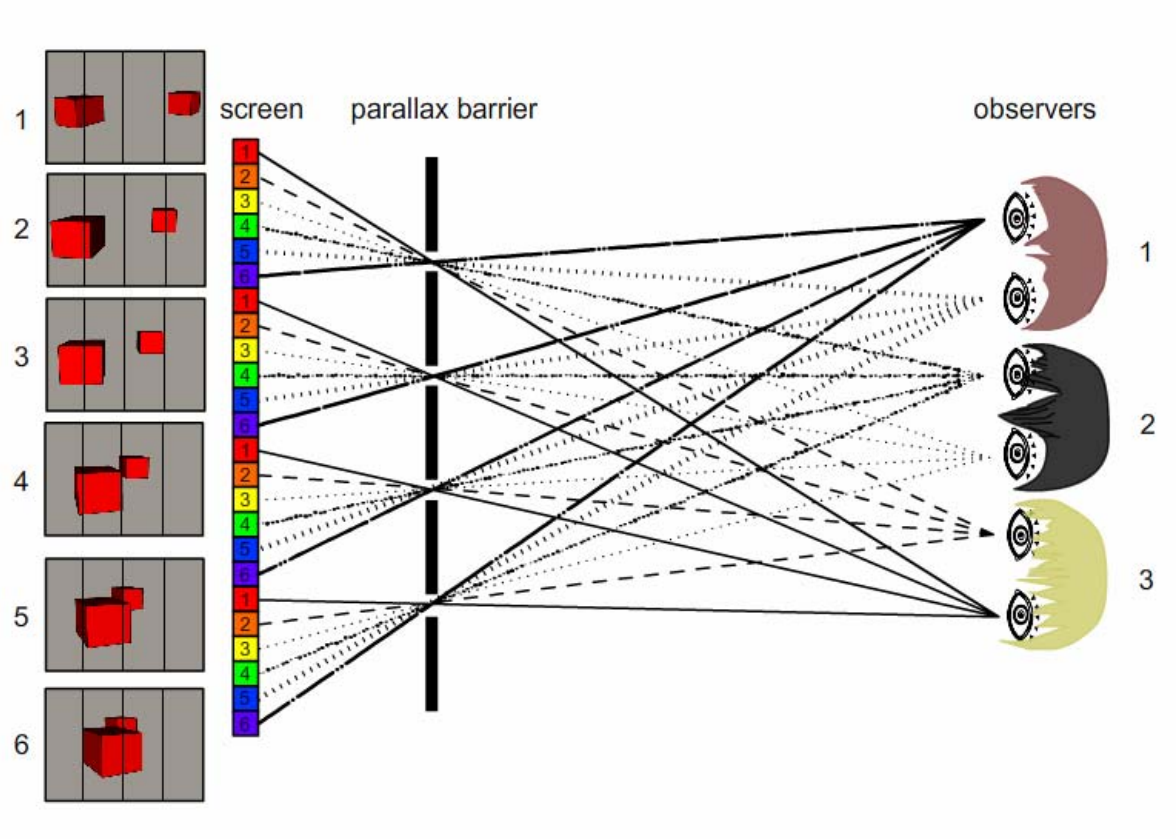

Figure 2-7: Simple diagram of multi-view parallax display system. Three observers see different images. Observer 1 sees image 6 with right eye and image 5 with left eye. Observer 2 sees image 4 (right eye) and 3 (left eye) and observer 3 sees image 2 (right eye) and 1 (left eye). Observers must be seated in a designated position to see a proper image.

2.3.2.2 Computer-generated holography

In 1947, holography was invented by Dennis Gabor. Holography is a wavefront reconstruction technique that produces three-dimensional images by using interference and diffraction [31]. Brown and Lohmann introduced computer-generated holograms (CGH) in early 1960's [32]. Computer-generated holography is a technology that doesn't require a delicate interferometric recording process in photographic emulsions. Instead, a computer calculates a holographic fringe pattern and drives light modulators and/or beam scanners to modulate and diffract a laser beam to generate real-time holographic images. Since CGH generally uses lasers as a light source their color gamut is very wide. It also provides most of the human depth cues. A research group in MIT demonstrated the concept of CGH but the set-up was too bulky and displayed image size was too small (see Figure 2-8) [33].

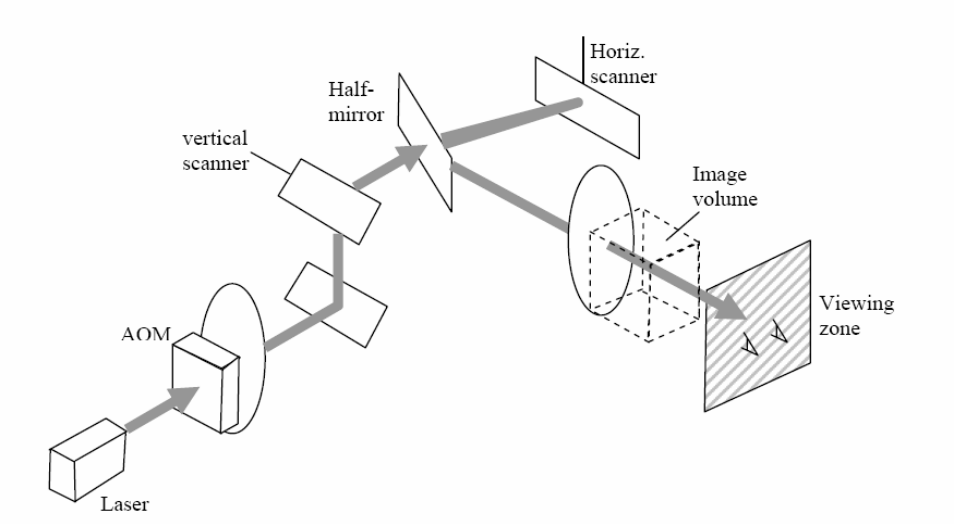

Figure 2-8: Holographic display set-up (Holovideo) developed by at MIT [29][34]

The group at MIT is working on improving the system [35] and a company called QienetiQ succeeded in increasing the size of image by utilizing an image tiling technique (see

Figure 2-9). However, CGH system is still expensive and to become a commercial display system and will require very large computing power.

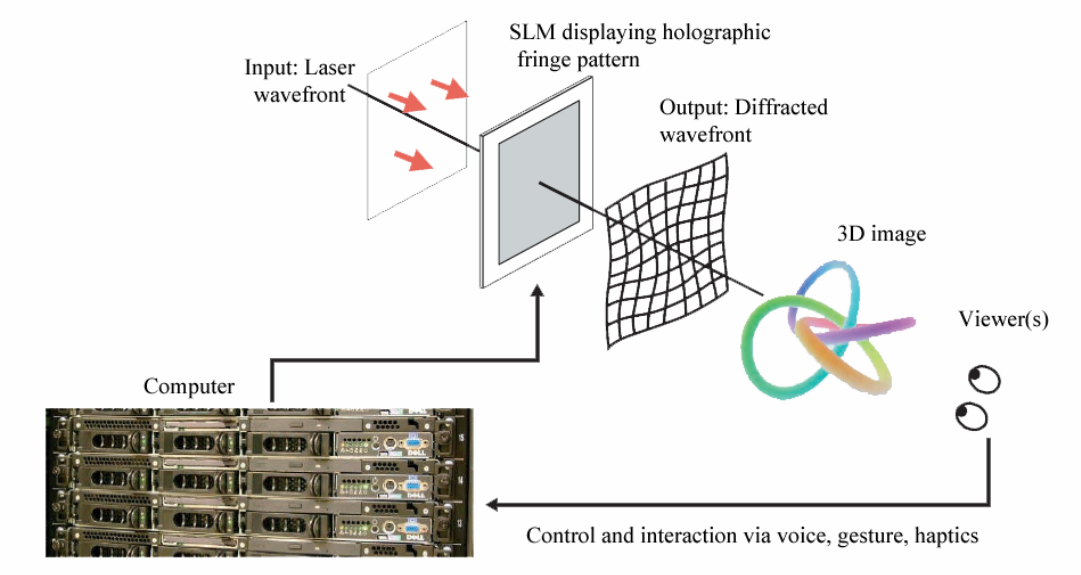

Figure 2-9: Computer-generated holography system developed by QinetiQ [36][37]

2.3.2.3 Volumetric

Volumetric 3D display, the main important subject of this dissertation, falls into the autostereoscopic display category since it doesn't requires additional equipment to see three-dimensional images. . Therefore, we will discuss it in detail in the following separate section.

2.4 Volumetric 3D display

A volumetric display generates volume filling images in a real three-dimensional space. Since the images are drawn in a three-dimensional volume most of the depth cues such as binocular, motion parallax and accommodation are naturally satisfied without any additional apparatus that the viewer must wear.

Volumetric 3D displays can be classified roughly into two categories: swept-volume and static-volume. A swept-volume 3D display is one in which the image space (where the image is formed) moves (translational or rotational) to create volume-filling 3D image. If the image space does not move the system is classified as a static-volume 3D display [1].

2.4.1 Swept volume 3D display

In two-dimensional display the fundamental element of an image is a pixel (picture element). A voxel (volume pixel) is the basic building block of 3D image in volumetric 3D display. A voxel should take the form of a sharply defined source of visible radiation and the voxel attributes should be invariant with respect to viewing directions [1]. Swept volume 3D display systems can be divided according to the method by which the image space is created and by the voxel generation subsystems (Figure 2-10).

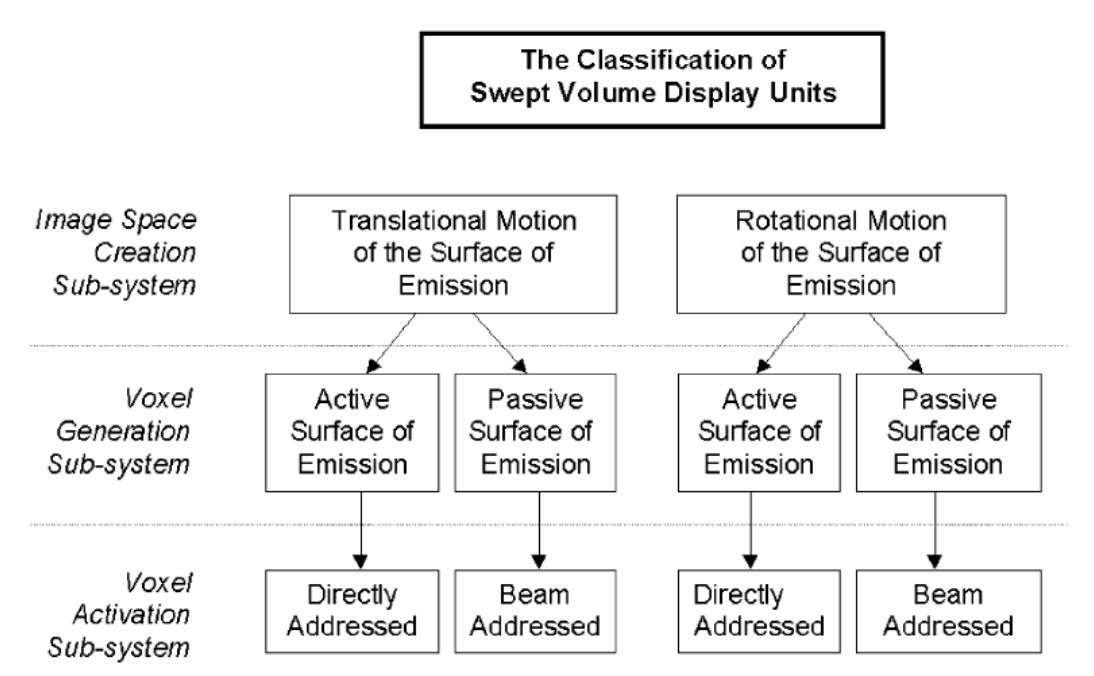

Figure 2-10: Classification of the types of swept volume display [9].

2.4.1.1 Swept volume display utilizing translational motion of the screen

This type of swept volume display utilizes a screen that moves up and down or forward and backward [39][40][41]. For example, an oscillating CRT screen with images synchronized to the screen's position can generate volumetric images. However, the CRT's heavy mass made it impossible to obtain desirable fast acceleration and deceleration at its turning point from forward to backward movement and vice versa [39]. Another type of display using a reciprocating screen has been proposed by C. Tsao et el. (Figure 2-11). Instead of moving a heavy CRT screen, this concept utilizes a moving screen and projection system. While a screen moves back and forth, an LED projector and a slide projector with high speed LCD shutter projects images onto the screen. Displays in this category suffer problems related to their

screens' acceleration and deceleration, because of their inertial forces, which generate vibration and noise and also limit the oscillation frequency that causes flicker of images.

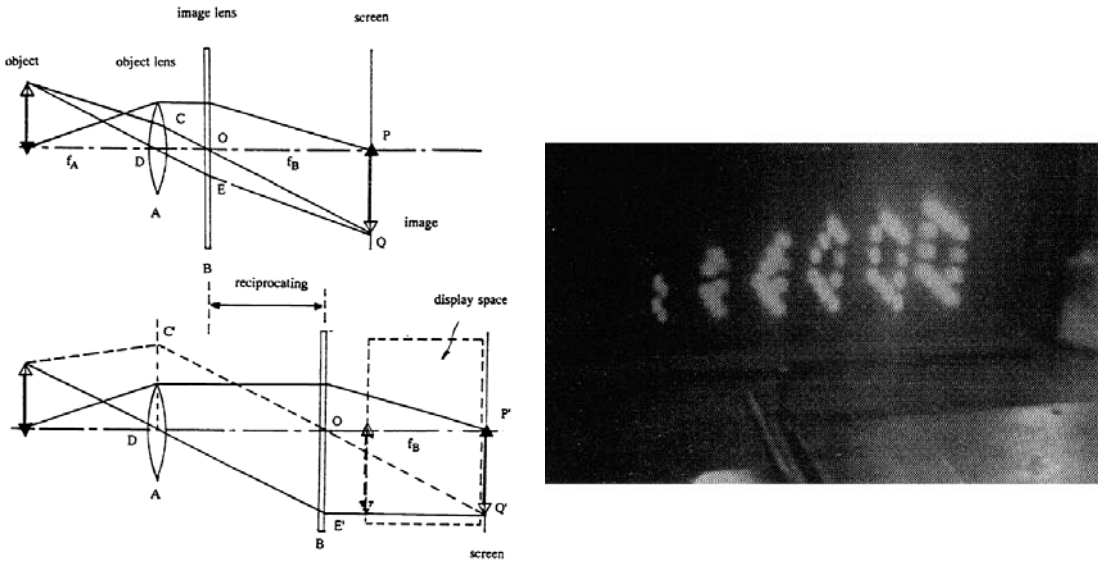

Figure 2-11: Basic concept of the moving screen projection by reciprocating approach (left) and generated image [40]

2.4.1.2 Swept volume display utilizing rotational motion of the screen

Swept volume display systems in this category exploit rotational motion of its screen regardless of the screen shape. Screens with various shapes were proposed in addition to the rotating flat screen [42] such as rotating spiral or Archimedes spiral [43], rotating helix [38], and vibrating disk [39]. Such displays can be subdivided into two categories based on how voxels are generated. For example, a voxel can be generated by an external beam addressing or projection onto the screen. That is, the screen is not itself emissive but it diffusely reflects the light projected onto it. Images, acquired from different perspectives using many different

cameras, are projected onto the screen. When projected in the proper time sequence to match the motion of the screen viewers are able to see different views of an object when they move around the display (Figure 2-12).

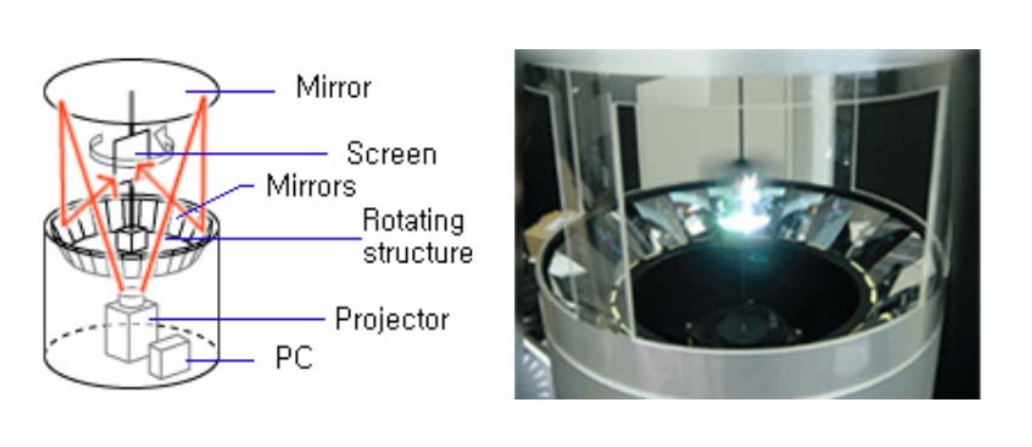

Figure 2-12: Swept volume display employing a rotating screen. The voxels are generated by projection of light onto the rotating surface (Hitachi Transpost) [43][44].

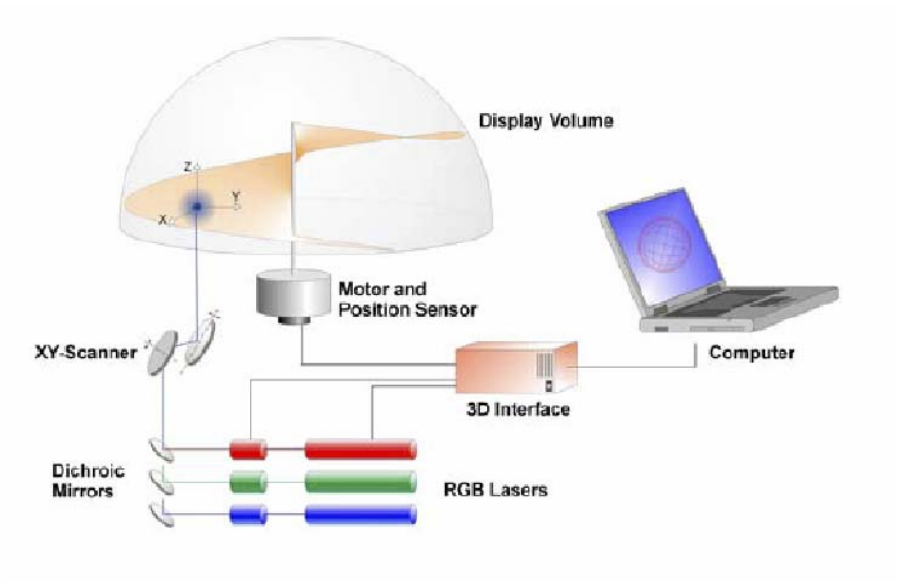

Figure 2-13: Swept volume display utilizing a rotating helical screen (FELIX 3D display [38]).

In the case of rotating helix screen, each individual voxel is addressed by laser beams. The beam scanners determine where the voxel will be generated in x-y plane while the timing of when to project the laser light onto the rotating helical screen determines the z-coordinate of the voxel (Figure 2-13).

If the screen is made up of light sources such as LEDs it can actively generate a voxel by direct addressing (Figure 2-14). Turning on and off desired LEDs at appropriate times will generate volumetric 3D images in real time.

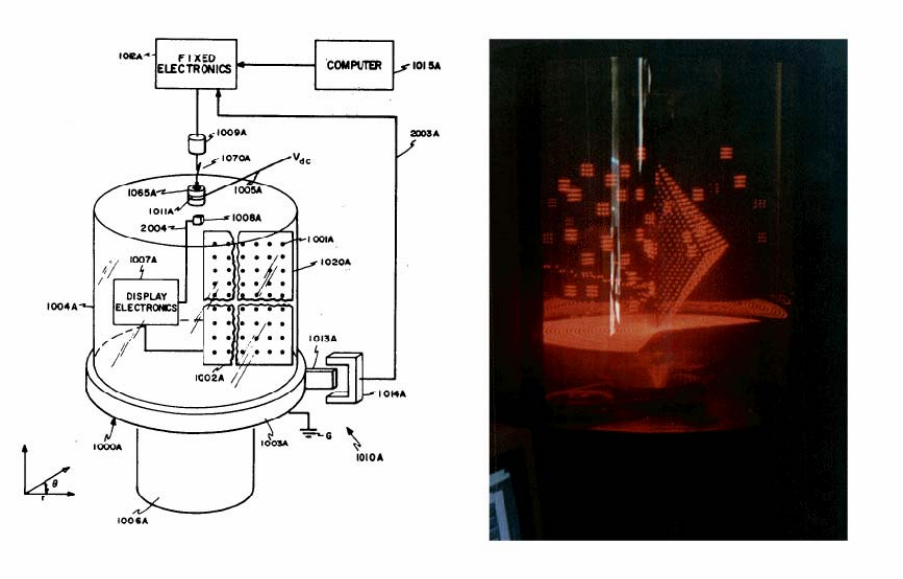

Figure 2-14: Swept volume display employing a rotating flat screen with LEDs [46][47][48][49].

2.4.2 Static volume display

A major advantage of static volume display is that there are no mechanical moving parts in the system. The image space is made up of a static-volume of material or array of materials within which voxels may be generated. Static volume displays can be classified in many

different ways [9][50], but can be simply grouped by the method of voxel addressing and visualization: external optical-electric and all external optical addressing (Figure 2-15).

The static volume displays that use an optical-electrical voxel addressing method usually exploit a stack of liquid crystal panels as an image space which stay transparent in the off state but when on, the pixels in a panel change into scattering state to scatter light to every direction (Figure 2-16, 2-17). Unlike the conventional 2D LCD screen, they are stacked and spaced without polarizers hence each pixels will occupy a volume in three-dimensional space. Each liquid crystal panel is turned on and off sequentially in synchronization with light sources and each panel is controlled to generate an image slice of an object so that in total they can form a volumetric image of an object.

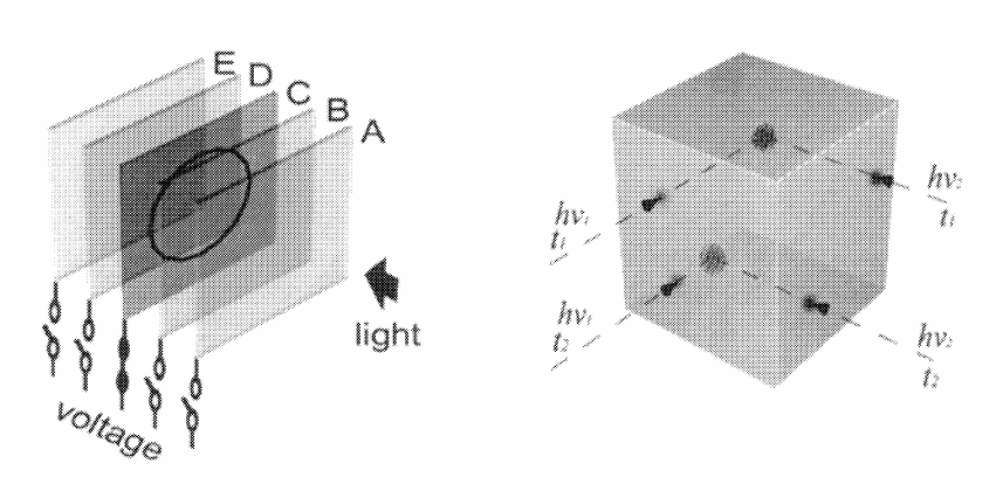

Figure 2-15: Static volume display classified by the methods of voxel addressing. (left: optical-electrical, right: all optical) [51].

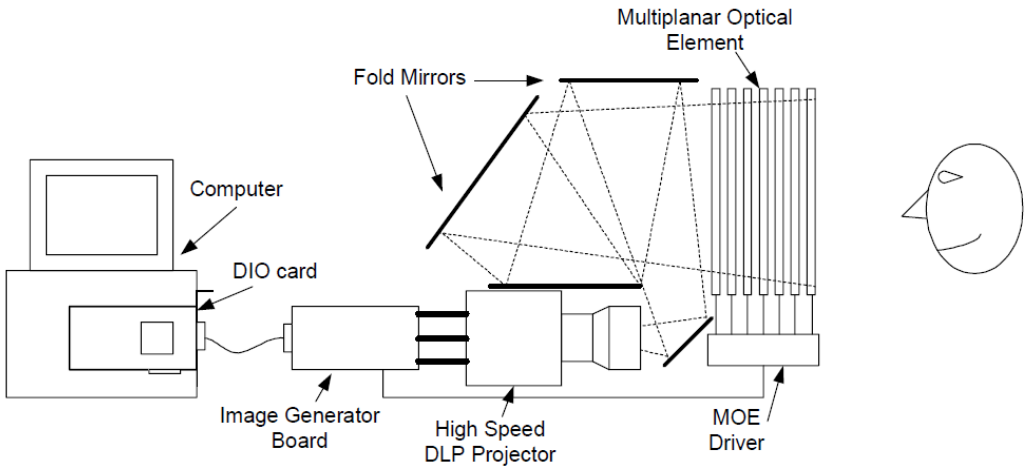

Figure 2-16: Schematic diagram of the DepthCube 3D Display System. [53]

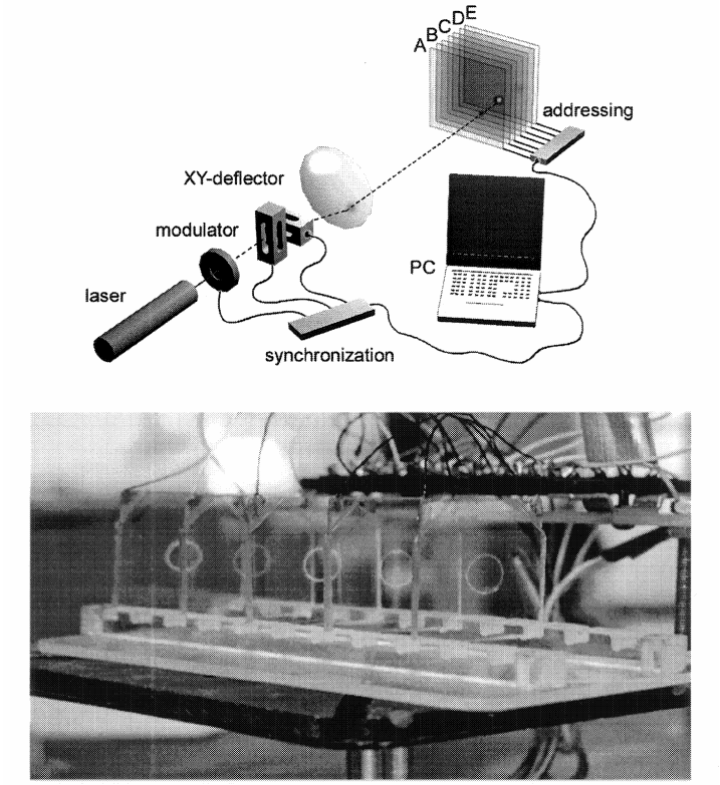

Figure 2-17: Schematic diagram of static volume display utilizing a stack of ferroelectric liquid crystal panels by the joint research team from the Lebedev Physical Institute and Moscow State Engineering Physics Institute (Russia) [51].

Optical voxel addressing can be performed by one or two laser beams. When using a single laser beam to address a voxel the laser beam has to be focused [54][55][56]. The usual problem of one beam pumping in static volume display is the shape of voxel generated by up-conversion fluorescence. The ideal voxel shape is spherical since it will have the same shape when observed from any direction. However, in one-beam pumping the shape of voxel is usually elongated along the laser beam direction of incidence (see Figure 2-18). Another problem in one beam pumping is the necessity of rapid focus change of the pump beam. Since the voxel is generated where the beam is focused, to generate an image made up of hundreds of voxels, quick beam focus change is required additional to beam scanning. However, compared to the two-beam pumping, its system can be simpler and doesn't need to deal with the precise overlap of two pump beams.

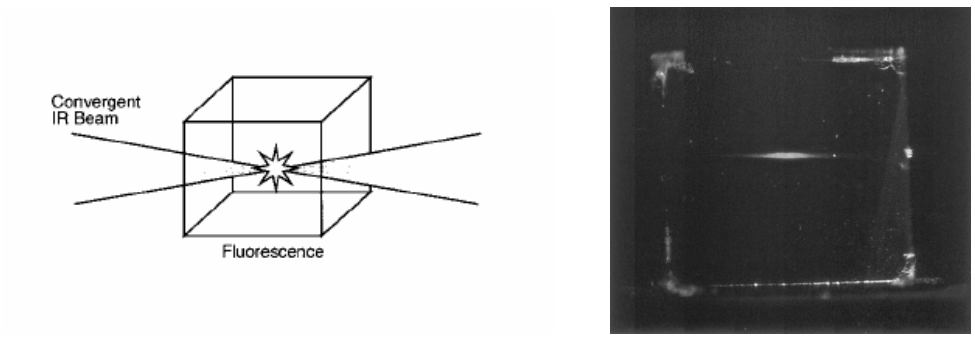

Figure 2-18: One beam pumping scheme of a static volume 3D display (left) and its usual voxel shape (right) [56].

In a static volume display utilizing optical voxel addressing, the voxel generation process is based on up-conversion of infrared light into visible fluorescence. Therefore, the up-

conversion efficiency is one of the most important factors to attain displays with practical brightness. Different materials can be used as a display medium (see Chapter 3.1).

There is a different type of static volume display that doesn't require display material and employs a different physical process not an up-conversion process (Figure 2-19).

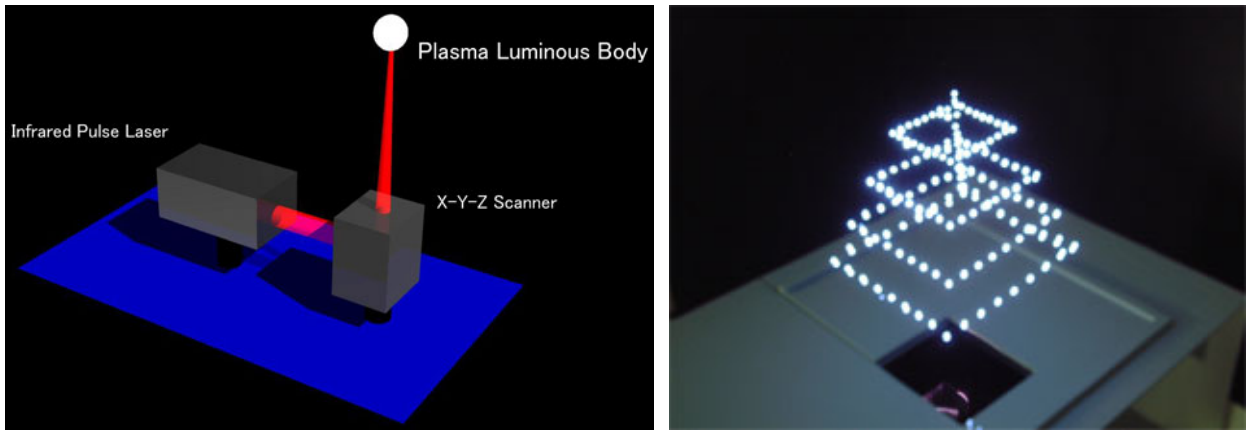

Figure 2-19: The static volume 3D display system developed by the National Institute of Advanced Industrial Science and Technology (AIST) in Tokyo, Japan, in collaboration with Burton Inc and Keio University. [57].

National Institute of Advanced Industrial Science in Japan and Keio University in collaboration with Burton Inc. have demonstrated a 3D display that generates images in the air (see Figure 2-19) [57]. The display utilizes an ionization effect which occurs when a beam of laser light is focused to a point in air. The laser beam itself is invisible to the human eye but, if the intensity of the laser pulse exceeds a threshold, the air breaks down into glowing plasma that emits visible light. By controlling the position of the focal point in the direction of the x, y, and z-axes, 3D images can be constructed by voxels in the air. Currently, these can be projected

between two and three meters from the apparatus, in a space of about a cubic meter. Each flashpoint generates a noisy popping sound, resulting in a constant crackling when the display is in operation [57][58].

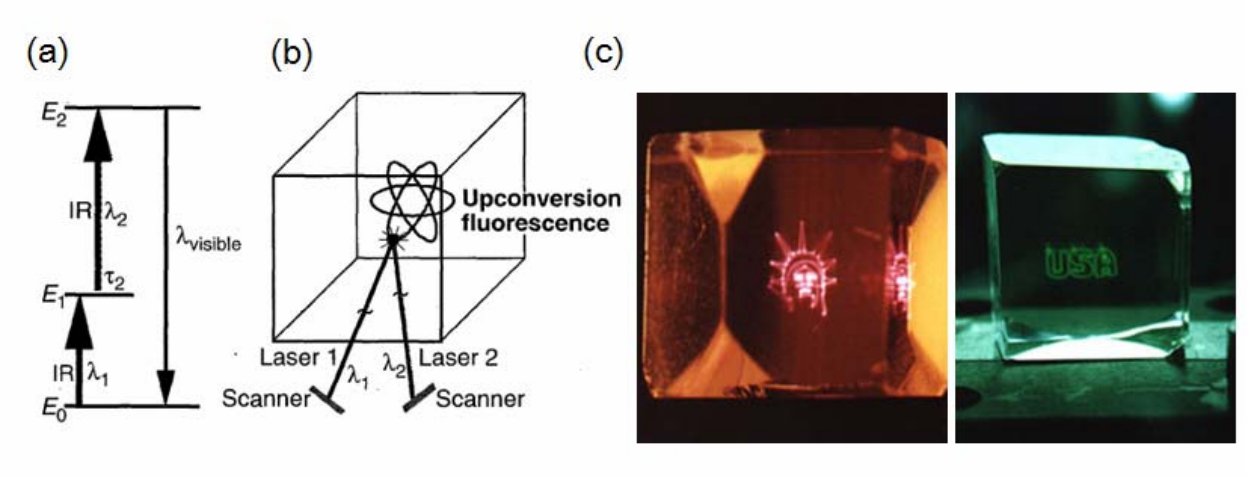

Figure 2-20: (a) Energy level diagram of an active ion (b) Two intersecting laser beams are used to address voxels and draw objects in a transparent material doped with such an ion. (c) Volumetric images created in rare-earth doped ZBLAN glass [7][61]

Unlike the single-beam addressing, two-beam addressing employs stepwise excitation of up conversion by two different wavelengths. This process of stepwise excitation of fluorescence has been known since the 1920s [59]. D. Lewis et al. described a display based on this concept in 1971 [60]. They generated two voxels in erbium-doped CaF_2 crystal with two filtered xenon lamps as a pump sources. The voxels were activated by sequential absorption of light from two invisible near infrared light beams as shown in Figure 2-20. At the intersection of the two pump beams in this display medium electrons were excited from the ground state (E_0) to some intermediate energy level (E_1) and then to an upper energy level (E_2) by sequential two-photon

absorption. That is, a first absorption of near infrared light populated the intermediate level. This was followed by a second absorption that excited the medium in the intermediate state into the upper level and it is due to fluoresent transitions of the medium in this state that visible light is emitted. This mechanism is called two-step two-frequency up-conversion (TSTF-UC). Downing and et al. demonstrated its application to 3D displays within rare-earth doped heavy metal fluoride glasses using a crossed-beam display (CBD) technique in 1996 [7] (Figure 2-20).

2.5 Summary: Different types of 3D displays

As we have discussed in Chapter 2-3 and 2-4, there are many different ways to display 3D information. Each has its own strengths and weaknesses. Below is list of advantages and disadvantages of the different types of 3D displays.

Stereoscopic

Stereoscopic displays are simple and good for large numbers of viewers. But they require viewers to wear devices (e.g., goggles) and accommodation-convergence mismatch makes many viewers uncomfortable. Also, the system does not provide different perspectives for the viewers at different viewing angles.

Autostereoscopic

Autostereoscopic displays do not require the viewers to wear any additional devices but still retain the binocular parallax. In the case of multi-view system, different observers sitting in different angles from the display can see different perspective. This means that a single viewer

who moves around the display will see different aspects of the object (e.g., this means the display has look around capability). However, observers need to be in proper position to see correct images. Also, to have more views, it is necessary to sacrifice image resolution in inverse proportion to the number of views (image resolution = resolution of display / # of views)

Computer-generated holography

Computer-generated holography provides most of the human depth cues. CGH generally uses lasers as light source enabling a very wide color gamut. However, CGH involves enormous computations which needed to be done in real time. Currently, the image size that CGH can generate is limited. Image tiling techniques can solve this problem but will increase the display costs significantly.

Swept volume display

Swept volume displays provide most of the depth cues a human needs to perceive a 3D image. However, there are some problems related to the mechanical motion of the screen. Since the screen needs to move with high speed, to prevent image jittering, such high speed moving parts in a system may experience short life, will make noise and can be unstable. Also the image will be dim because the rapid refresh rate allows only short illumination of any point on the rotating screen negating taking advantage of the integration of light in the retina.

Static volume display

A static volume display also provides most of the human depth cues and there are no moving parts. Since images are drawn in a volume of a certain display medium, the display

material is the most important factor in the vability of the system. The display medium must be easily visible and scalable to enable large displays. The first problem is about efficient display materials which convert infrared light(s) into visible fluorescence (or scatter the visible light) and still retain optical clarity. Second issue is about making a larger display medium. Currently, the dimensions of static volume 3D displays utilizing up-conversion process are on the order of a few cm.

CHAPTER THREE: MATERIALS FOR STATIC VOLUME 3D DISPLAY

3.1 Display medium

There are different types of materials that can be used as a display medium. For example, gaseous materials such as mercury vapor [62], iodine monochloride vapor [63], and rubidium vapor [64] were reported as possible display media for static volume 3D displays. Also, some organic dyes in liquid or polymeric solutions can serve as 3D display media [65]. Solid-state materials such as rare-earth doped fluoride crystals can also be used as the display medium.

A gaseous material has is easy to produce, fills the allotted display volume and its refractive index is close to air so there will be minimal distortion of generated images. However, most gases used in this kind of displays are toxic and need to be kept in a chamber at high pressure. In this dissertation organic dyes and rare-earth doped fluoride crystals are examined as 3D display media.

3.2 Organic dyes

Organic dye doped liquids could serve as a 3D display medium but it is not always easy to confine the liquid and the dyes and solvents may have hazardous properties. On the other hand, dye doped polymers may serve as 3D display media. As discussed by Rapaport and colleagues [65] some dyes in liquid and polymeric solutions that can be excited to emit visible light by simultaneous absorption of two infrared light sources of different wavelengths (non-degenerate two-photon absorption (TPA) as indicated in Figure 3-1) can be attractive candidates

for 3D display media. Since organic dyes can be tailored for desired properties there is a continuous and wide range of wavelengths accessible for both two-photon absorption (TPA) and visible emission. Additionally, dyes can be doped in polymeric hosts to produce clear, non-scattering solid volumes that can easily be scaled up. However, dyes have several disadvantages. They almost always present some residual degenerate TPA which causes an undesirable line of visible emission along one or both of the laser beam paths (see Figure 3-2, 3-3). There can be significant self-absorption of the emitted visible signal in dye solutions due to too small a Stokes shift. Since TPA in dyes is not a stepwise absorption but involves simultaneous absorption of two photons through a virtual intermediate state, it is not likely to be efficient enough for practical use. The exciting beams for such a process must overlap both spatially and temporally (i.e., intersect at the same point in space at the same time) and this requires long pulses (>several nsec) with high peak powers.

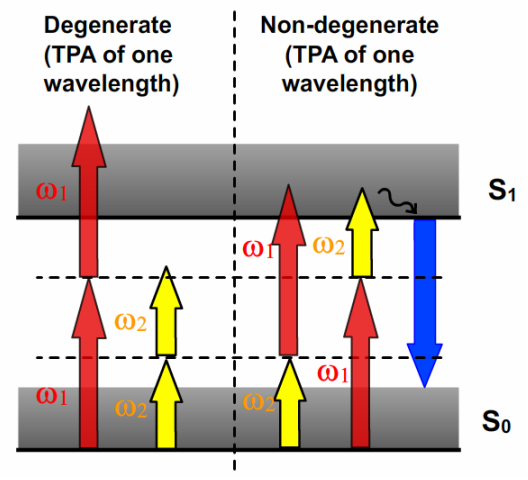

Figure 3-1: Energy diagram of an organic dye solution. Two-photon absorption of a single wavelength (left) and two different wavelengths (right) are shown.

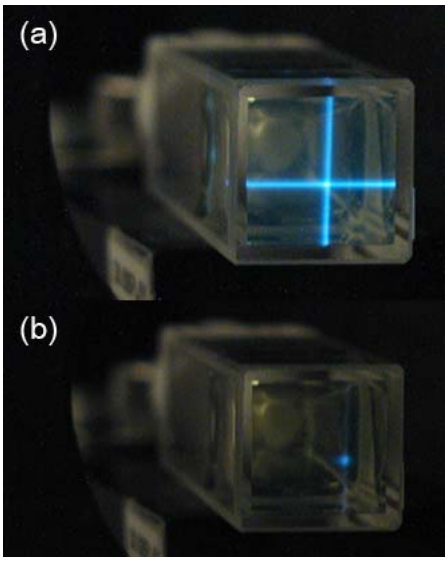

Figure 3-2: A voxel in the dye DPABz in a polymeric binder. (a) TPA excited by a single wavelength. (b) TPA excited by two different wavelengths.

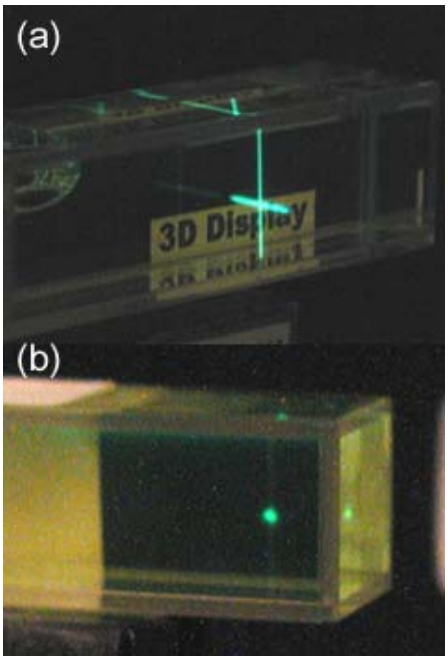

Figure 3-3: A voxel in the dye Coumarin 6 in THF. (a) TPA excited by a single wavelength. (b) TPA excited by two different wavelengths.

3.3 Rare-earth doped materials

There are several advantages to using RE doped materials as the 3D display medium. Since stepwise excitation implies the succession of two linear processes, it is efficient at lower peak power than non-degenerate simultaneous two-photon absorption in organic dyes. This relaxes the requirements on the pump sources to achieve bright voxels. Furthermore, the real intermediate energy level can be used to store energy and the temporal overlap of the addressing beams is not a necessity.

Using fluoride materials as a host adds more advantages. Fluoride materials containing trivalent ions, mainly Y^{3+} cations, are very advantageous because they can be substituted easily by rare earth ions of the same valence. Moreover, the fluoride materials compared with oxides have low phonon energies that make it possible to reduce the nonradiative de-excitation phenomena by multiphonon emissions, thus ensuring good fluorescence quantum yields for the principal emitting levels (see Table 3-1). They also have a reasonably high thermal conductivity compared to chlorides and bromides known as having very low phonon energies. Fluorides also have good thermo-mechanical properties and a high chemical stability [66].

Table 3-1: Optical Properties of KY_3F_{10}, and YLF [67][68][69][70].

	Phonon energy $\hbar\omega_m$ (cm^{-1})	Index of refraction n_D or $(n_e; n_o)_D$
KY_3F_{10}	~400	1.4876
YLF	460	1.476; 1.453

We conducted several experiments with rare-earth doped fluoride crystals provided by AC Materials: 1% Ho:YLF, 1% Er:YLF, 2%Pr:KY_3F_{10} and 2%Er:KY_3F_{10}. Crystallographic properties of potassium triyttrium decafluoride (KY_3F_{10}), lithium yttrium fluoride ($LiYF_4$ or YLF) are shown in Table 3-2. The crystal structure of KY_3F_{10} is cubic and it is isotropic crystal. This is another strong advantage of KY_3F_{10} crystal as a candidate for scalable volumetric display medium. This will be discussed in Chapter 4-1.

Table 3-2: Crystallographic properties of KY_3F_{10} and YLF [71].

Host	KY_3F_{10}	YLF
Structure	Cubic (fluorite)	Tetragonal (Scheelite)
Space group (Schoenflies)	Fm3m (O_h^5)	$14_{1/a}$ (C_{4h}^6)
Crystallographic positions for Y^{3+} ions ~coordination number!	$C_{4v}(8)$	$S_4(8)$
Cell parameters	a=11.536 Å	a=5.16 Å c=10.85 Å
Number of elements by cell	8	4
Anisotropy	Isotropic	Uniaxial
Melting point	~ 990 °C (congruent)	~810 °C (uncongruent)

Two optical parametric oscillators were used in a Master Oscillator-Power Oscillator configuration (MOPO) pumped by the same flashlamp pumped, Q-switched neodymium-doped yttrium aluminum garnet (Nd:YAG) laser as the sources for the two different pump wavelengths. The experimental set-up is shown in Figure 3-4. A delay was introduced in one of the laser paths

to make sure that the first excited state was populated before hitting the material with the second-step pump wavelength.

.

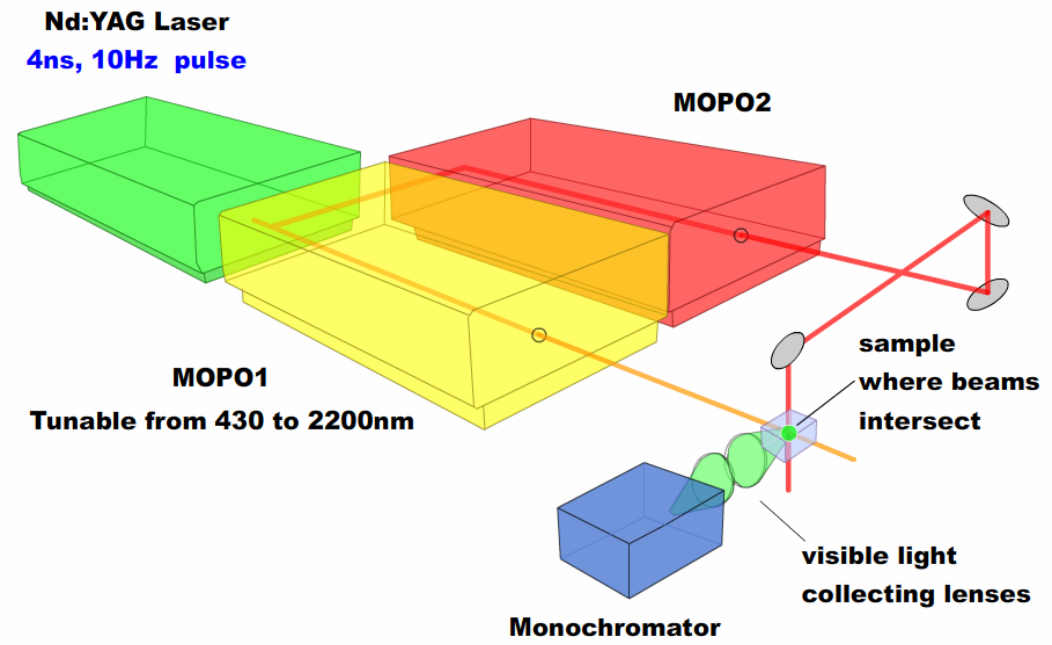

Figure 3-4: Setup for fluorescence and excitation spectral measurements using two-step two-frequency up-conversion.

The brightest green, 543 nm, TSTF up-conversion emission was obtained with Er:KY_3F_{10} when it was pumped with 1494.1 nm first and then with 848.4 nm (see Figure 3-5 and 3-6). These two frequencies were identified by monitoring the fluorescence strength at 543 nm using monochromator in Figure 3-4 when we fix the first pump at a certain wavelength which can excite ground state ions to one of the intermediate states shown in Figure 3-7, and then scan the wavelength of the second pump beam so that the ions in the intermediate state can be excited into the third level to emit green light.

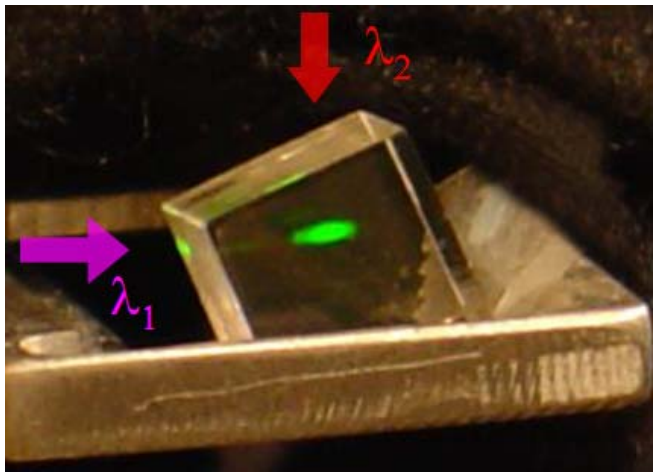

Figure 3-5: A voxel in a 2%Er:KY3F10 single crystal excited by two different pump beams (λ_1=1494.1 nm from left-hand side of the picture, λ_2 = 848.4 nm from the top).

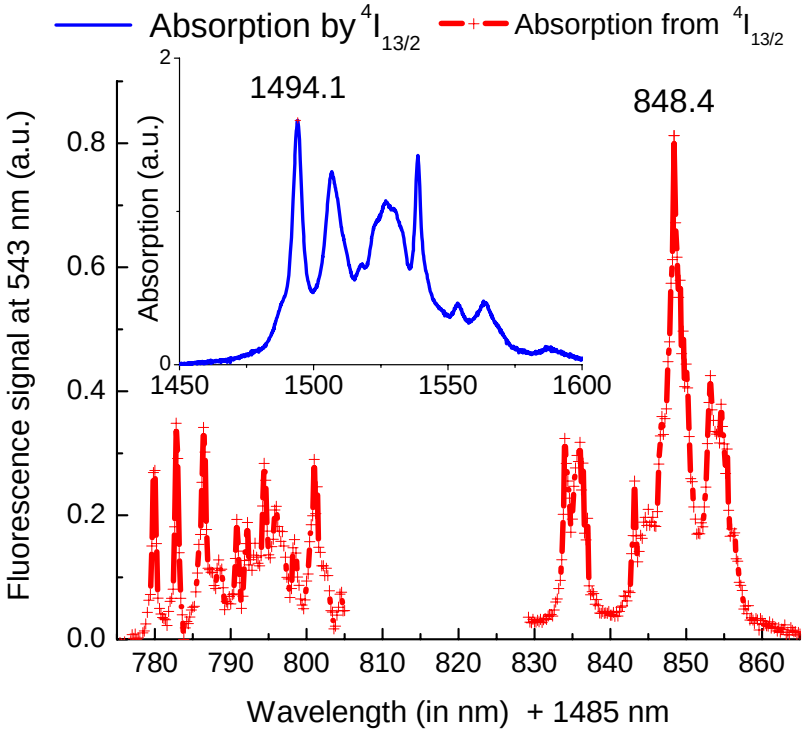

Figure 3-6: Absorption (inset) and excited state absorption in Er:KY_3F_{10} .

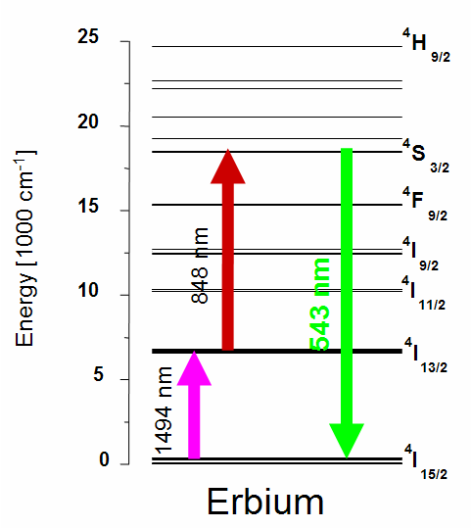

Figure 3-7: Energy level diagram of triply ionized erbium.

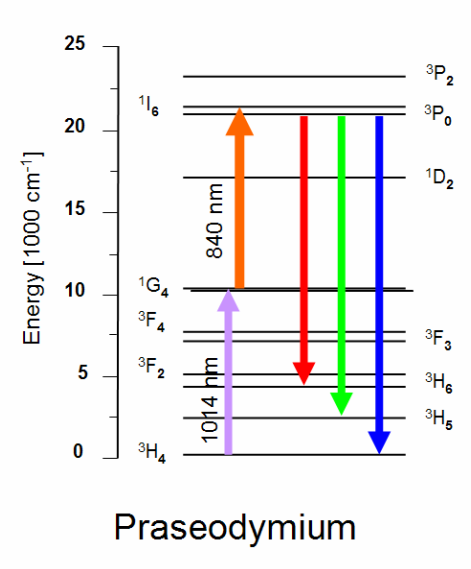

Figure 3-8: Energy level diagram of triply ionized praseodymium.

The same experiment was carried out for $Pr:KY_3F_{10}$ instead of $Er:KY_3F_{10}$ and two pump wavelengths were found that resulted in bright fluorescence. The first pump beam (1014 nm) excites praseodymium ions from the $^3H_4$ to the $^1G_4$ state and then second pump (840nm) excited

them from the $^1G_4$ to the $^1I_6$ state (See Figure 3-8). The ions then decay and give off red, green and blue emission (Figure 3-9) resulting in white voxels (see Figure 3-10).

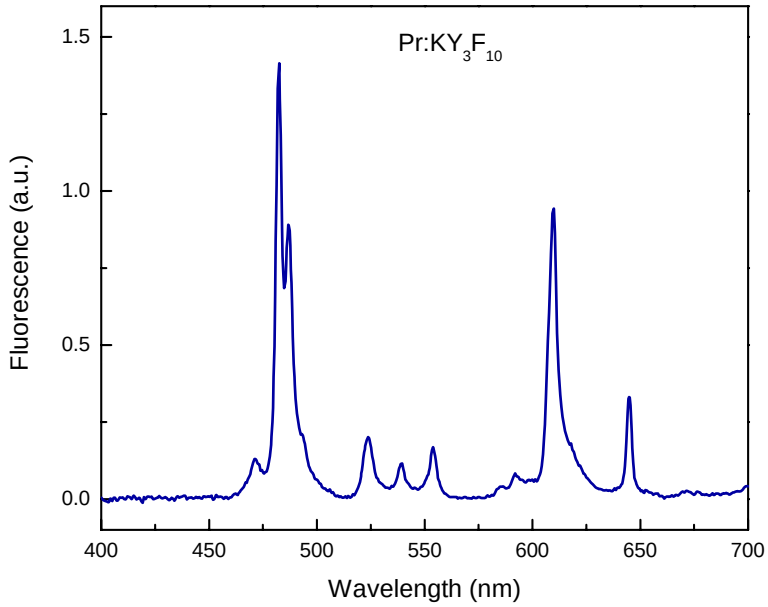

Figure 3-9: Emission spectrum of praseodymium doped KY_3F_{10} crystal when pumped with 1040 and 840 nm.

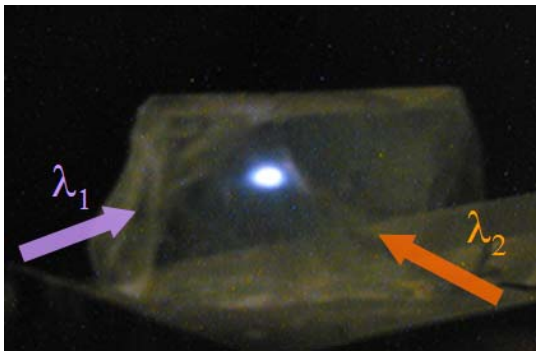

Figure 3-10: A voxel in a 2%Pr: KY_3F_{10} single crystal excited by two different pump beams (λ_1 = 1040 nm, λ_2 = 840 nm from the direction shown in the figure)

Efficient up-conversion alone makes Er:KY_3F_{10} and Pr:KY_3F_{10} strong 3D display candidates. However, Er:KY_3F_{10} and Pr:KY_3F_{10} have several more advantages over other materials as discussed below. Using these fluoride single crystals directly as the 3D display medium presents some difficulties. First, growing large single crystals is not easy. Second, even if it were possible to make single crystals big enough for a display medium it would be very expensive to do so. As a solution to the 3D display medium scalability issues, M. Bass and H. Jenssen proposed a 3D display based on a dispersion of emitting particles in a transparent host [72].

3.4 Summary: Organic dye & Rare-earth doped crystal

Organic dyes and rare-earth doped fluoride crystals have been reviewed in this chapter to find efficient display medium candidates for volumetric 3D display. Their pros and cons are summarized in Table 3-3 and Table 3-4 respectively.

An advantage of an organic dye based display medium is that a dye can be made to have desired properties such as convenient absorption or emission wavelengths. Dyes can be doped in polymeric hosts to produce clear, non-scattering solid volumes that can be scaled up. However, they almost always have residual degenerate TPA and due to small Stokes shifts there can be significant self-absorption of the emitted visible light. Further, dyes are not very efficient two photon absorber-emitters. Two-photon excitation requires long pulses (>several nsec) with high peak powers.

Table 3-3: Summary of advantages and disadvantages of organic dye as a volumetric display medium.

Physical attribute	Pros	Cons
Organic dyes can be specifically designed and engineered	Wide range of wavelengths for absorption	Almost always some residual degenerate TPA
	Wide range of wavelengths for emission	Self-absorption of emitted visible signal
	Can dope a polymer matrix (no scattering problem)	
Virtual intermediate state	No ghost pixel	No energy storage
		Simultaneous temporal and spatial overlap difficult: needs long pulses
		Inefficient non-linear absorption: needs high peak power

The major advantage of rare-earth doped fluoride crystal is its efficient, sequential linear absorption. This can provide bright voxels and thus bright images. However, this also increases the likelihood of ghost voxels. Ghost voxels can be made when the second voxel is generated without enough time after the first voxel is generated in the same spatial plane. Because the lifetime of the intermediate state of the active ion is normally on the order of a millisecond, even after the generation of the first voxel is completed the intermediate state can still be populated along the path of the first excitation pump beam (λ_1). When the second pump beam for the second voxel generation (λ_2) crosses the previous first pump beam path the ions in the intermediate state can be excited and then emit unintended visible light. This unwanted voxel is called a ghost voxel and is sketched in Figure 3-11.

Table 3-4: Summary of advantages and disadvantages of rare-earth doped single crystal as a volumetric display medium.

Physical attribute	Pros	Cons
Rare earth have discrete, well defined levels	Diode lasers available at many of the desired wavelengths	Few specific, narrow linewidth sources are needed
	Cubic crystalline hosts can be index matched to polymer matrix	Cannot dope a polymer matrix: needs crystalline host. Scattering issues
Real intermediate state	Efficient, sequential linear absorption	Possibility of ghost pixels
	Energy storage	One beam is always linearly absorbed through the material: needs to be taken into account by adjusting the second beam intensity while scanning
	No need to get temporal and SIMULTANEOUS spatial overlap	

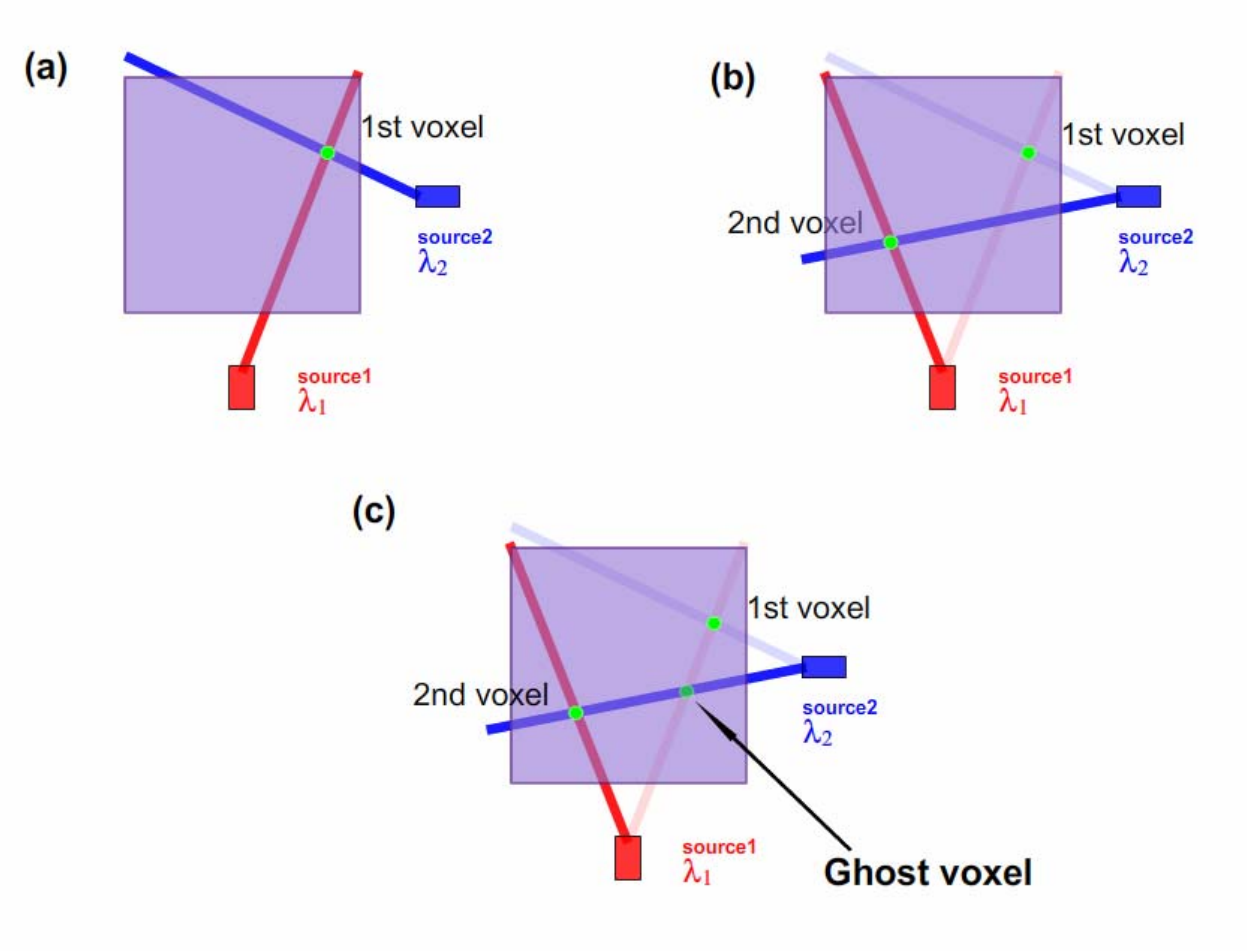

Figure 3-11: A ghost voxel generation process. (a) The first voxel is generated. (b) The second voxel is made in the same plane as the first voxel. (c) When the second pump beam (λ_2) for second voxel crosses the previous pump (λ_1) beam path for the first voxel generation, the not yet decayed excited state electrons can be excited to fluoresce and generate the ghost voxel.

CHAPTER FOUR: SCALABLE 3D DISPLAY MEDIA

4.1 Concept

Instead of struggling to grow a large single crystal of rare earth doped fluoride, it is preferable to make whatever small single crystals are easily grown, grind these small crystals into powder, and then place them in an index-matched passive host such as a polymer. In this manner, it should be possible to make the 3D display medium any size that is required. The proper amount of crystal powder must be mixed into the proper polymer. Other advantages, compared to the same size single crystal display medium are reduced weight and cost. Such a medium would be much lighter since the polymer's density is about one quarter that of KY_3F_{10}. It would cost much less because growing very large crystals, if possible, is a very expensive and time consuming process. Another advantage of the concept of placing crystal particles in a passive host to form the 3D display medium is that different crystal powders can be mixed into the polymer, for instance Er:KY_3F_{10} and Pr:KY_3F_{10}, forming a single display medium. Then by choosing different sets of pump wavelengths we can select different colors of emission from the display medium.

One of the most important reasons for choosing KY_3F_{10} as the host crystal for this type of scalable 3D display medium is its crystal structure. It is cubic and isotropic, which means it can be characterized by a single index of refraction (see Table 3-1 and 3-2). This is important when we want to grind the crystal into powder and disperse the powder into an index-matched passive host to eliminate scattering. Since KY_3F_{10} is a cubic material, it is possible to index-match the

host for any orientation and polarization. In addition, Er:KY_3F_{10} has refractive index of 1.4876 (n_d) and there are commercially available polymers of the same index of refraction suggesting that the display medium is possible.

4.2 Experiments using different polymers

Experiments were performed on dispersions of Er:KY_3F_{10} crystal powders ranging in size from 10 to 400 μm in different polymer hosts. A major objective of these experiments was to make 3D display media with as high a density of homogeneously distributed emitting material as possible to assure efficient and uniform voxels and transparency of the entire medium. When making a static volumetric 3D display, the active medium used has to be transparent to let the pump light in and the emitted light out. Index-matching the particles and the polymer is therefore a very important factor to consider as it reduces light scattering at the interfaces. An extensive search to find the proper polymer is reported.

4.2.1 PMMA (Polymethylmethacrylate)

Polymethylmethacrylate (PMMA) is very versatile material and has been used in many applications because of its excellent clarity, UV damage resistance, good abrasion resistance, hardness and stiffness [73][74]. A solid pellet/bead type of PMMA was used and mixed with solvents such as Tetrahydrofuran (THF), dioxane and acetone.

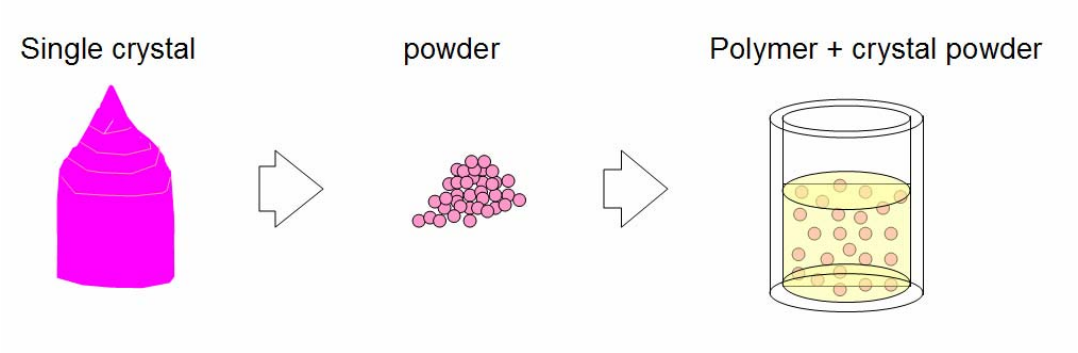

Figure 4-1: Sample making procedure (1) make powder from a bulk single crystal (2) mix the powder with an index-matched polymer in a sample container (3) carry out the polymerization process (depending on the polymer)

Samples were prepared by the following simple procedure: Bulk crystals were broken down to small particles size between 10 and 400 μm. These particles were sieved to select a range of sizes and were then mixed with an index-matched polymer. The performed polymerization process was carried out depending on the polymer selected (see Figure 4-1). A couple of critical problems are found with the sample making procedure using PMMA.

A major problem was caused by the use of solvent in the mixture. Since the polymerization occurs while the solvent evaporates into the air from the surface of the sample in a container, the surface of the sample mixture contacting the air will start to dry out first. Then the remaining solvent inside the sample may not evaporate easily. As a result, the polymerization speed slows down and often prevents samples from complete polymerization. In addition the evaporation of the solvent frequently leaves bubbles inside the sample (See Figure 4-2). Because a thick volumetric bulk sample is sought using a polymer that requires any kind of solvent may not be desirable.

Figure 4-2: Fully polymerized PMMA samples. No crystal particles were included in this sample. Many bubbles can be seen trapped inside the samples.

Index of refraction control was another problem. As shown in Figure 4-3, the refractive indices of PMMA (numbers in parenthesis stand for different product number) are much higher than that of KY_3F_{10} crystal over the entire range of wavelengths. Index-matching of KY_3F_{10} crystal and the polymer is essential to make scalable display medium. It is reported that in some polymers, chlorine atoms or chlorinated side-groups generally increase the refractive index of small molecules and polymers; whereas the incorporation of fluorine atoms or fluorinated side-groups decreases the refractive indices of similar polymers [76][77]. Synthesizing polymers to have different refractive indices may be achieved but in addition to the desired refractive index, good mechanical and optical quality must be maintained. It may take some time to develop such a PMMA. Also a PMMA that does not require solvent for polymerization seems to be required before further experiments are conducted using PMMA

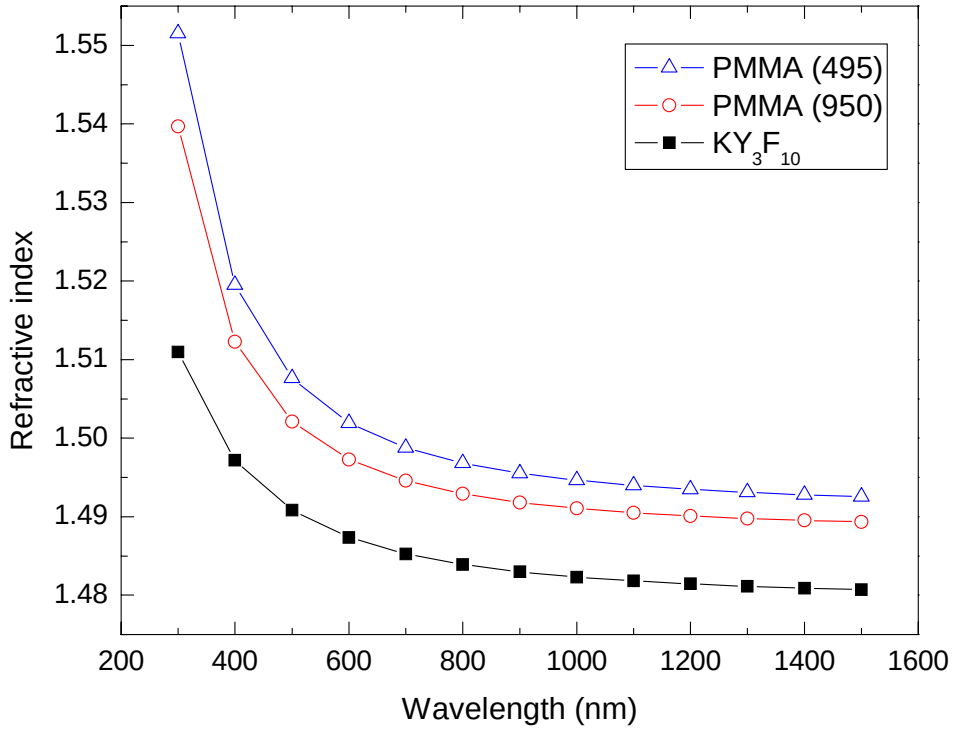

Figure 4-3: Index of refraction dispersion curves of PMMA and KY_3F_{10}. Two different PMMA dispersion curves were drawn using Cauchy coefficients from Ref. [75].

4.2.2 PFCB (Perfluorocyclobutyl)

Perfluorocyclobutyl (PFCB) polymer, provided by Dr. Dennis Smith of Clemson University, has good optical properties and can be prepared to have the desired index of refraction [78] (Figure 4-4). Different types of PFCB polymers were studied to enable a transparent scalable display medium which containing powdered up-conversion materials without any bubbles or cracks.

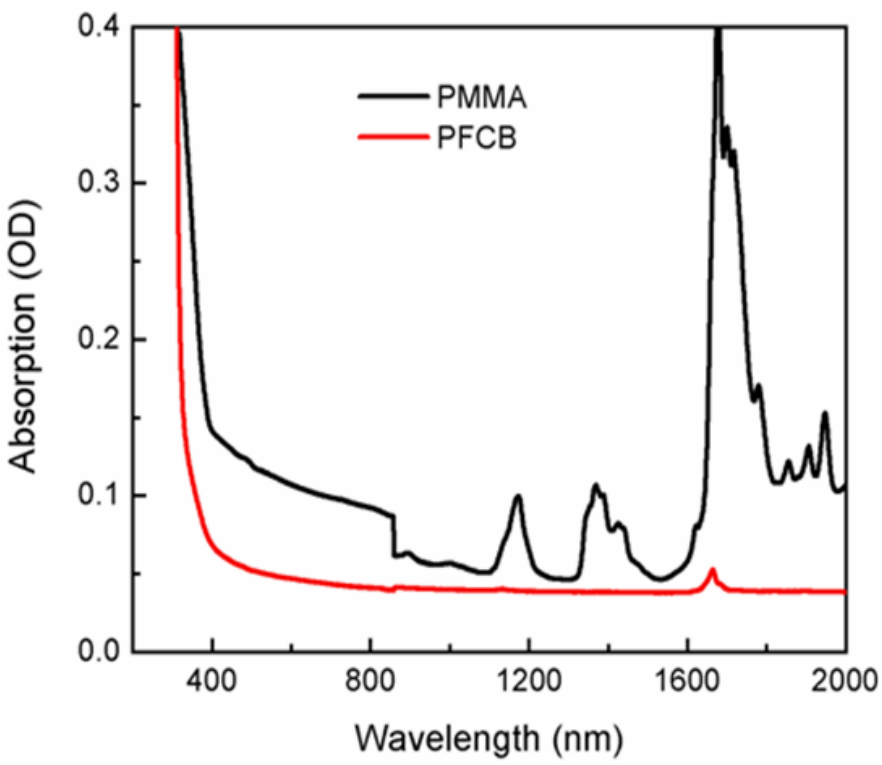

Figure 4-4: Absorption spectra of PMMA and PFCB [79] PFCB polymer shows lower absorption than PMMA.

4.2.2.1 Thermoplastic PFCB

Thermoplastic polymer is a polymer that can be remelted or redissolved in a solvent and remolded. Thermoplastic PFCB properties were shown in Table 4-1. THF, and cyclopentanone were used as a solvent to dissolve a powder form of PFCB polymer. However, as in the case of PMMA, making sample without bubbles was almost impossible. When the polymer was mixed with Er:KY_3F_{10} particles the solvent evaporation frequently made voids near the particles. Also, solvent evaporation took too long.

Table 4-1: Typical properties of thermoplastic PFCB [79].

Typical Properties	Thermoplastic Polymer
Number average molecular weight (Mn, GPC)	20,000 - 40,000
Refractive Index (1550nm)	1.442 - 1.505
Glass Transition Temperature (°C, DSC)	110 – 155
Thermal Decomposition Temperature (°C, TGA)	> 450
Typical solvents	Mesitylene, THF, Cyclopentanone

4.2.2.2 Thermosetting PFCB (solventless)

Because using solvent causes many problems, solventless polymers were sought. A different type of PFCB polymer was obtained from Tetramer Technologies L.L.C. Unlike the thermoplastic, thermosetting polymer cannot be remelted or redissolved once it has been molded. Figure 4-5 shows the schematic representation of the formation of PFCB polymers.

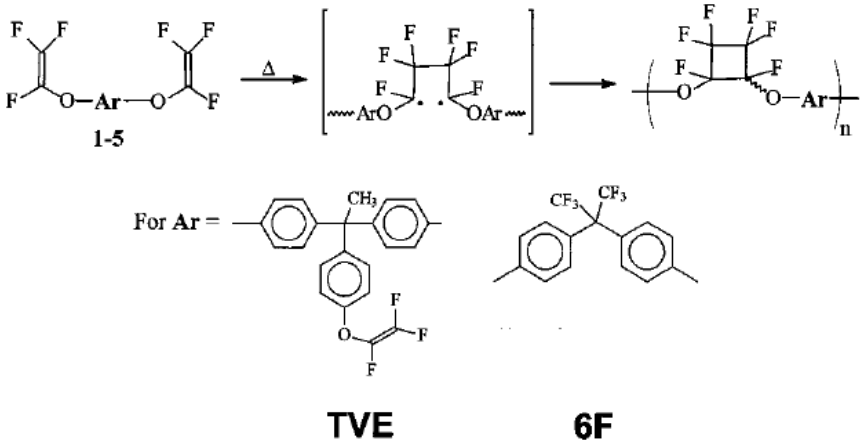

Figure 4-5: (Top) Schematic representation of the formation of PFCB polymers by the thermally induced dimerization of trifluorovinylaryle-ethers. (Bottom) Specification of aryl substituents [80]. The ratio of TVE and 6F in the PFCB polymer allows the refractive index to be selected

The refractive index of the polymer was determined by controlling the aryl substituents. The refractive index of 6F is about 1.455 at 633 nm and 1.5 for TVE (Figure 4-6). By mixing 6F and TVE in appropriate ratios we could make a PFCB polymer with different refractive indices between 1.455 and 1.5. Once we decided the refractive index required and mixed the polymer with Er:KY_3F_{10} powder the mixture was kept it in a vacuum oven under nitrogen atmosphere at 150 °C for about 12 to 14 hours. Then the temperature was increased to 220 °C to harden the polymer further. However, when the mixture was cooled to room temperature, many cracks were observed to form inside the sample (Figure 4-7). This may have caused by rapid cooling and partly because of the polymer gets too hard and stiff the polymer-particle interfaces suffer too much stress.

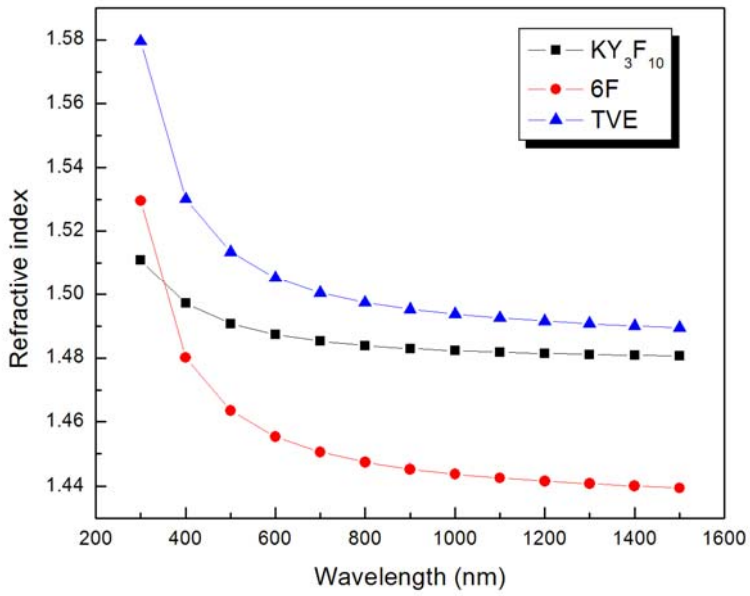

Figure 4-6: Dispersion curves of 6F and TVE compared to KY_3F_{10} crystal [78]. By mixing 6F and TVE with different ratio we can get the PFCB polymer with different refractive indices.

Figure 4-7: Fully polymerized PFCB samples (curing temperature ~ 220 °C). Many cracks were generated between particles and polymer. The sample on the right includes fewer particles than to the sample on the left.

Complete polymerization can still be achieved around 150 °C. Consequently, the sample can be less rigid. To take advantage of this feature, the sample was formed at 150 °C and cooled slowly by decreasing the temperature by 10 °C every couple of hours. Samples prepared in this manner had fewer or no internal cracks. However, cracks did form over time and after a couple of hours the samples appeared similar to the samples made at 220 °C.

Even lower temperature curing was tried to reduce the stress between particles and polymer. For example, 125 °C was tried and the sample held much longer at this temperature. The resulting sample was very soft and no cracks were observed.

Matching the refractive index of PFCB polymer to the Er:KY_3F_{10} crystal's index of refraction in the visible drastically reduced the visible light scattering from the crystal powder in the polymer as shown in Figure 4-8. But, in this case sample became opaque a couple of days later. The reason can be that the temperature was not high enough to complete cross-link all the monomers in the sample. This allows the non-polymerized monomers to precipitate out and cause the sample to become opaque.

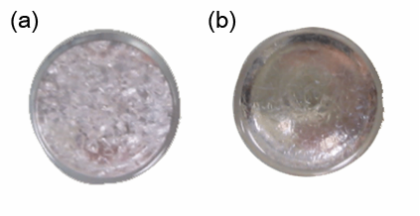

Figure 4-8: 2%Er:KY_3F_{10} powder in (a) a not index matched PFCB polymer and (b) when the index of refraction of the polymer is matched to the crystal. Light scattering from the interfaces of the particles and polymer were reduced when properly index matched.

4.2.2.3 Sulfonated PFCB

In the work described above, it became clear that some kind of modification to the polymers was necessary to prepare a polymer to hold inorganic particles such as Er:KY_3F_{10} particles better. Sulfonated PFCB was provided by Dr. Smith from Clemson University. Since the sulfonated PFCB require using solvent, it was not possible to make thick samples without bubbles. Thus, thin film samples were prepared to test the feasibility of this modified polymer. The making of this type of sample is explained in Figure 4-9.

In Figure 4-10 it is clear that some particles are well contacted to the sulfonated polymer (encircled with dotted line). However, it still is not perfect and the refractive index of sulfonated PFCB polymer was hard to control. Also, the polymer itself is opaque because of its poor quality.

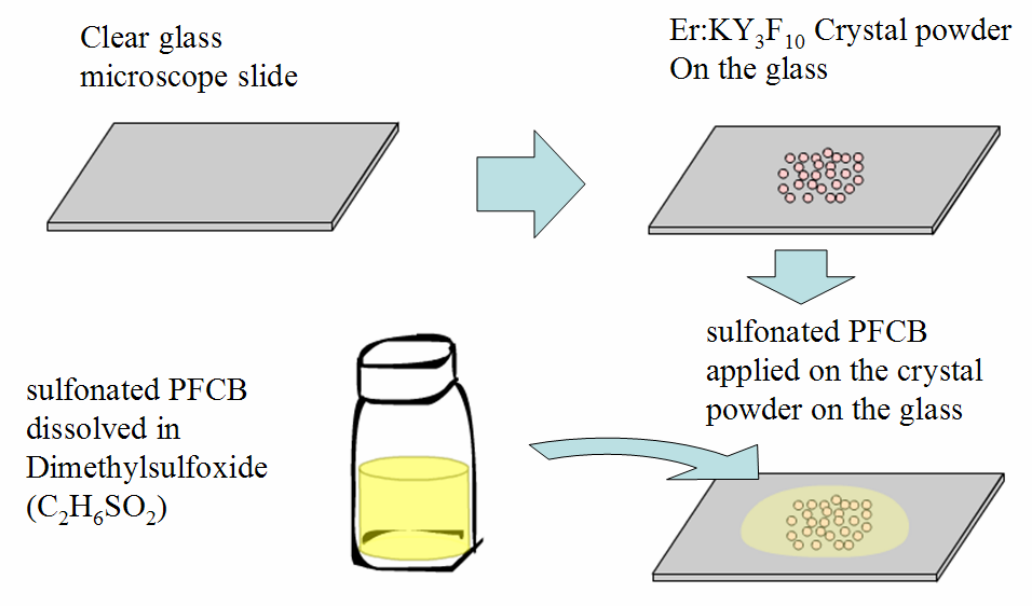

Figure 4-9: Sulfonated PFCB polymer test procedure. Sample was held at room temperature until all the solvent evaporated. It required more than 10 days to dry just one layer

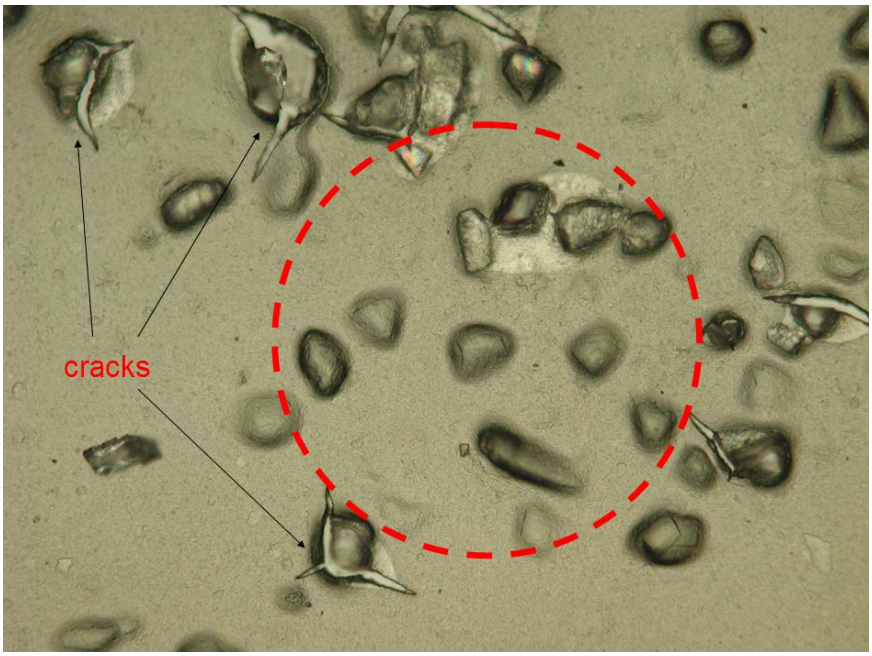

Figure 4-10: Sulfonated PFCB test result. Particle size ranges from 30~100 mm. Some particles are well contacted with polymer (encircled in the photo)

Modification in PFCB polymer can improve its ability to hold inorganic crystal particles. However, a solventless polymer (thermal curing) is desirable to make bulk samples and more work is required on refractive index control, and on the degree of modification to the polymer that is necessary.

4.2.2.4 Thermosetting PFCB (solventless) with ligand

Making samples with no defects such as cracks or bubbles has proven to be a difficult process. A properly chosen polymer and polymerization process can reduce this problem. Bubbles could be eliminated by slow thermal polymerization of solventless polymer in a vacuum oven and samples were obtained with very low scattering (see Figure. 4-11).

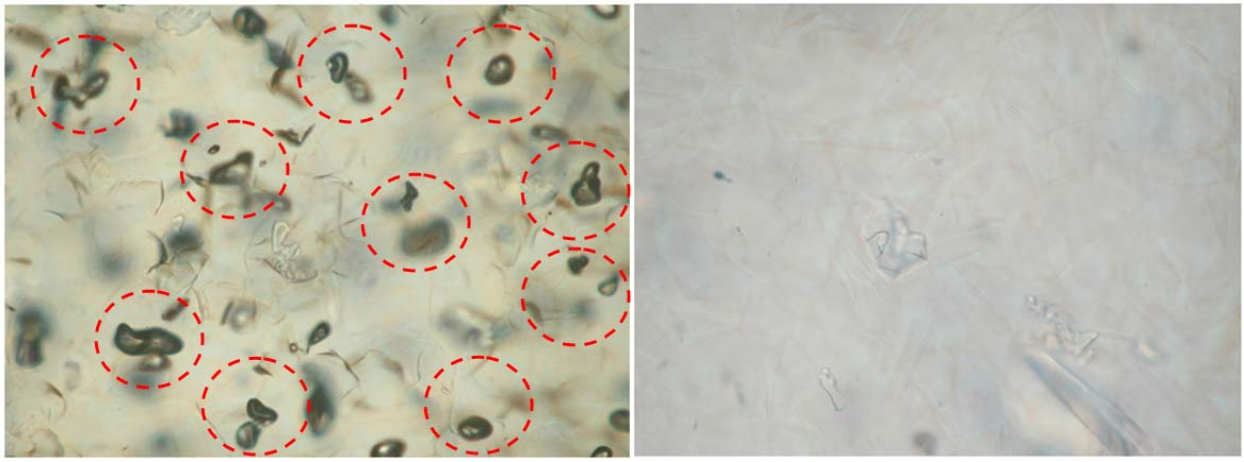

Figure 4-11: Er:KY_3F_{10} crystal particles mixed with PFCB polymer. Many bubbles (encircled with dotted line) were trapped inside the sample because the polymerization took place too quickly (left). Bubbles were eliminated by slow thermal polymerization in a vacuum oven as seen in the photo on the right.

However, after a few days cracks formed and voids between the crystallites and the host polymer could be seen. This is most likely due to the difference between their thermal expansion coefficients. Phosphorylating the polymer host helped the polymer hold the crystalline powder and prevented cracks in our optically-written 2D display studies [81][82][83]. Phosphorylation should help similarly with the PFCB polymers used as index-matched passive hosts for 3D displays.

Phosphate trifluoroethanol (TFE) ligand (figure 4-12) mixed with PFCB polymer was tested to help the polymer hold particles with less surface tension between particles and polymer.

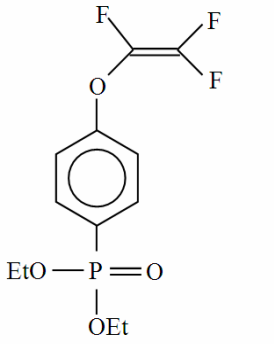

Figure 4-12: Phosphate Trifluoroethanol (TFE) used as a ligand when Er:KY3F10 particles were mixed in a PFCB polymer host

Some ligand was added to the polymer and then mixed with Er:KY_3F_{10} crystals. This mixture was then placed in the vacuum oven. Samples were kept at 80 °C for about 1 hour to get rid of any bubbles. After the bubbles were removed, the the temperature was increased to 150 °C and held there for about 16 hours for the complete polymerization. The temperature was then decreased little by little slowly down to room temperature to prevent abrupt contractions.

Figure 4-13(a) shows the samples 3 hours after being removed from the oven, and figure 4-13(b) is the samples a week later. It seems that ligand helped only for a short time. However, it was discovered that insufficient ligand had been used in these samples in follow-up experiments.

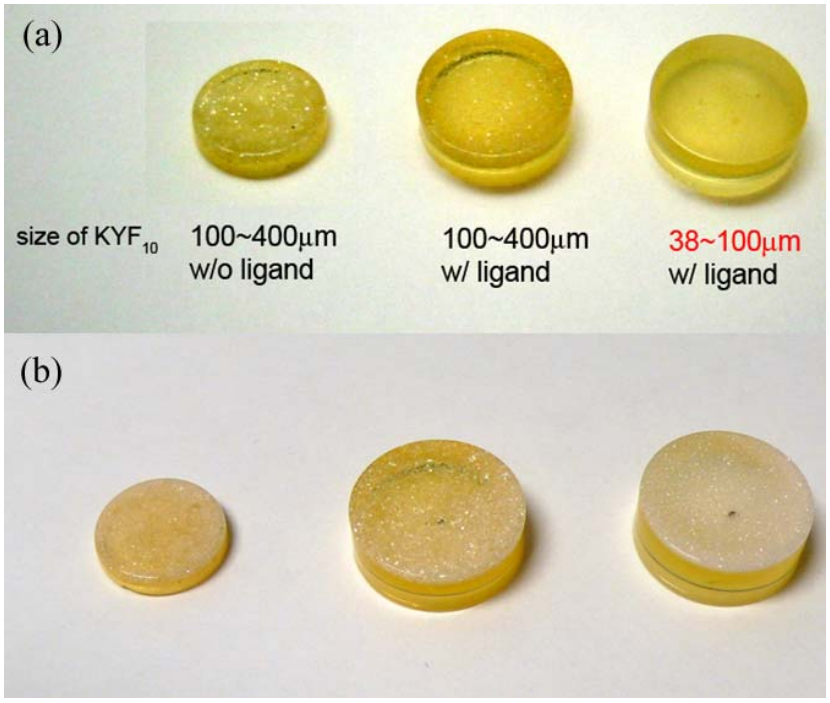

Figure 4-13: Er:KY_3F_{10} particles mixed with PFCB with or without ligand.(a) 3 hours after removal from the oven. (b) a week later. Not enough ligand had been used.

Further experimenting revealed the proper amount of ligand and produced samples with better quality. Significant regions of samples could be found as seen in the right hand microscope photo in Figure 4-14. However, there are still some macroscopic cracks. This may improve further when using a more optimized ligand and sample preparation conditions.

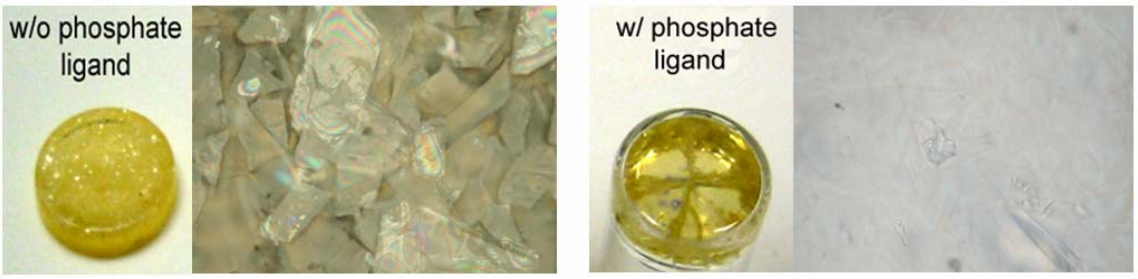

Figure 4-14: Er:KY_3F_{10} particles mixed with PFCB only (left) and with PFCB and ligand (right). This result shows that inclusion of a proper ligand will help prevent the medium from cracking.

4.2.3 Polymer-gel

Another type of host that will not crack is a polymer that even after the completion of the polymerization process remains soft. Optical-gels (or polymer-gel) from Nusil Technology (Light Span) were chosen for this purpose because of their softness after polymerization and because they could be obtained with the desired refractive indices. It also has a curing time that is long enough to allow the powder dispersion and sufficient for any trapped air bubbles to escape. Typical properties of the polymer-gels are shown in Table 4-2

Different refractive indices could be obtained by mixing these three polymer-gels in different ratios. For instance, by mixing LS-3246 and LS-3249 in different proportions polymer-gels can be formed having refractive index between 1.46 and 1.49 at 589 nm. To have refractive index between 1.49 and 1.52 LS-3249 and LS-3252 could be mixed. However, when LS-3246 and LS-3252 were mixed the polymer became opaque. A typical dispersion curves of a polymer-gel is shown in Figure 4-15. Cauchy coefficients were provided by the manufacturer. Polymer-gel is transparent in the visible and near infrared (Figure 4-16).

Table 4-2: Typical properties of polymer-gel from Lightspan [84].

Typical Properties	LS-3252	LS-3249	LS-3246
Uncured Properties			
Viscosity (mixed)	400 cP	150 cP	1,600 cP
Work Time (2x viscosity)	8 hours	5 hours	8 hours
Cure Time	24 hours	72 hours	24 hours
Cured Properties			
Consistency	Soft, self-healing gel	Soft, self-healing gel	Soft, self-healing gel
Durometer, Type 00	10	15	10
Specific Gravity	1.07	1.06	1.04
TGA Take-off (1% wt. Loss, 10°C/min. in air)	>250°C	>250°C	>250°C
Appearance	Clear	Clear	Clear
Refractive Index, 589 nm	1.52	1.49	1.46
Refractive Index vs. Temperature, 589 nm	-3.9 x 10^{-4}/°C	-3.8 x 10^{-4}/°C	-4.0 x 10^{-4}/°C

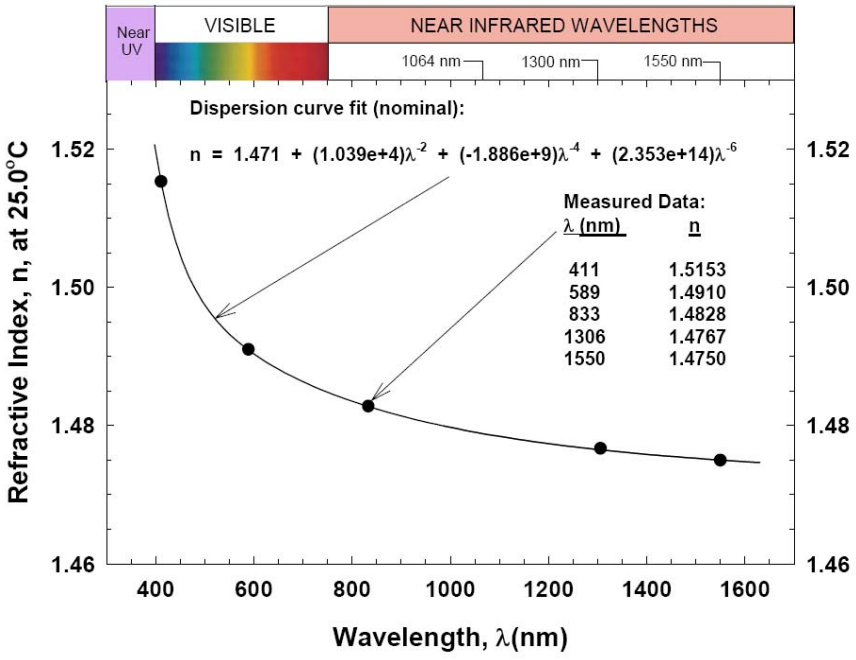

Figure 4-15: Typical dispersion curve of polymer-gel (LS-3252 is shown here) [84].

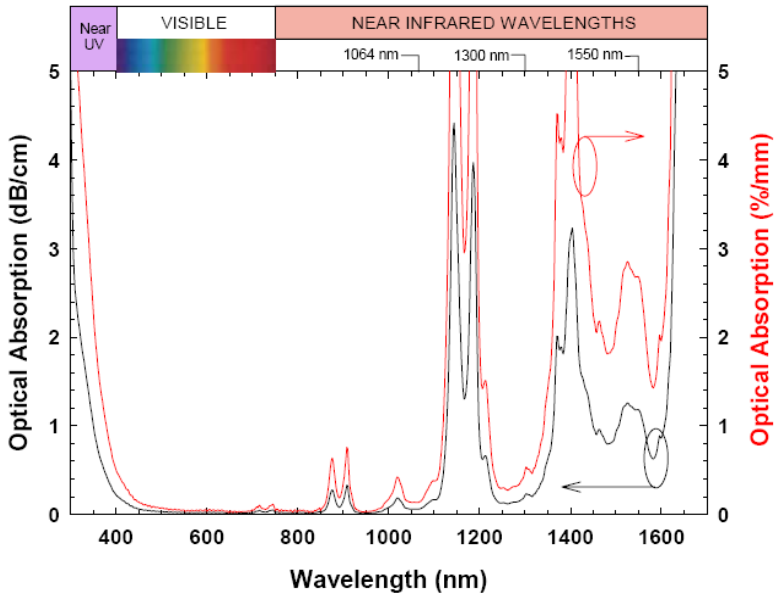

Figure 4-16: Typical absorption spectrum of polymer-gel (LS-3252 is shown here) [84].

There are some polymer-gel absorption peaks in near infrared but the absorption is not too strong throughout the visible and at the pump wavelengths near 850 nm. The absorption at 1494 nm.is not too weak to ignore but it can be acceptable for small displays. However, to make a large display medium, it is essential to minimize the polymer-gel absorption at 1491 nm.

Dispersion of crystalline powder in the polymer is important to achieve a homogeneous display medium. Uniform dispersion of crystalline powder using optical-gel as a polymer host was achieved with fairly small particles as shown in Figure 4-17 (particle size <20 μm, 20~38 μm). Precipitation of particles was observed from the samples with particles larger than 38 μm.

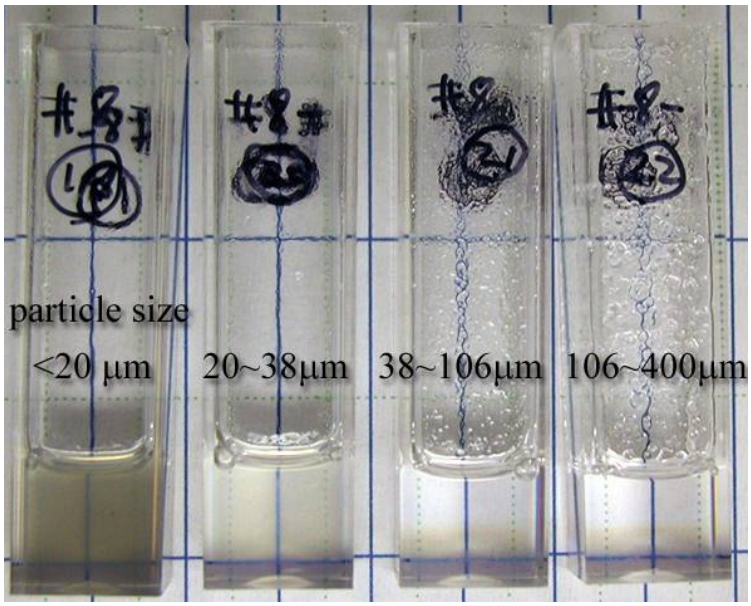

Figure 4-17: Different sizes of Er:KY3F10 particles in Polymer-gel index-matched at 600 nm. Uniform dispersion is observed from samples with particles smaller than 20 μm and between 20 and 38 μm. Precipitation of particles can be observed using particles larger than 38 μm.

Different index-matched samples were made to find the optimum index-index matching condition (Figure 4-18). 20~38 μm Er:KY_3F_{10} particles were used in different polymer-gel index-matched at various wavelengths. It can be clearly seen that the sample index-matched in the visible wavelength shows better transparency than those index-matched in the near infrared. Also samples with different weight percent (wt%) were prepared (Figure 4-19). Er:KY_3F_{10} particles were mixed in a polymer-gel index-matched at 600 nm with different particle size and different wt%. With more particles, samples exhibit more scattering of visible light. However, those samples with more particles are expected to give more fluorescence so there is a trade off to be made between scattering and emission strength.

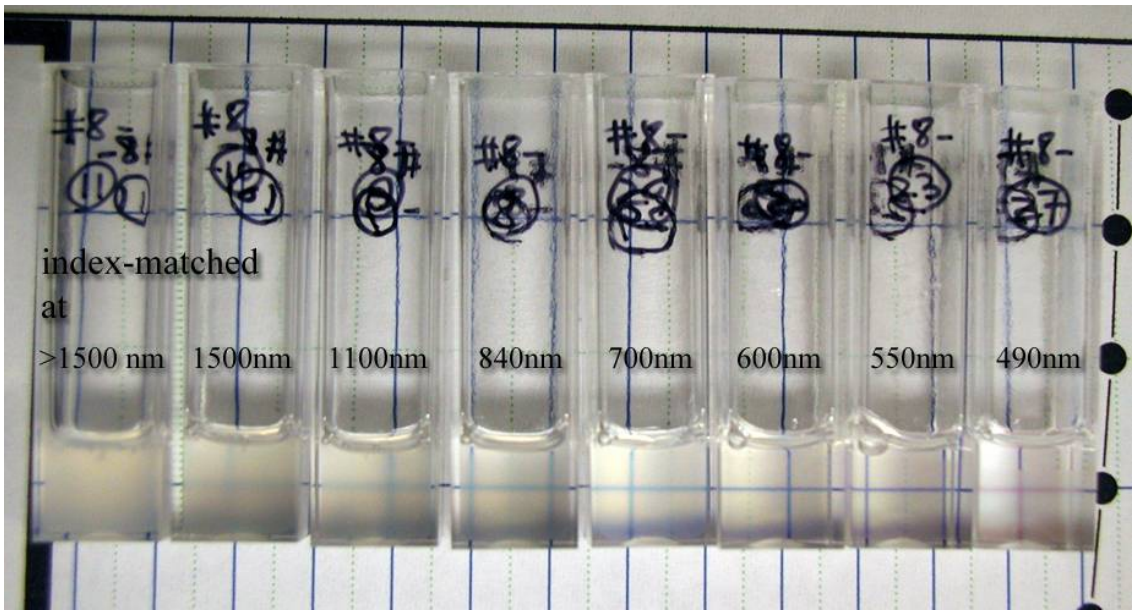

Figure 4-18: 20~38 μm size Er:KY3F10 particles in a Polymer-gel index-matched at various wavelengths. The sample that was index-matched in the visible wavelengths shows better visible transparency as expected.

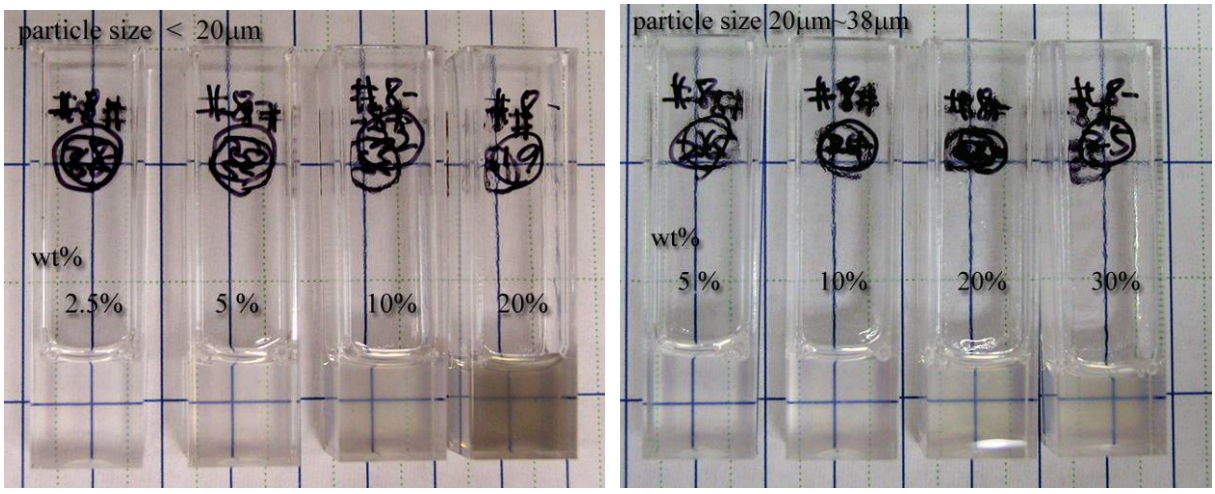

Figure 4-19: Er:KY3F10 particles in a Polymer-gel index-matched at 600 nm with different particle size and different wt % of particles to Polymer-gel. With more particles, samples exhibit more visible light scattering.

Samples index-matched at 550 nm with crystallite particle size about 10~20 μm were prepared to demonstrate the scalable display medium 'proof-of-principle' (Figure 4-20). Uniform dispersion of particles was achieved and transparency was retained.

Figure 4-20: 2%Er:KY_3F_{10} powder in the index matched Polymer-gel. Different weight percents of crystal particles were suspended in the polymer and transparency was retained.

Two different pump beams were incident on the samples, to generate a voxel in the prototype scalable display medium (Figure 4-21). The first pump beam was incident from left-hand side of the picture, and second one was from the direction perpendicular to the page. Optimum pump wavelengths found earlier for the Er:KY_3F_{10} crystal were 1494.1 nm for the first pump beam and 848.4 nm for the second. Bright voxels were generated inside the scalable display medium. A voxel similarly excited in a single crystal 2%Er: KY_3F_{10} is shown for comparison in Figure 4-21(c).

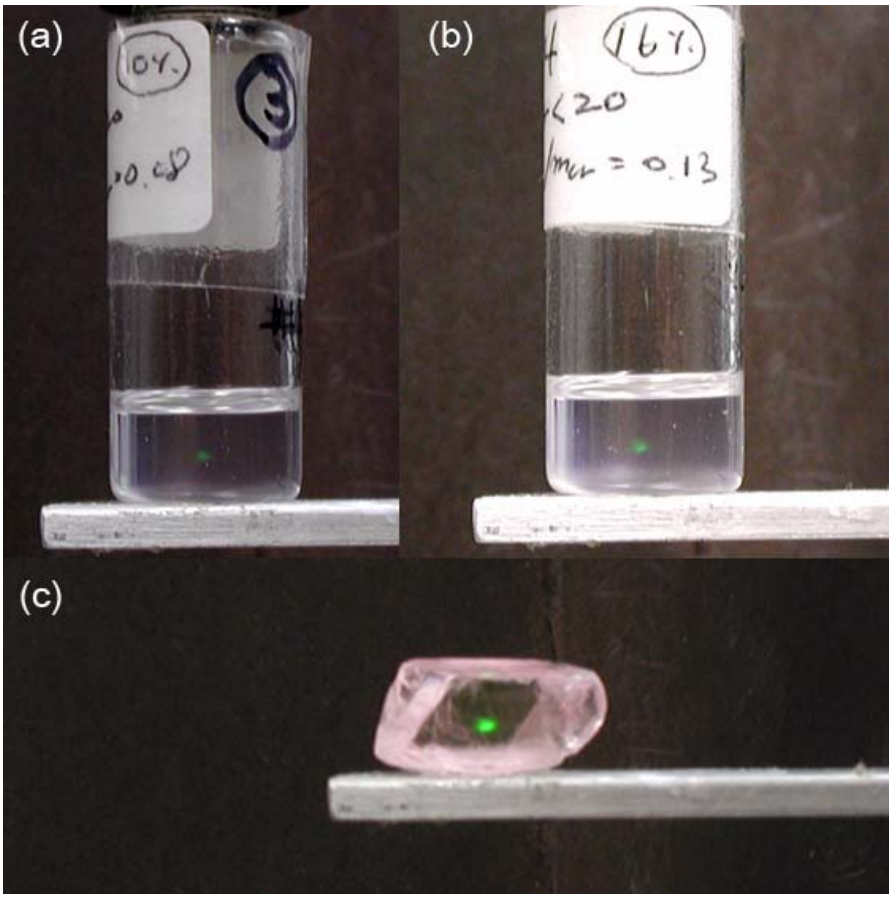

Figure 4-21: (a),(b) Photo of the emission from 2%Er: KY_3F_{10} powder (particle size 10~20 μm (a) 10 wt% (b) 16 wt%) in optical-gel excited by two different pump beams (λ_1=1494.1 nm from left-hand side of the picture, λ_2=848.4 nm perpendicular to the page.) (c) Emission from a single crystal 2%Er: KY_3F_{10} under the same pump conditions shown for comparison.

4.3 Index matching

Bright visible voxels were generated in the display medium. However, the medium isn't perfectly transparent. One of the reasons that the medium looks opaque stems from index mismatch. The dispersion curves of Er:KY_3F_{10} and the polymer-gel with different refractive indices are shown in Figure. 4-22 (PFCB has dispersion curve similar to that of the polymer-gel.).

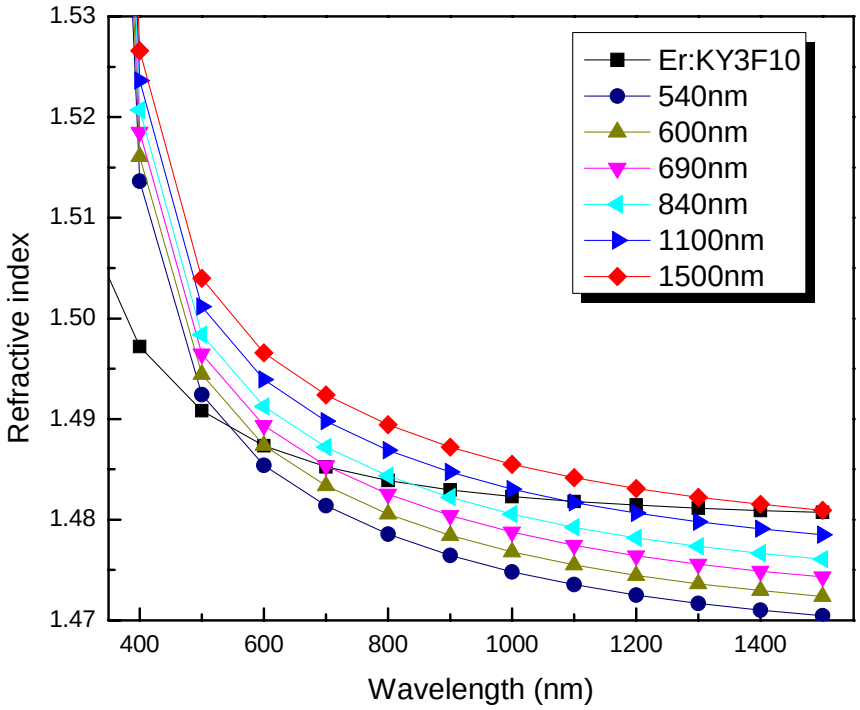

Figure 4-22: Dispersion curves of Er:KY_3F_{10} and polymer-gel with different indices. The dispersion curves for the polymer-gel are labeled with the wavelength at which the refractive index matches that of Er:KY_3F_{10}.

If the refractive index of the polymer-gel is matched to Er:KY_3F_{10}'s index at one single wavelength there will be mismatches at other wavelengths: for example, if it were matched at one of the visible wavelengths, then other visible wavelengths and the pump wavelengths in near infrared cannot be matched. Since it is not easy to control the dispersion of the polymer-gel, experiments were conducted to find the optimum index-matching condition for better display medium quality.

To determine the index-matching conditions of the samples, their absorbance was measured using a Cary 500 Spectrophotometer shown in Figure 4-23. The absorbance measured in this manner is a combination of the scattering in the sample and the absorbances of the polymer-gel and the Er:KY_3F_{10} measured individually (see Figure 4-24 and 4-25)

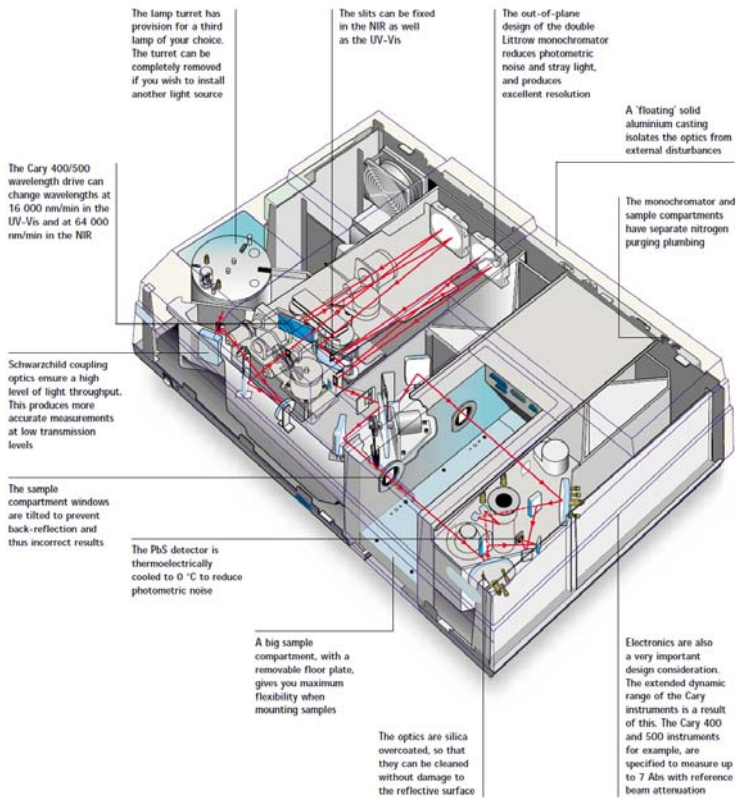

Figure 4-23: Schematic of the Cary 500 spectrophotometer used in the absorbance measurements

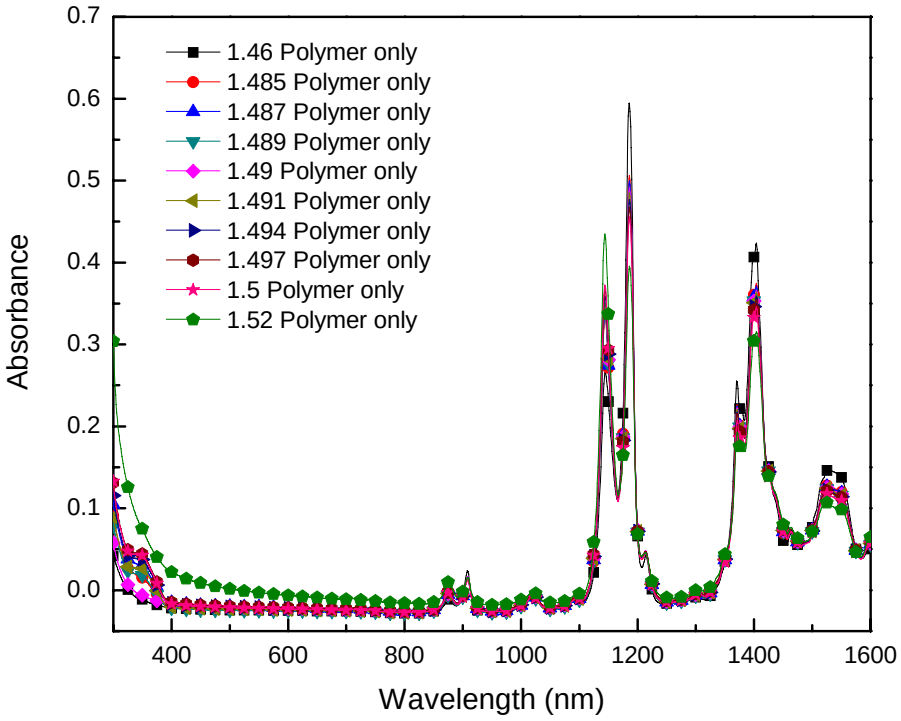

Figure 4-24: Absorbance spectra of the polymer-gels with different indices. The legend indices are polymers' indices at 589 nm.

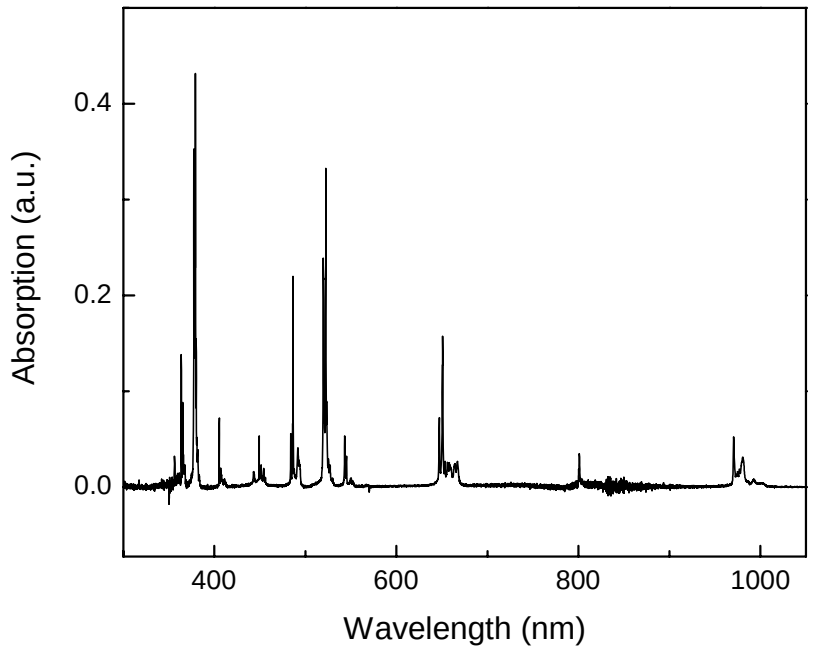

Figure 4-25: Absorption spectrum for Er:KY_3F_{10} crystal.

Since the absorbances of the components of the sample do not change when they are mixed together, the difference between the components absorbances and the absorbance of the mixed sample represents the scattering due to index mismatch. If a given wavelength of the beam undergoes pronounced scattering the observed absorbance of the mixed sample will be high. Many different polymers with different refractive indices were tested: index-matched to Er:KY_3F_{10} at 540 nm (visible), 1500 nm, and in between. Many different samples were made by mixing Er:KY_3F_{10} powder with these polymers. The absorbance spectra of some of these samples are shown in Figure 4-26. The sample index-matched at 540 nm showed minimum absorbance, meaning minimum scattering, around 540 nm, but significant absorbance or

scattering in the near IR. On the other hand, the sample matched at 1500 nm had minimum scattering in near IR but a huge amount of absorbance or scattering in the visible. The sample index-matched at 690 nm showed balanced scattering in both the visible and near IR. That is, compared with other samples, the sample that was index-matched at 690nm had the least overall scattering across the range of visible and near IR wavelengths.

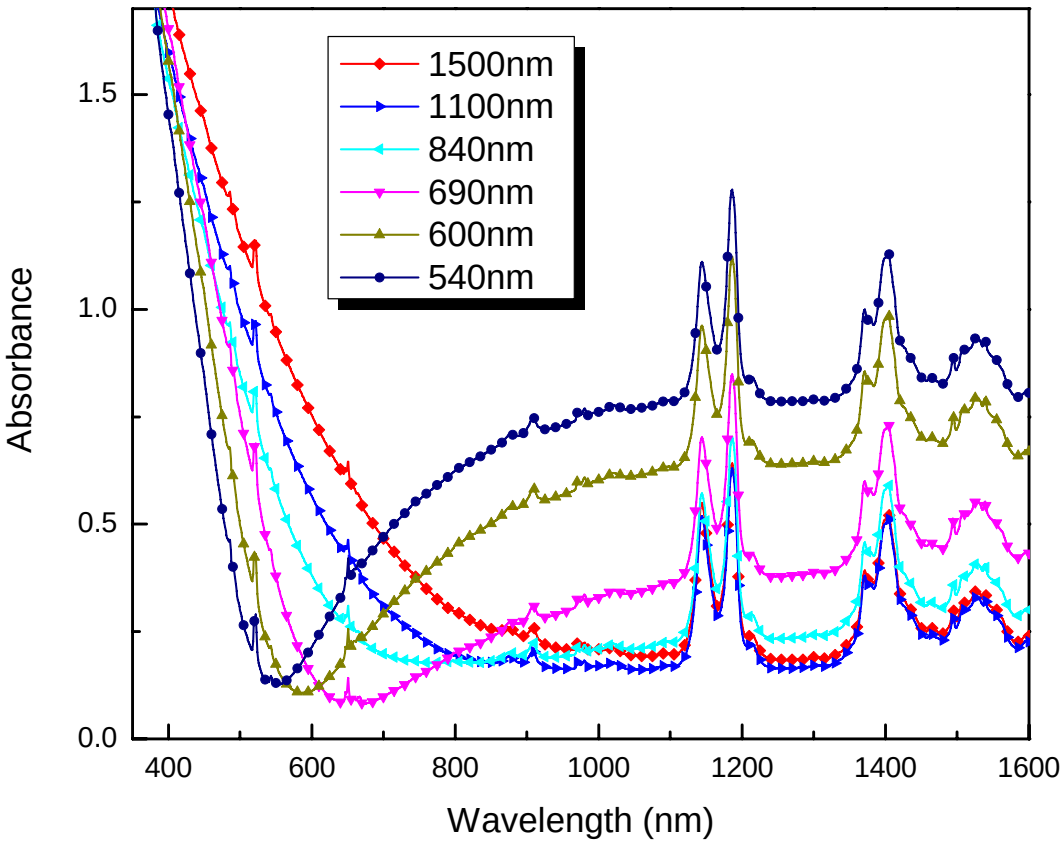

Figure 4-26: Absorbance spectra for samples index-matched at different wavelengths. The samples exhibit lowest absorbance at the wavelength at which they are index matched with Er:KY_3F_{10}.

The fluorescence strength was measured when each sample was pumped with the optimum pump wavelengths found earlier (848nm and 1491nm) to determine which sample produces the brightest voxel using the setup shown in Figure 4-27.

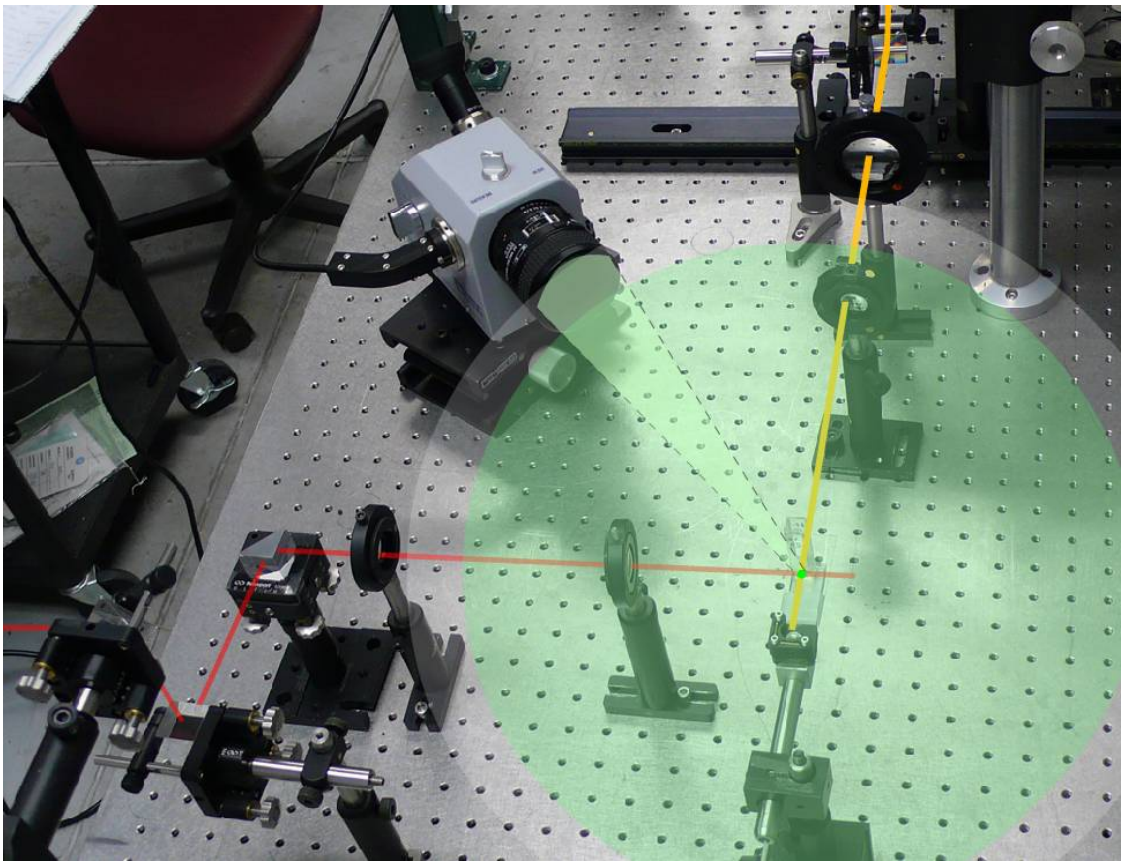

Figure 4-27: Fluorescence strength measurement setup. The TOP 100 optical probe with telescope lens collected the visible light emitted from a voxel in a certain solid angle (illustrated with dotted lines) and sent it through the optical fiber to the compact array spectrometer (CAS) 140B from Instrument systems.

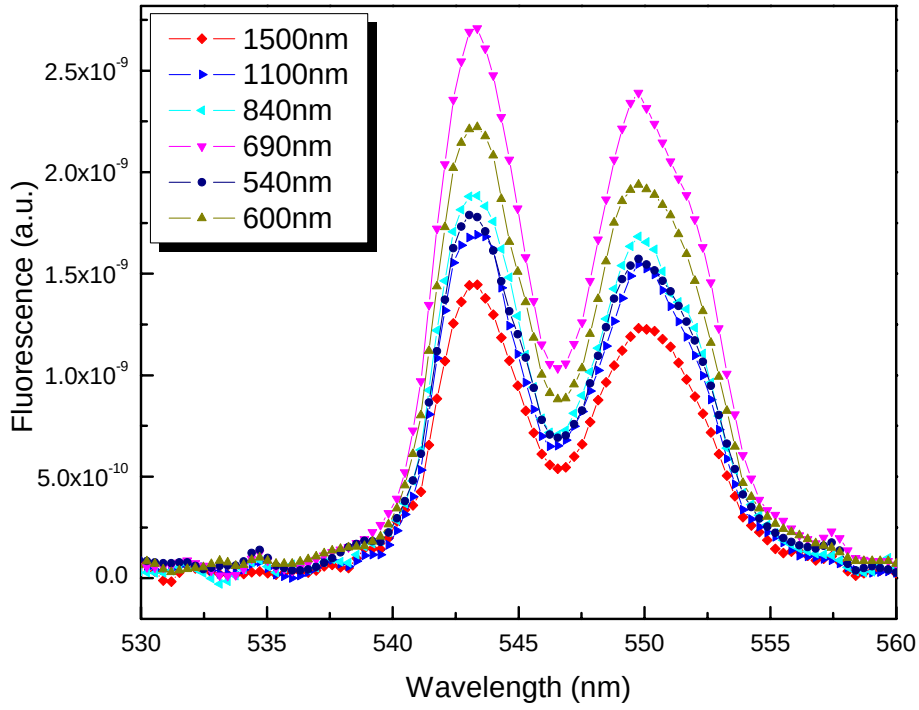

Figure 4-28: Fluorescence strength versus wavelength for Er:KY_3F_{10} for polymer gels index matched at the indicated wavelengths When the refractive index of the polymer gel is 1.489, same as the index of Er:KY_3F_{10} crystal at 690 nm, the strongest fluorescence was observed.

The result (Figure. 4-28) shows that the optimum index-matching, that which gives a good balance between visible and IR scattering, results in the brightest voxel within the medium. Since the voxel emission process involves three different wavelengths of light, i.e., two pump wavelengths and one visible, if any of these wavelengths experience serious scattering while entering or exiting the medium, it would be impossible to observe a well defined, bright voxel inside the medium. This means that when the host refractive index is chosen it is necessary to

consider all involved refractive indices. In the present case of Er:KY_3F_{10}, the active emitting material optimum index-matching occurs when the polymer-gel index is selected to match the crystal at 690 nm or when its index is 1.489 at 589 nm.

4.4 Other issues

Another issue in preparing this 3D display medium arises from the manner of makingcrystal powder. Since the crystals are mechanically ground into powder, it is likely that damage, cracks or fractures, is produced inside the crystal particles. If such cracks or fractures always resulted in completely separate particles then they would be of no concern. However, when they make an air gap inside the crystal particle those gaps cannot be reached by the index-matching polymersand so they cannot be index-matched. The microscope photo in Figure 4-29 shows that some particles are not index-matched, as one can clearly see some particles' silhouettes. This can be a more serious problem than the small index mismatch due to the dispersion because these air gaps scatter most of the visible lights regardless of the wavelengths.

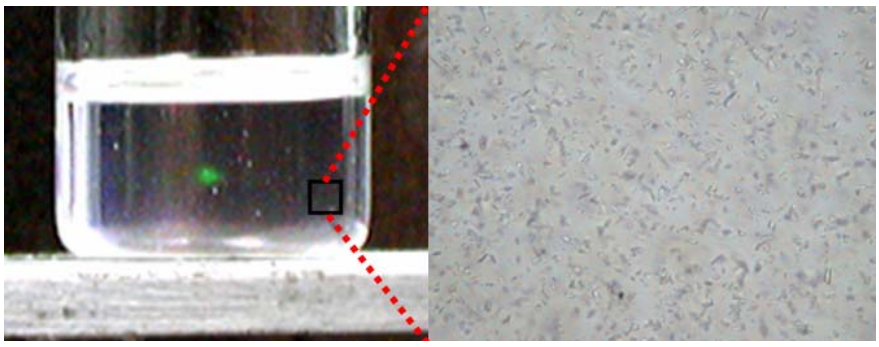

Figure 4-29: 200x microscope photo of the enclosed region of the prototype scalable display medium sample. It is clear that there are some particles that didn't index matched at all.

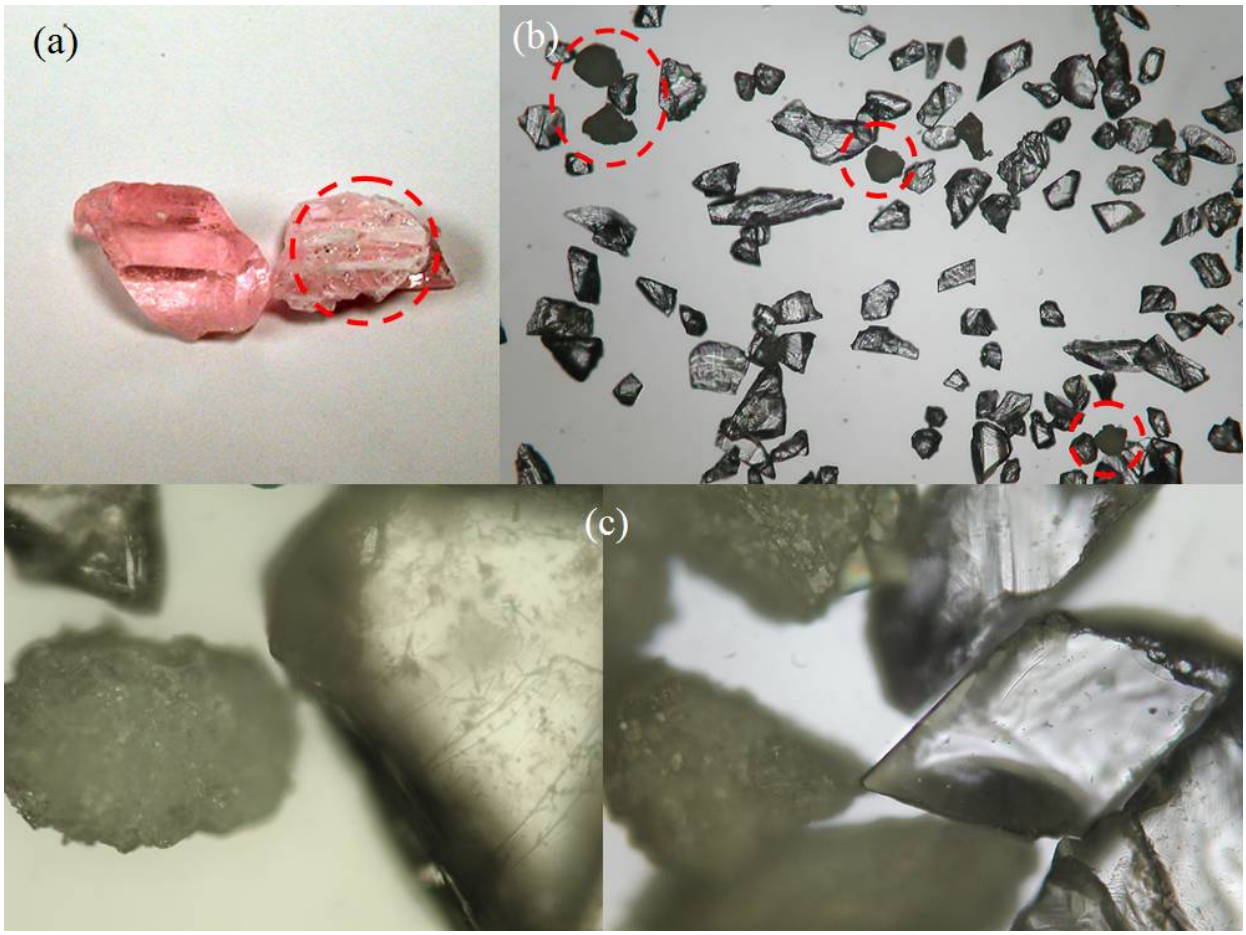

Figure 4-30: Structures appear in parts of single crystals. (a) Not magnified (b) 100x microscope photograph. Dotted red circle lines indicating particles with structure in them. (c) 200x microscope photograph.

When as received materials are inspected by eye (see Figure 4-30(a)), some part any single crystal is found to be not transparent. To observe it better, the single crystal was broken into small particles using an agate mortal and pestle. Microscope photographs show the damaged material more clearly (Figure 4-30 (b)(c)). Some of the crystal particles are found to have structure (encircled with dotted red lines). Light scattering caused by structures inside these particles make them opaque.

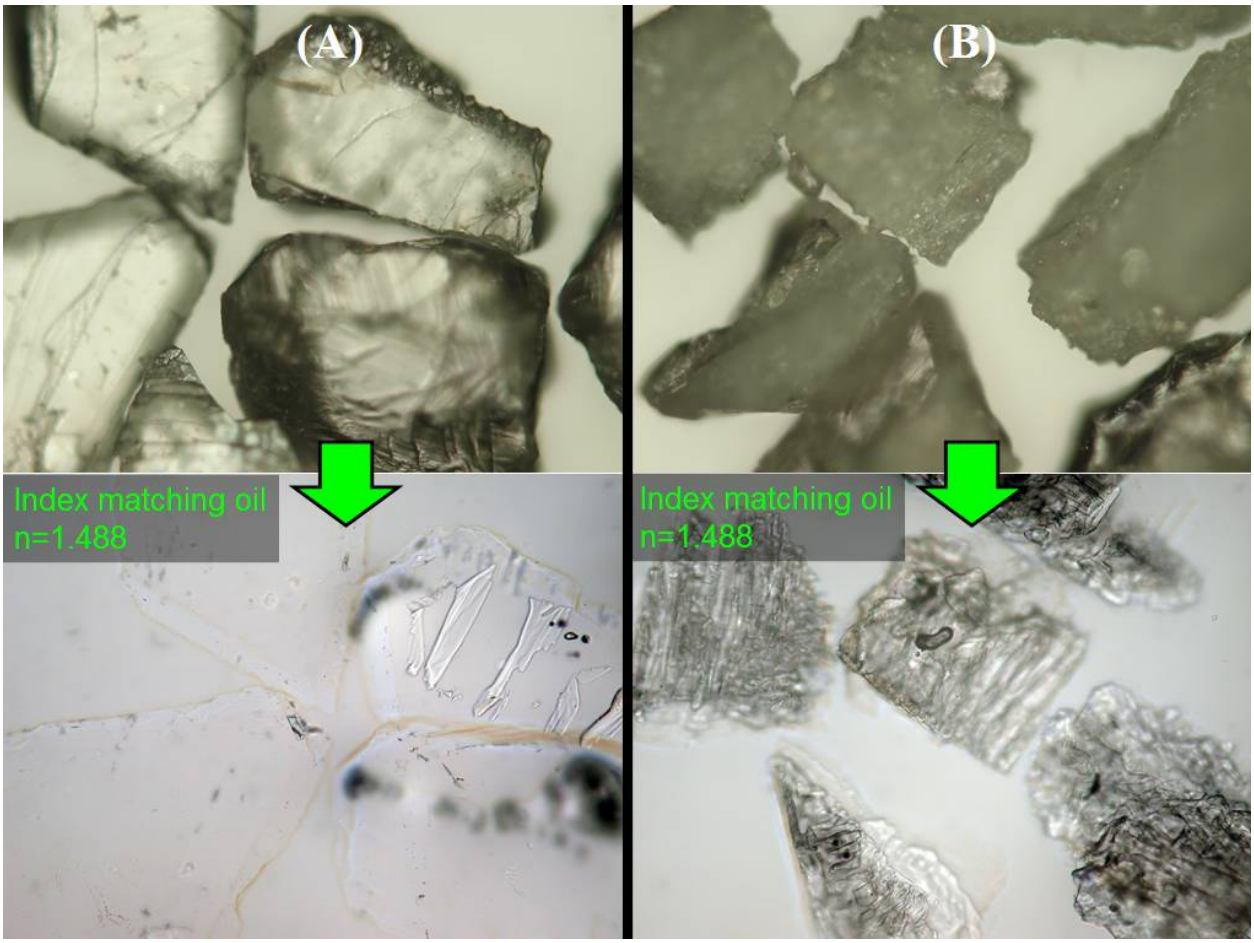

Figure 4-31: 200x microscope photo of two groups of particles (top): (A) clear particles of size about 400 μm. (B) opaque particles of the same size as group A. The upper micrographs were taken of dry particles and the lower when they were immersed in an index-matching oil.

The presence of structure within the raw particles is easily seen when they are placed in index-matching fluid. Two groups of particles were chosen to be compared to each other when they were placed in an index-matched oil: (A) a group of particles that looked transparent by eye, (B) group of particles that looked opaque. The sizes of particles in both groups was about 400 μm. These particles were then immersed in the index-matching oil of refractive index 1.488

which matches the refractive index of KY3F10 crystal at 550nm. It can be easily seen that there are structures inside some of the particles (Figure 4-31).

The particles with structure (group B) are very brittle. They easily broke into pieces as pressure was applied to them. When these separated particles were placed in index-matching oil the were found to still have structure within (see Figure 4-32). These particles are clusters of smaller crystallites which couldn't grow into the large single crystal.

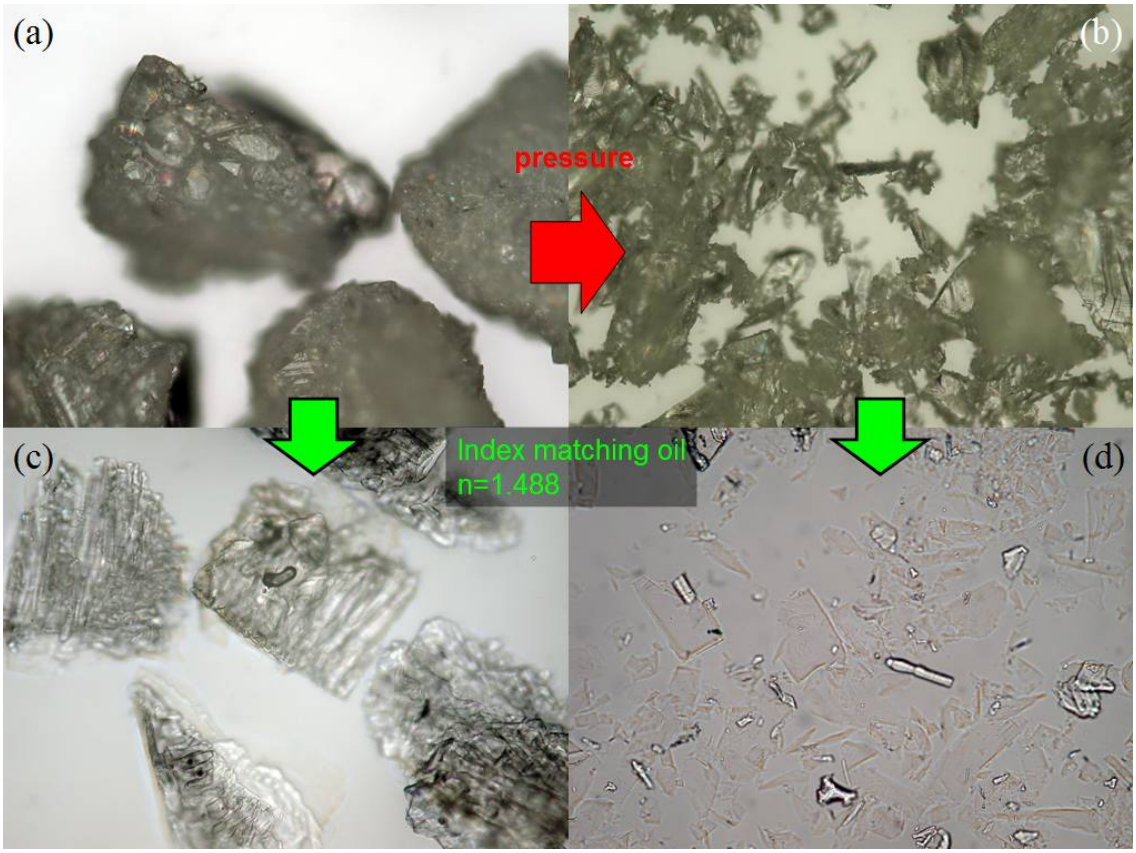

Figure 4-32: 200x microscope photo of the particles with surface structures. (a) particle size ~400 μm (b) when the 400 μm particles were mechanically stressed they broke into such smaller crystallites shown (c) when the particles in (a) were immersed in an index-matching oil. (d) when the particles in (b) were placed in index-matching oil

To find out how fine these structures were the 400 μm particles were ground down to about 20 μm. As shown in Figure 4-33, particles with internal structures were found as small as 20 μm or less. As the size gets smaller more of particles with internal structure were observed. Since all these particles contribute to scattering they can degrade a 3D display medium quality significantly.

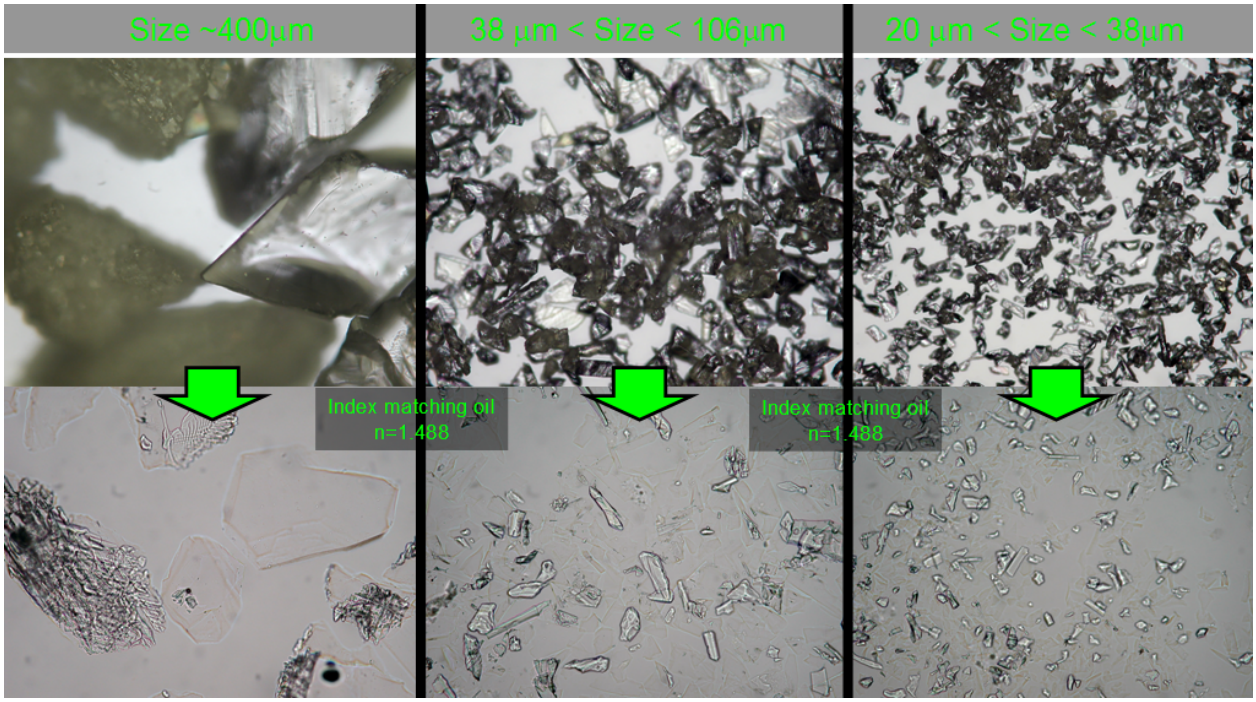

Figure 4-33: 200x microscope photo of particles with structures in them. When the particle size is reduced by mechanical grinding more such particles were observed.

A simple solution to the eliminating the scattering problems caused by such particles would be sorting them out and using only the particles without any internal damage or structure. Since, it is impossible to sort millions of ~10 μm particles in a reasonable time, particles were prepared by starting with fairly large particles, about 400 microns or larger and selected only

those showing no internal damage. These selected particles into smaller particles. Such sorting of the starting crystal particles prior to making the small particle powder led to a significant reduction in the presence of damaged crystal particles. As one can see in Figure 4-34, scattering caused by the internal damages or structures within the crystal particles was dramatically reduced.

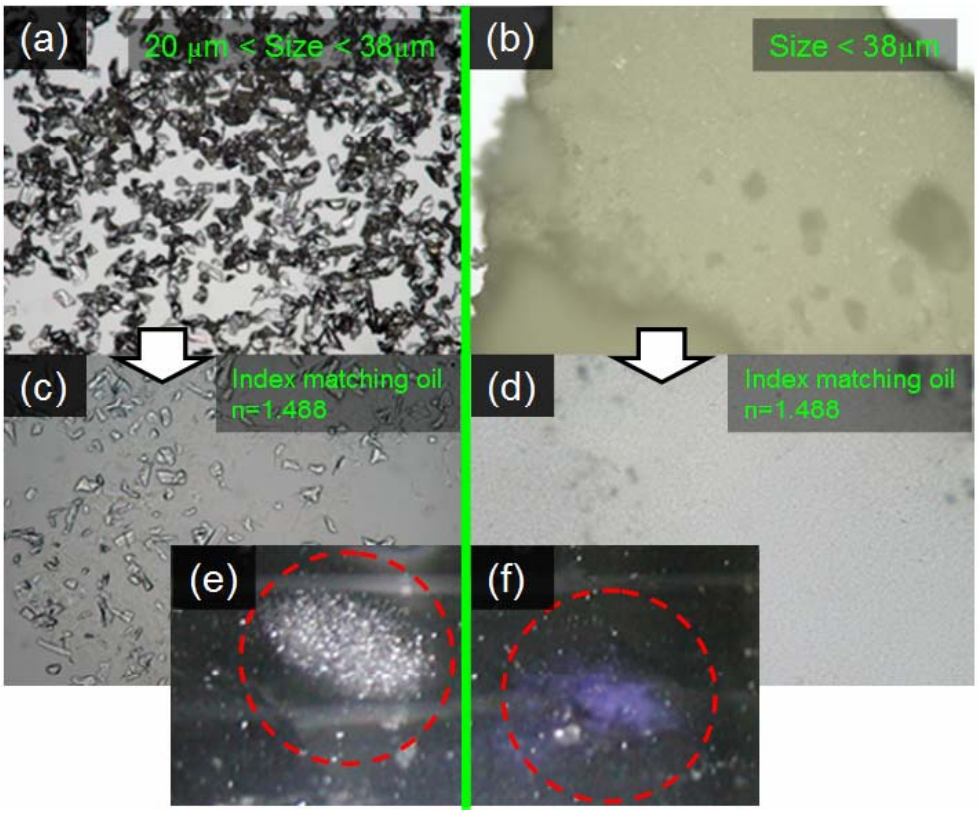

Figure 4-34: Comparison between particles and selected particles. Left hand side: (a) 200x microscope photo of crystal particles (c) 200x photo of particles in an index-matching oil (e) particles in an index matching oil without magnification. Right hand side: (b) 200x photo of selected particles (d) 200x photo of selected particles in an index-matching oil (f) selected particles in an index-matching oil without magnification.

4.5 Other factors: particle size, concentration

There are other important factors that can influence the sample quality such as transparency and brightness. As shown in Figure 4-19, different particles size and different concentration of samples were made to examine how these factors affect to the quality of samples.

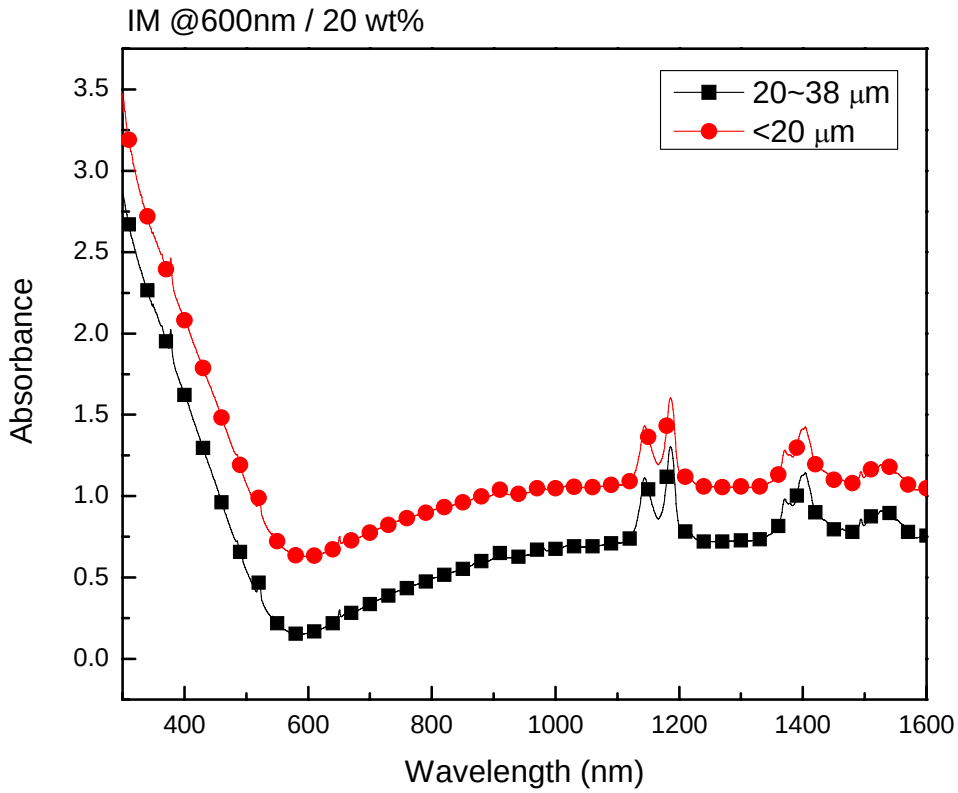

Figure 4-35: Absorbance spectra of samples index-matched at 600 nm with different particle sizes but fixed weight percent concentration of particles in the polymer. Smaller particles exhibit more scattering

Figure 4-35 shows the absorbance spectra of sample with different size particles. All other parameters are the same for both samples (index matched at 600 nm and 20 wt% in polymer-gel). The sample containing smaller particles exhibits more scattering than the sample with larger particles. This may be because of the number of particles in the sample with smaller particles is much larger than that of sample with larger particles. The number of particles in the sample with 20~38 μm particles is 4.3×10^3 particles/mm^3. On the other hand, the sample with particles smaller than 20 μm, assuming an average particle size of 10 μm, gives 3.1×10^4 particles/mm^3.

The samples used in Figure 4-36 had much higher concentration of particles. Because of the difficulty in dispersing large particles uniformly in the polymer caused by settling in gravity, the samples were fully packed with particles in the bottom of the sample vial. Even though the concentrations of KY_3F_{10} particles were much higher than the samples used Figure 4-35, the particle size was much larger so the number of particles in the same volume was much smaller. For example, the number of particles in the sample containing particles between 108 and 400 μm is ~9.7 particles/mm^3. Thus, these samples show the same tendency as observed with smaller particles of more scattering. However, because of the smaller number density of particles, they exhibit quite low overall absorbance.

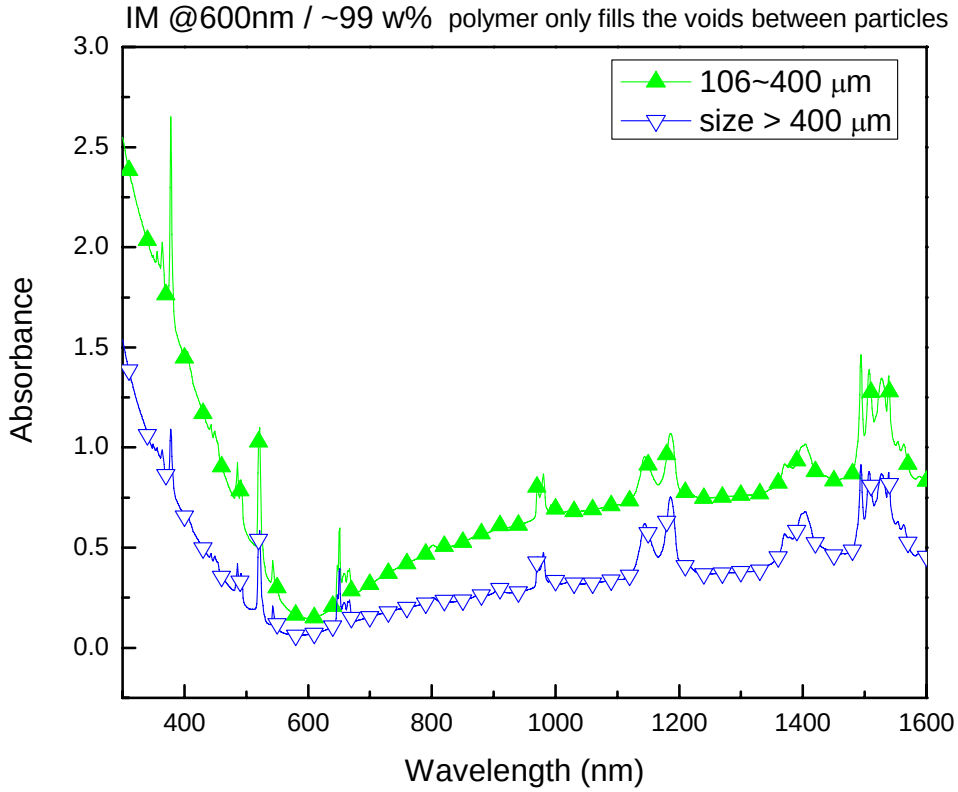

Figure 4-36: Absorbance spectra for samples index-matched at 600 nm with different particle sizes (size between 106~400 μm and size bigger than 400 μm) but fixed concentration of particles to the polymer. Smaller particles exhibit more scatterings

Within samples with same size particles the concentration of particles will determine the degree of transparency and the brightness of the voxel. Figure 4-37 and 4-38 show that the absorbance spectra depend on the concentration of particles for particles between 20 and 38 μm and for particles smaller than 20 μm, respectively. Both graphs demonstrate that higher concentration gives higher absorbance. Since absorption by the polymer and the KY_3F_{10} does not depende on particle size, the difference in absorbance comes from the difference in scattering. Hence, the result tells us that higher concentration gives more scattering.

The brightness of a voxel will depend directly on the density of the active material. In this case, the active material is KY_3F_{10} particles because the index-matched polymer is a passive matrix. To achieve a brighter voxel a higher concentration of the active material is necessary. However, more KY_3F_{10} particles implies more interfaces between particles and polymer which will cause more scattering because of index mismatch at wavelengths other than the index-matched wavelength.

Since it is impossible to achieve scattering-free scalable display medium without perfect index-matching over the complete wavelength range, the degree of concentration of crystallites needs to be determined depending on several criteria such as display medium size and voxel brightness. For instance, if the application of this scalable display medium is for relatively large size display, then the concentration may be lower than in a smaller display to maintain a certain degree of transparency so that the images made inside can be seen by the observers even though the brightness will be less. The display medium criteria depend on the application and so it must be designed appropriately.

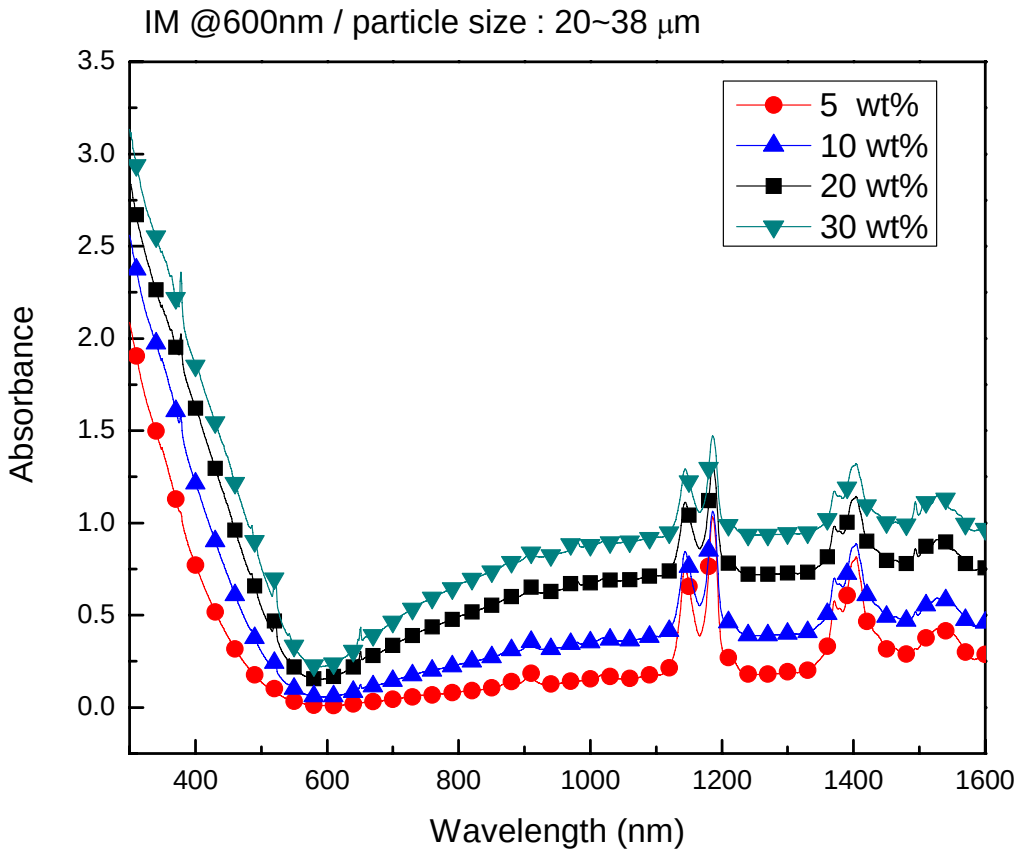

Figure 4-37: Absorbance spectra for samples index-matched at different wavelengths for weight percent of particles to polymer from 5 to 30%. The samples exhibit lowest absorbance at the wavelength at which they are index matched with Er:KY_3F_{10}.

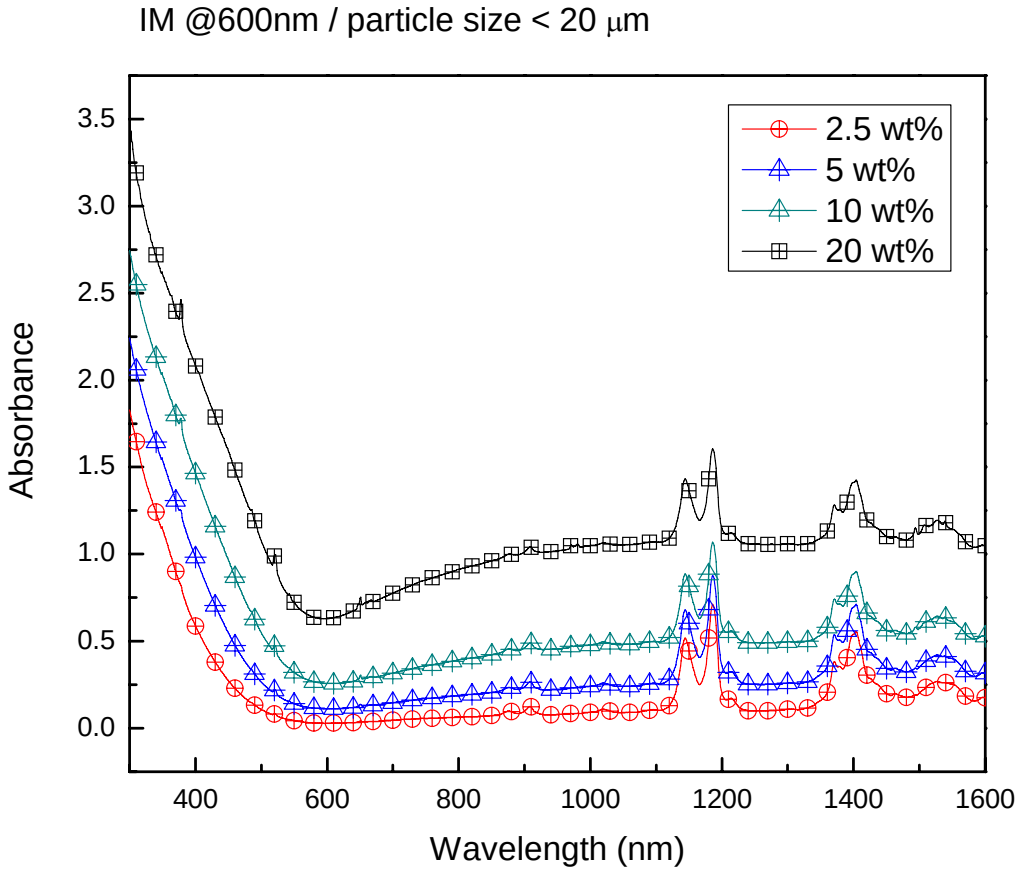

Figure 4-38: Absorbance spectra for samples index-matched at different wavelengths for weight percent of particles to polymer from 2.5 to 20%. The samples exhibit lowest absorbance at the wavelength at which they are index matched with Er:KY_3F_{10}.

CHAPTER FIVE: CONCLUSIONS AND FUTURE WORK

5.1 Scalable 3D display media

Different materials as display medium candidates for static volumetric 3D display were studied such as organic dyes and rare-earth doped single crystals. Several rare-earth doped fluoride crystals that are excited to emit visible light by sequential two photon absorption have been investigated as display medium candidates for static volumetric three dimensional displays. KY_3F_{10} crystals doped with erbium and praseodymium were found to be the most promising display material for static volumetric 3D display. As a solution to a the demand for a larger size display scalable display medium concepts were explored. Dispersion of powders of these materials in a refractive index-matched polymer was demonstrated as a scalable display medium. Detailed experiments on many different polymers were described. Polymers which stay soft and do not require solvent are shown to be most appropriate polymers for 3D display purposes. The scattering problem in such a medium is greatly reduced by index-matching the polymer to the particles. A prototype scalable display medium was demonstrated and an index-matching condition that optimizes the performance was identified.

5.2 Future work

5.2.1 Dispersion control

Several problems were identified in realizing a scalable 3D display medium such as residual scattering problem caused by dispersion mismatch and the use of defective crystalline particles. The dispersion mismatch problem can be investigated further by using other polymers which have dispersion to that of KY_3F_{10} than does PFCB or polymer-gel. For example, it may be possible to make a fluorinated-PMMA which has a dispersion curve similar to KY_3F_{10}. Since the index of refraction of normal PMMA is much higher than that of KY_3F_{10} crystal the polymer has to be modified so that its index of refraction is decreased. J. Gaynor et al. showed that fluorination of commercially available PMMA lowers the refractive index.[76] By changing fluorine density by adding fluorinated side groups to the methacrylate monomer, they were able to lower the refractive index up to 0.1 (from 1.489 to 1.383) which is more than enough for our purposes.

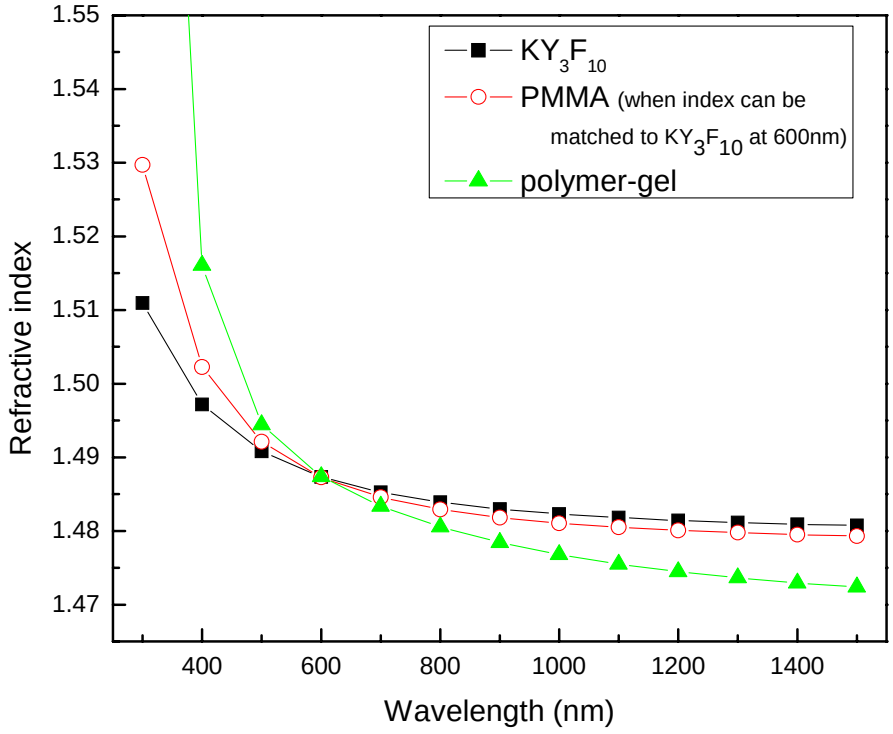

Figure 5-1: Dispersion curves of PMMA (when the refractive index can be matched to KY_3F_{10} at 600nm), polymer-gel and KY_3F_{10}. The dispersion differences between PMMA and KY_3F_{10} crystal are much smaller than that of the polymer-gel and the KY_3F_{10} crystal

In Figure 5-1, the dispersion curve of PMMA (when the refractive indices are lowered over entire wavelengths by 0.01 from the commercially available PMMA) is presented along with that of polymer-gel and KY_3F_{10}. As one can see from the graph, the dispersion difference is much smaller using this PMMA-KY_3F_{10} combination compared to polymer-gel-KY_3F_{10}. Thus, future work should seek a solventless type of PMMA with lower index of refraction or a dispersion controlled polymer to make scalable 3D displays.

5.2.2 Smaller crystallite particles

If the particle size is decreased and/or the particles are more concentrated there will be more scattering in the sample. Since a higher density of particles is essential for brighter voxels it is necessary to increase the concentration of particles without or with the least amount of degradation to the transparency of the 3D display medium. One way to realize this is by using smaller particles, especially, nanoparticles. The important wavelengths in this TSTF-UC scheme are all the visible wavelengths and the near infrared. Because, the shortest wavelength in the visible is about 450 nm, the use of nanoparticles smaller than this wavelength (about tens of nanometers) might result in a significant decrease in scattering.

In recent experiment conducted using fluoride crystals, nanoparticles were made about 50 nm in size (Figure 5-2). A micronizing mill and an ultrasonic processor system incorporated with flow cell and were used to prepare these particles. No attempt was made to make KY_3F_{10} nanoparticles but it can be done by using a similar process. It is also necessary to determine the emission characteristics of nanoparticles.

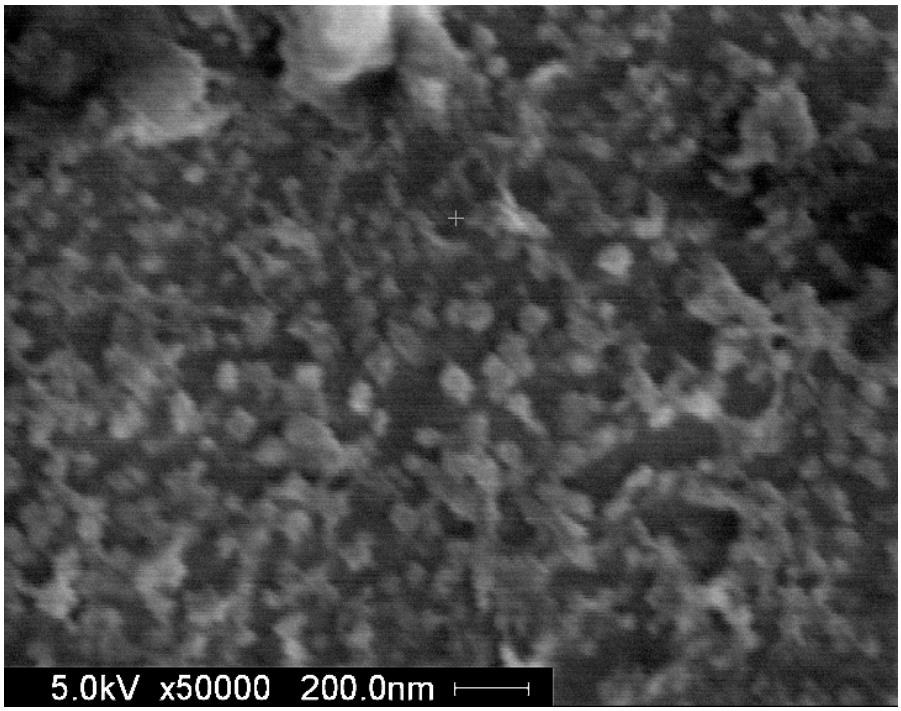

Figure 5-2: SEM photograph of the 1% Er, 18% Yb:NYF nanoparticles. The average size shown is about 50 nm.

5.2.3 Ceramic crystal

Another way to increase the concentration of particles with least amount of degradation to the transparency is to prepare large ceramic crystals of KY_3F_{10}. A. Ikesue and other researchers were able to reduce scattering in ceramic crystal YAG and make laser quality ceramic crystal materials [85][86]. Ceramic crystal of KY_3F_{10} can be possibly made from the KY_3F_{10} single crystal powder [87]. If ceramic crystals of KY_3F_{10} can be made with comparable properties, ceramic crystal KY_3F_{10} will be a strong candidate for a scalable 3D display medium.

Collaboration with Dr. A. Ikesue and A.C Materials is under way to achieve this goal.

LIST OF REFERENCES

[1] B. G. Blundell, A. J. Schwarz, "Volumetric three dimensional display systems", Wiley-Interscience, 2000.

[2] T. Ando, K. Mashitani, M. Higashino, H. Kanayama, H. Murata, Y. funazou, N. Sakamoto, H. Hazama, Y. Ebara and K. Koyamada, "Multi-view image integration system for glass-less 3-D display", Stereoscopic Display and Virtual Reality Systems XII, Proc. SPIE-IS&T, 5664, pp 158-166, 2005.

[3] T. Hashiba, and Y. Takaki, "Development of a 3D pixel module for an ultra large screen 3D display", Three-dimensional TV, Video, and Display III, Proc. SPIE, 5599, pp 24-31, 2004.

[4] H. Choi, S.-W. Min, S. Jung, J.-H. Park, and B. Lee, "Multiple-viewing-zone integral imaging using a dynamic barrier array for three-dimensional displays", Opt. Express 11, pp 927-932, 2003.

[5] G. Favalora, D. M. Hall, M. Giovinco, J. Napoli, R. K. Dorval, "A Multi-Megavoxel Volumetric 3-D display System for Distributed Collaboration", Application of Virtual Reality Technologies for Future Telecommunication System, San Francisco, CA, 2000.

[6] D. G. Hopper, "Reality and Surreality of 3-D Displays: Holodeck and Beyond", Electronic Information Display Conference, SID, 2000.

[7] E. Downing, L. Hesselink, J. Ralston, and R. Macfarlane, "A three-color, solid-state, three-dimensional display", Science 273 1185-1189, 1996.

[8] K. Langhans, C. Guill, E. Rieper, K. Oltmann, D. Bahr, "SOLID FELIX: A Static Volume 3D-Laser Display", Stereoscopic Displays and Applications X, Andrew J. Woods, Mark T. Bolas, John O. Merritt, Stephen A. Benton, Proc. SPIE, 5006, pp 161-174, 2003.

[9] B. G. Blundell, A. J. Schwarz, "The Classification of Volumetric Display Systems: Characteristics and Predictability of the Image Space", IEEE Transactions on Visualization and Computer Graphics, 8, pp 66-75, 2002.

[10] J. Cho, H. Jenssen, M. Bass, “Development of a Scalable Volumetric Three-Dimensional Up-Conversion Display Medium”, SID Symposium Digest of Technical Papers, Vol. 38, Issue 1, pp. 1228-1231, May 2007

[11] http://www.rp-photonics.com/luminescence.html

[12] F. Auzel, "Upconversion processes in coupled ion systems," Journal of Luminescence, vol. 45, pp. 341, 1990.

[13] J. Cao, U. Parasuraman, J. Liu, and T. Sun, “Design and implementation of an advanced three-dimensional volumetric display based on up-conversion phosphors”, Cockpit and Future Displays for Defense and Security, ed. by Darrel G. Hopper, Eric W. Forsythe, David C. Morton, Charles E. Bradford, Henry J. Girolamo, Proc. of SPIE Vol. 5801, pp. 278-286, 2005.

[14] C. Xiaobo, F. Yan, Z. Guangyin, L. Meixian, L. Kun, S. Feng, B. Shizhang, S. Meiru, S. Zengfu, S. Yinguan, F. Shiping, X. Jun, H. Chenjuan, L. Xiangang, Z. Zhe, "A initial research of threedimensional volumetric display based on di-frequency upconversion", SPIE Vol. 3560, pp. 122-131, 1998.

[15] W. N. Dember, and J. S. Warm, “Psychology of depth perception”, 2nd ed., Holt, Rinehart and Winston, New York, 1979.

[16] N.S. Holliman, “Three-dimensional display systems” in “Handbook of Optoelectronics”, Vol.II, Ed. J.P. Pakin and R.G.W. Brown, Taylor & Francis, 2006.

[17] S. Y. Edgerton, “The Renaissance rediscovery of linear perspective”, Basic Books, New York, 1975.

[18] C. D. Wickens, “Engineering Psychology and Human Performance”, 2nd ed., HarperCollins Publishers Inc., New York, 1992.

[19] D. S. Falk, D. R. Brill, and D. G. Stork, “Seeing the Light”, Optics in Nature, Photography, Color, Vision and Holography, John Wiley & Sons, New York, 1986.

[20] C. Wheatstone, “Contributions to the theory of vision: part the first, on some remarkable, and hitherto unobserved, phenomena of binocular vision”, Philosophical Transactions of the Royal Society, 128, 371-394, 1838.

[21] I. P. Howard and B. J. Rogers, “Binocular Vision and Stereopsis”, Oxford psychology series No. 29, Oxford university press, New York, 1995.

[22] B. Lane, “Stereoscopic displays”, Proceedings of the SPIE, Vol. 367, Aug. 1982.

[23] L. Lipton, “Foundations of stereoscopic cinema”, Van Nostrand Reinhold, New York, 1982.

[24] D. F. McAllister, “Stereo computer graphics and other true 3D technologies”, Princeton University Press, 1993.

[25] T. Okoshi, “Three-dimensional imaging techniques”, Academic press, New York, 1976.

[26] M. G. Lippmann, “Epreuves reversibles donnant la sensation du relief”, Journal of Physics [4 th series], 7, 821-825, 1908.

[27] C. B. Burckhardt, “Optimum parameters and resolution limitation of integral photography”, Journal of the Optical Society of America, 58(1), 71-76, 1968.

[28] T. Toda, S. Takahashi and F. Iwata, “Three-dimensional (3D) video system using grating image”, SPIE Proceedings, 2652, 54-61, 1996.

[29] A. Schwerditner, “Autostereoscopic 3D display”, Stereoscopic Display and Virtual Reality Systems XIII, Proc. SPIE-IS&T, 6055, 2006.

[30] P. Surman, I. Sexton, R. Bates, W. K. Lee, K. Hopf, T. Koukoulas, “Latest developments in a multi-user 3D display”, Three-dimensional TV, Video, and Display IV, Proc. of SPIE Vol. 6016, 2005.

[31] E. Hecht, “Optics”, 4 th edition, Addison Wesley, San Francisco, 2002.

[32] B. R. Brown, and A.W. Lohmann, “Computer generated binary holograms”, IBM Journal of Research & Development, 13, 160-167, 1969.

[33] Lucente, Hilaire, Benton, Watlington, “New Approaches to Holographic Video”, Holographics International '92, SPIE Vol. 1732, July 1992.

[34] http://alumni.media.mit.edu/~lucente/holo/holovideo.html

[35] D. E. Smalley, Q. Y. J. Smithwick, and V. M. Bove, Jr., "Holographic Video Display Based on Guided-Wave Acousto-Optic Devices," Proc. SPIE Practical Holography XXI, v. 6488, 2007.

[36] C. Slinger, C. Cameron, M. Stanley, "Computer-Generated Holography as a Generic Display Technology", Computer, IEEE Computer Society, August 2005.

[37] M. Stanley, M. AG Smith, A. P S., P. J Watson, S. D Coomber, C. D Cameron, C. W Slinger, and A. D Wood, "3D electronic holography display system using a 100 Mega-pixel spatial light modulator", Optical Design and Engineering, edited by Laurent Mazuray, Philip J. Rogers, Rolf Wartmann, Proceedings of SPIE Vol. 5249, pp. 297-308, 2004.

[38] K. Langhans, D. Bezecny, D. Homann, D. Bahr, C. Vogt, C. Blohm, K. Scharschmidt, "New portable FELIX 3D display", Projection Displays IV, Proceedings of SPIE, Vol. 3296, 24-30 January 1998.

[39] E. L. Withey, "Cathode-Ray Tube Adds Third Dimension", Electronics engineering edition, pp. 81-83May 1958.

[40] C. Tsao and J. Chen, "Moving Screen Projection: a new approach for volumetric three-dimensional imaging", Projection Displays II, Proceedings of SPIE, Vol. 2650, pp. 254-261, San Jose, CA, 1996.

[41] V. V. Saveljev, P. E. Tverdokhleb, and Y. A. Shchepetkin, "Laser system for real-time visualization of three-dimensional objects," Proc. SPIE, vol. 3402, pp. 222–224, 1998.

[42] R. G. Batchko, "Rotating flat screen fully addressable volume display system," U.S., Patent 5 148 310, 1992.

[43] H. Yamada, K. Akiyama, K. Muraoka, and Y. Yamaguchi, "The comparison of three kinds of screens for a volume scanning type 3-D display," in Proc. 1st Int. Symp. Three Dimensional Image Communication Technologies 1993, pp. S-5-3-2–S-5-3-10.

[44] R. Otsuka, T. Hoshino, and Y. Horry, "Transpost: A Novel Approach to the Display and Transmission of 360 Degrees-Viewable 3D Solid Images", IEEE Transactions on visualization and computer graphics, Vol. 12, No. 2, March/April 2006.

[45] http://hhil.hitachi.co.jp/products/transpost.html

[46] http://www.holoverse.com/hv_volumetric1.htm

[47] E. P. Berlin, “Three-dimensional display“, U.S. Patent 4160973, 1979.

[48] Y. Lin, X. Liu, Y. Yao, X. Zhang, X. Liu, and F. Lin, “Key factors in the design of a LED volumetric 3D display system”, Light-Emitting Diode Materials and Devices, edited by Gang Yu, Chuangtian Chen, Changhee Lee, Proc. of SPIE Vol. 5632, pp. 147-154, 2005.

[49] Y. Yao, X. Liu, Y. Lin, H. Zhang, X. Zhang, X. Liu, "Data Acquirement and Remodeling on Volumetric 3D Emissive Display System", Light-Emitting Diode Materials and Devices, edited by Gang Yu, Chuangtian Chen, Changhee Lee, Proc. of SPIE Vol. 5632, pp. 184-191, 2005.

[50] J.-Y. Son, B. Javidi, AND K.-D. Kwack, “Methods for Displaying Three-Dimensional Images”, Proceedings of the IEEE, Vol. 94, No. 3, March 2006.

[51] I. N. Kompanetsa, S. A. Gonchukov, and P.N.Lebedev, “Volumetric displays”, Current Research on Image Processing for 3D Information Displays,edited by Vladimir V. Petrov, Proceedings of SPIE Vol. 5821, pp. 125-136.

[52] D. L. MacFarlane, “Volumetric three-dimensional display”, Appl. Optics, Vol. 33, No.31, pp. 7453-7457, 1994.

[53] A. Sullivan, “DepthCube solid-state 3D volumetric display”, Stereoscopic Displays and Virtual Reality Systems XI, edited by Andrew J. Woods, John O. Merritt, Stephen A. Benton, Mark T. Bolas, Proc. of SPIE-IS&T Electronic Imaging, SPIE Vol. 5291, pp. 279-284.

[54] T. Honda, T. Doumuki, A. Akella, L. Galambos, and L. Hesselink, “One-color one-beam pumping of Er3+-doped ZBLAN glasses for a three-dimensional two-step excitation display”, Optics Letters, Vol. 23, No. 14, July 1998.

[55] X. B. Chen, M. X. Li, Z. C. Ying, K. Liu, G. W. Wang, “The Physics of one-beam pumping upconversion three dimension volumetric display based on erbium doped glass”, Cockpit Displays IX: Display for Defense Applications, Darrel G. Hopper, Eidtor, Proceedings of SPIE Vol. 4712, 2002.

[56] D. Miyazaki, M. Lasher, and Y. Fainman, “Fluorescent volumetric display excited by a single infrared beam”, Applied Optics, Vol. 44, No. 25, Sep. 2005.

[57] http://www.aist.go.jp/aist_e/latest_research/2006/20060210/20060210.html

[58] http://technology.newscientist.com/article/dn8778.html

[59] C. Füchtbauer, “Excitation of mercury spectral lines”, Phys. Z., Vol. 21, pp. 635-638, 1920.

[60] J. D. Lewis, C. M. Verber, and R. B. McGhee, “A True Three-Dimensional Display”, IEEE Transactions on Electron Devices, Vol. ED-18(9), pp. 724-732, 1971.

[61] http://www.3dtl.com/

[62] Ralph Zito, Jr., “Rate Analysis of Multiple-Step Excitation in Mercury Vapor”, Journal of Applied Physics, Volume 34, Number 5, pp. 1535-1543, 1963.

[63] R. H. Barnes, C. E. Moeller, J. F. Kircher and C. M. Verber, “Two-step excitation of fluorescence in iodine monochloride vapor“, Applied Physics Letters, Volume 24, Number12, pp 610-612, 1974.

[64] I. I. Kim, E. Korevaar, and H. Hakakha, “Three-dimensional volumetric display in rubidium vapor”, Proceedings of SPIE, Vol. 2650, pp. 274-284, San Jose, CA, 1996.

[65] A. Rapaport, K. Ayrault, E. St. Mattew-Daniel, M. Bass, “Visible light emission from dyes excited by simultaneous absorption of two different frequency beams of light”, Applied Physics Letters, 74, pp. 329-331, 1999.

[66] E. Boulma, M. Diaf, J. P. Jouart, M. Bouffard, J. L. Doualan and R. Moncorge, “Anti-Stokes emissions and determination of Stark sub-level diagram of Er^{3+} ions in KY3F10”, J. Phys., Condens. Matter, 18, pp. 6721-6727, 2006.

[67] F. W. Ostermayer, J. P. van der Ziel, H. M. Marcos, L. G. Uitert, and J. E. Geusic, "Frequency upconversion in YF3:Yb,Tm," Physical Review B (Solid State), vol. 3, pp. 2698, 1971.

[68] P. Porcher and P. Caro, "Crystal field parameters for Eu in KY3F10. III. Radiative and nonradiative transition probabilities," Journal of Chemical Physics, vol. 68, pp. 4183-4187, 1978.

[69] C. A. Morrison and R. P. Leavitt, "Spectroscopic properties," in Handbook on the Physics and Chemistry of Rare Earths, vol. 5, K. A. Gschneider and L. Eyring, Eds.: Elsevier, 1982.

[70] A. J. Milliez, "Up-conversion in rare-earth doped micro-particles applied to new emissive 2D displays", PhD. Dissertation paper, 2006.

[71] A. Braud, S. Girard, J. L. Doualan, M. Thuau, R. Moncorge, and A. M. Tkachuk, "Energy-transfer processes in Yb:Tm-doped KY3F10, LiYF4, and BaY2F8 single crystals for laser operation at 1.5 and 2.3 μm," *Physical Review B (Condensed Matter)*, vol. 61, pp. 5280, 2000.

[72] M. Bass, H. Jennsen, "Display medium using emitting particles dispersed in a transparent host", U.S. patent 6,327,074 B1, 2001.

[73] http://en.wikipedia.org/wiki/Acrylic_glass

[74] http://www.matweb.com/search/SpecificMaterial.asp?bassnum=O1300

[75] http://www.microchem.com/products/pdf/PMMA_Data_Sheet.pdf

[76] J. Gaynor, G. Schueneman, P. Schuman, J. P. Harmon, "Effects of fluorinated substituents on the refractive index and optical radiation resistance of methacrylates" ,J. of Applied Polymer Science, Vol. 50, 9, pp. 1645 – 1653.

[77] H. R. Allcock, J. D. Bender, and Y. Chang, "Controlled Refractive Index Polymers: Polyphosphazenes with Chlorinated- and Fluorinated-,Aryloxy- and Alkoxy- Side-Groups", Chem. Mater. 2003, 15, 473-477.

[78] J. Ballato, S. Foulger, D.W. Smith, "Optical properties of perfluorocyclobutyl polymers", J. Opt. Soc. Am. B, 20, pp. 1838-1843, 2003.

[79] http://www.tetramertechnologies.com/

[80] J. Ballato, S. Foulger, D.W. Smith, “Optical properties of perfluorocyclobutyl polymers. II. Theoretical and experimental attenuation”, J. Opt. Soc. Am. B, 21, No. 5, pp. 958-967, 2004.

[81] M. Bass and K. Belfield, “Composites of inorganic luminophores stabilized in polymer hosts”, US. Patent No. 6,844,387.

[82] A. Rapaport, F. Szipocs, J. Milliez, H. Jenssen, K. J. Schafer, K. D. Belfield, and M. Bass, “Optically written displays based on up-conversion of near infrared light”, Projection displays VII, Ming H. Wu, Editor, Proceedings of SPIE Vol. 4294, 2001.

[83] A. Rapaport, J. Milliez, M. Bass, A. Cassanho, and H. Jenssen, "Review of the Properties of Up-Conversion Phosphors for New Emissive Displays", Journal of Display Technology, Vol. 2, Issue 1, pp. 68-78, 2006.

[84] http://www.light-span.com/products/engineering/photonics/optical_gels.aspx

[85] A. Ikesue and K. Yoshida, “Influence of pore volume on laser performance of Nd:YAG ceramics”, Journal of Materials Science, 34, pp. 1189-1195, 1999.

[86] A. Ikesue, K. Yoshida, T. Yamamoto, and I. Yamaga, “Optical Scattering Centers in Polycrystalline Nd:YAG Laser”, Journal of the American Ceramic Society, 80, 6, pp. 1517-1522, 1997.

[87] Personal communication, H. Jenssen.